Functional and genetic dissection of mechanosensory organs of *Drosophila melanogaster*

Funktionelle und genetische Analyse von mechanosensorischen Organe in *Drosophila melanogaster*

Doctoral thesis for a doctoral degree
at the Graduate School of Life Sciences,
Julius-Maximilians-Universität Würzburg,
Section Neuroscience

submitted by

Chonglin Guan
from
Zhengzhou

Würzburg 2016

Submitted on:

Members of the Thesis Committee:

Chairperson: Prof. Michael Sendtner

Primary Supervisor: Prof. Tobias Langenhan

Supervisor (Second): Prof. Georg Nagel

Supervisor (Third): Dr. Robert J Kittel

Supervisor (Fourth): Prof. Manfred Heckmann

.

Date of Public Defence:

Date of Receipt of Certificates:

Affidavit

I hereby confirm that my thesis entitled *Functional and genetic dissection of mechanosensory organs of Drosophila melanogaster* is the result of my own work. I did not receive any help or support from commercial consultants. All sources and / or materials applied are listed and specified in the thesis.

Furthermore, I confirm that this thesis has not been submitted as part of another examination process neither in identical or similar form.

Würzburg, Signature

Eidesstattliche Erklärung

Hiermit erkäre ich an Eides statt, die Dissertation *Functional and genetic dissection of mechanosensory organs of Drosophila melanogaster* eigenständig, d.h. insbesondere selbstständig und ohne Hilfeeines kommerziellen Promotionsberaters, angefertigt und keine anderen als die von mir angegebenen Quellen und Hilfsmittel verwendet zu haben.

Ich erkläre außerdem, dass die Dissertation weder in gleicher noch in ähnlicher Form bereits in einem anderen Prüfungsverfahren vorgelegen hat.

Würzburg, Signature

1 Summary

In *Drosophila* larvae and adults, chordotonal organs (chos) are highly versatile mechanosensors that are essential for proprioception, touch sensation and hearing. Chos share molecular, anatomical and functional properties with the inner ear hair cells of mammals. These multiple similarities make chos powerful models for the molecular study of mechanosensation.

In the present study, I have developed a preparation to directly record from the sensory neurons of larval chos (from the lateral chos or lch5) and managed to correlate defined mechanical inputs with the corresponding electrical outputs. The findings of this setup are described in several case studies.

(1) The basal functional lch5 parameters, including the time course of response during continuous mechanical stimulation and the recovery time between successive bouts of stimulation, was characterized.

(2) The calcium-independent receptor of α-latrotoxin (dCIRL/Latrophilin), an Adhesion class G protein-coupled receptor (aGPCR), is identified as a modulator of the mechanical signals perceived by lch5 neurons. The results indicate that dCIRL/Latrophilin is required for the perception of external and internal mechanical stimuli and shapes the sensitivity of neuronal mechanosensation.

(3) By combining this setup with optogenetics, I have confirmed that dCIRL modulates lch5 neuronal activity at the level of their receptor current (sensory encoding) rather than their ability to generate action potentials.

(4) dCIRL´s structural properties (e.g. ectodomain length) are essential for the mechanosensitive properties of chordotonal neurons.

(5) The versatility of chos also provides an opportunity to study multimodalities at multiple levels. In this context, I performed an experiment to directly record neuronal activities at different temperatures. The results show that both spontaneous and mechanically evoked activity increase in proportion to temperature, suggesting that dCIRL is not required for thermosensation in chos. These findings, from the development of an assay of sound/vibration sensation, to neuronal signal processing, to molecular aspects of mechanosensory transduction, have provided the first insights into the mechanosensitivity of dCIRL.

In addition to the functional screening of peripheral sensory neurons, another electrophysiological approach was applied in the central nervous system: dCIRL may impact the excitability of the motor neurons in the ventral nerve cord (VNC). In the second part of my work, whole-cell patch clamp recordings of motor neuron somata demonstrated that action potential firing in the *dCirl*^{KO} did not differ from control samples, indicating comparable membrane excitability.

1 Zusammenfassung

In *Drosophila* Larven, sowie in adulten Tieren, sind die Chordotonalorgane (Chos) sehr vielseitige Mechanosensoren und von wesentlicher Bedeutung für die Propriozeption, das Tastgefühl und die auditive Wahrnehmung. Chos teilen molekulare, anatomische und funktionelle Eigenschaften mit Innenohrhaarzellen der Säugetiere und machen sie somit zu leistungsstarken Modellen um molekulare Mechanismen der Mechanosensorik zu untersuchen. In der vorliegenden Studie habe ich ein Präparat entwickelt, um direkt von sensorischen Neuronen der larvalen Chos (von lateralen Chos oder lch5) abzuleiten und definierte mechanische Eingänge mit den korrelierenden elektrischen Ausgängen zu verbinden. Im Folgenden sind die Ergebnisse dieses experimentellen Setups zusammengefasst.

(1) Die basalen funktionellen Parameter von lch5 insbesondere der Zeitverlauf der Reaktion während kontinuierlicher mechanischer Stimulation und die Erholungszeit zwischen aufeinanderfolgenden Stimulationen wurden bestimmt.

(2) Der Calcium-unabhängige Rezeptor von α-Latrotoxin (dCIRL/Latrophilin), ein Adhäsion Klasse G-Protein-gekoppelter Rezeptor (GPCR) wurde als Modulator der von lch5 Neuronen perzipierten mechanischen Signale identifiziert. Die Ergebnisse zeigen, dass dCIRL/Latrophilin für die Wahrnehmung der externen und internen mechanischen Reize erforderlich ist und die Empfindlichkeit neuronaler Mechanosensorik modelliert.

(3) Mit Hilfe optogenetischer Werkzeuge konnte ich bestätigen, dass dCIRL die Aktivität von lch5 Neuronen auf Ebene des Rezeptorstroms (sensorische Kodierung) und nicht der Generierung von Aktionspotentialen moduliert.

(4) Die strukturellen Eigenschaften von dCIRL (z.B. Ektodomänenlänge) sind wesentlich für die mechanosensitiven Eigenschaften von Chos.

(5) Die Vielseitigkeit der Chos bietet des Weiteren die Möglichkeit, Multimodalitäten auf mehreren Ebenen zu untersuchen. In diesem Zusammenhang wurde die neuronale Aktivität der Chos bei verschiedenen Temperaturen analysiert. Die Ergebnisse zeigen, dass sich sowohl spontane als auch mechanisch evozierte Aktivität im Verhältnis zur Temperatur erhöhen, was darauf hindeutet, dass dCIRL keine Rolle in der Temperaturwahrnehmung spielt.

Diese Erkenntnisse, von der Entwicklung des Präparats der Ton/Vibrations Wahrnehmung, über die neuronalen Signalverarbeitung bis hin zu molekularen Aspekten der Mechanotransduktion, haben erste Einblicke in die Mechanosensitivität von dCIRL gewährt.

Neben der funktionellen Charakterisierung peripherer sensorischer Neurone wurde ein weiterer elektrophysiologischer Ansatz im larvalen Zentralnervensystem gewählt, um zu untersuchen, ob sich dCIRL auf die Erregbarkeit motorischer Nervenzellen im Strickleiternervensystem (VNC) auswirkt. Im zweiten Teil meiner Arbeit wird mit Hilfe des *whole-cell-patch-clamp*-Verfahrens gezeigt, dass die Aktionspotentialfrequenz in Motoneuronen von *dCirl*^{KO} Mutanten ähnlich derer von Kontrolltieren ist, d.h. ihre Membranerregbarkeit ist vergleichbar.

2 Introduction

2.1 Mechanosensory transduction in *Drosophila*

A permanent challenge for an animal´s nervous system is the presence of diverse stimuli. Their sensory system provides fundamental physiological functions to interact with the environmental conditions. Distinct classes of receptor neurons in sensory organs respond adequately to specific external and internal cues, providing for the the major senses of photoreception, proprioreception, chemoreception, thermosensation, touch and hearing. Mechanosensation refers to an important sensory modality converting mechanical cues into biological responses. This process relies on sensory receptors to absorb and transform a diverse range of physical forces such as sound, vibration and stretch into biological responses (Delmas et al., 2011).

Mechanosensitivity is based on unique receptor cells in which integral membrane proteins, namely ion channels, have been proposed as sensors of mechanical force. When the force is applied to mechanosensitive channels in the nerve ending, the subsequent ion influx-generated depolarization (receptor potential) brings the membrane potential towards a certain voltage threshold for triggering action potentials (APs). Mechanoreceptors translate the parameters of the mechanical stimulus into a code of action potentials, where the firing frequency reflects the main features of the stimulus. The first electrophysiological recordings of auditory receptor cells suggested that the ion channels could be directly activated by mechanical force (Corey and Hudspeth, 1979).

Insects are endowed with a specialized fundamental unit scolopidium in order to obtain mechanical information. In the fruit fly *Drosophila melanogaster*, the Johnston´s organ (JO), located in the second antennal segment (a2), consists of approximately 227 scolopidia (Kamikouchi et al., 2006), which contain ca. 500 mechanosensitive neurons that specifically respond to sound-induced antennal vibrations (hearing) or detect gravity and wind (Kamikouchi et al., 2009; Kamikouchi et al., 2006; Yorozu et al., 2009). The JO has become one of the most intensely studied models for mechanosensation as it shares biological and functional features (Figure 1) with the hair cells of the mammalian inner ear (Eberl et al., 2000; Kernan, 2007; Robert and Gopfert, 2004). In the mammalian inner ear, the ear ossicles transduce sound into a fluid motion that in turn deflects hair bundles towards the adjacent taller stereocilia. The stereocilia

are inter-connected through tip-links (Figure 1A). In comparison, the arista of the fly ear act as primary receivers and transmit air displacements associated with sound waves into stretched ciliated chordotonal cells (Figure 1B) (Gopfert and Robert, 2001; Kamikouchi et al., 2006; Schwander et al., 2010). Both sensor types have primary cilia and both receptors gate the associated channels that are bathed in a potassium-rich endolymph of very similar composition (Corey and Hudspeth, 1979; Gopfert and Robert, 2001; Lumpkin et al., 1997; Ohmori, 1985). However, it has remained elusive as to whether mutual molecular processes underlie the transduction mechanisms.

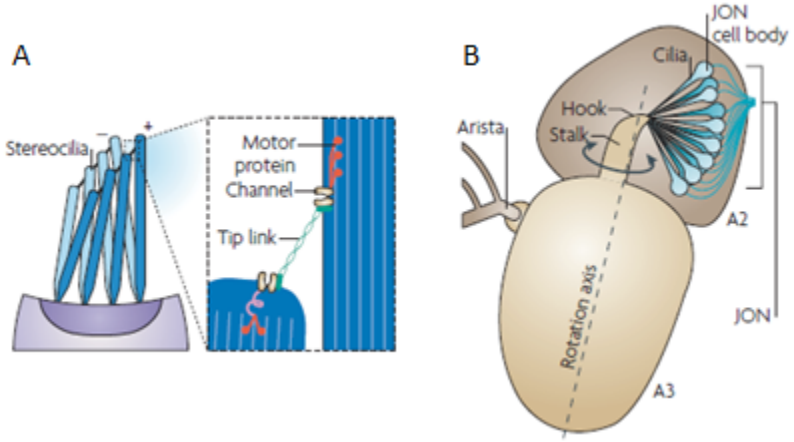

Figure 1. Cilium-based mechanotransduction in mammalian and fruit fly ear. Modified from Christensen and Corey (2007)

Schematic representation of mechanical organelle: hair cell of the inner ear of vertebrate (A) and Johnston`s organ of fruit fly (B).

(A) The excitatory deflection of the hair bundle in the positive direction, which increases tension in the gating spring. In the box region, the transduction model supposes that ion channels located at both ends of a tip link are pulled open by tip link tension. Channels are linked intracellularly to the actin filaments of stereocilia (pale blue lines) by motor proteins and part of the linkage is elastic (red).

(B) Sound-induced movement of air particles oscillates feathery arista in the Antennal segment 3 (A3). The associated stalk and hook vibrate rotationally in response to sound waves and stretch the ciliated neurons. As a result, action potentials are generated by neurons within segment 2 (A2).

2.2 Larval Chordotonal Organs

The peripheral nervous system (PNS) of *Drosophila* larvae provides a model to study the physiological function of sensory neurons. Generally sensory organs of *Drosophila* can be classified as either Type I organs (monociliated sensory neurons with accessory structures) (Keil, 1997) or Type II organs (non-ciliated, multidendritic neurons with dendritic morphologies) (Tracey et al., 2003). Larval type I neurons are located in external organs and chos, whereas multidendritic (MD) neurons (type II neurons) can be further divided into tracheal dendrite (td) neurons and dendritic arborization (da) neurons (Bodmer et al., 1987). The function of MD neurons is critical for larval locomotion (Hughes and Thomas, 2007; Song et al., 2007) and nociception (Kernan, 2007).

Chos, a single subtype of the Type I organs, serve as the primary proprioceptors and mechanoreceptors of *Drosophila* larvae (Kernan, 2007). The single sensory unit of chos is the scolopidium and is comprised of a cap cell, a scolopale cell, a ligament cell and a sensory neuron. Each scolopale contains a ciliary sensory ending which attaches to the dendritic cap in order to receive extracellular stimuli as a stretch receptor (Figure 3). In each segment of the larval abdominal body wall groups of up to five scolopidia (lch5, the pentascolopidial organ) connect the body wall (Cap cells) to the hypodermis (Ligament cells)(Figure 2), through which the animals sense mechanical stimuli and provide proprioceptive feedback on larval locomotion (Caldwell et al., 2003; Hughes and Thomas, 2007; Kernan, 2007). Assembly of the scolopale and cilium is crucial in order to hold the tension between the apical and basal attachment sites and to transduce the mechanical forces. Moreover, disconnection between the dendritic cap and the cilium in *nompA* mutants dispels chordotonal response (Chung et al., 2001). The rootlets are the cytoskeletal structure of ciliated cells. The transcriptional activator RFX is involved in the functionalization of sensory cilia into a mechanosensory structure. In *Rfx* mutants neither rootles nor the cilium can be found, indicating that *Rfx* regulates the differentiation of the ciliated chordotonal neurons (Dubruille et al., 2002).

The chordotonal neurons are monodendritic, bipolar nerve cells, which carry distal dendrites and proximal axons. The mechanosensory properties are determined by the subcellular location of established marker proteins of the chordotonal cilia, namely the dendritic compartment (Kernan,

2007). The ciliary sensory ending is fully enclosed in the scolopale space, which is filled with a specialized endolymph that contains Na^+ and K^+ (Carlson et al., 1997) and allows mechanogated channels to generate a receptor current. The axons propagate the electrical signals to the CNS while the dendrites with inner and outer segments attach to cap cells with their dendritic caps. Extensions of the outer segments form the chordotonal primary cilia with the axonemal structure of the "9x2+0" (nine microtubule doublets and no central microtubules).

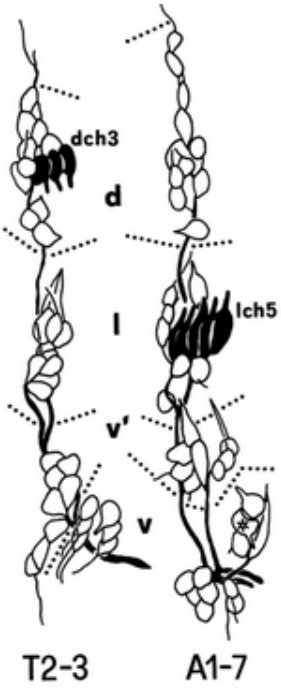

Figure 2. Layout of hemisegmental sensory neurons. (Meier and Reichert, 1995)

Pattern of peripheral sensory neurons in the Drosophila embryo. In each segment, sensory cells are arranged in four distinct clusters indicated by the dotted lines. Ventral is downwards and anterior is to the left. d: dorsal; l: lateral; v´ and v: two distinct parts of the ventral cluster. The dorsal chordotonal organ (dch3) in thoracic segments T2 and T3 comprises three sensory neurons and the lateral chordotonal (lch5) of abdominal segments A1–A7 is comprised of five sensory neurons.

2.3 TRP channels – the classical mechanotransducers

The mechanogated channels termed transient receptor potential (TRP) channels are ionotropic molecular sensors that are involved in a wide variety of neuronal signal transductions (Clapham et al., 2001; Minke and Cook, 2002). TRP superfamily channels are polymodal in that they are essential receptors for the transduction of a wide variety of sensations in flies, worms and mammals, e.g. for vision, olfaction, taste, thermosensation and mechanosensation (Arnadottir and Chalfie, 2010; Clapham, 2003; Delmas and Coste, 2013; Dhaka et al., 2006; Venkatachalam and Montell, 2007; Voets et al., 2005). TRP channels are non-selective cation channels (Cao et al., 2013b; Liao et al., 2013) and can be classified into seven categories based upon sequence homology: TRPA, TRPC, TRPM, TRPML, TRPN, TRPP and TRPV (Christensen and Corey, 2007).

Previous studies have demonstrated that two TRP superfamily channels (TRPN- and TRPV) are involved in mechanotransduction in *Drosophila*. The TRPN channels are encoded by *nompC*, loss of which reduces the sound-evoked response in adult *Drosophila* (Eberl et al., 2000). In *Drosophila* larvae, NOMPC (TRPN1) is expressed in Class III dendritic arborization neurons and is critical for the response to gentle touch (Walker et al., 2000; Yan et al., 2013) and sound stimuli in chordotonal neurons (Zhang et al., 2013). The TRPV channel subunits Nanchung (Nan) and IAV (Inactive) form a heteromeric complex in the proximal cilium of chordotonal neurons and are involved in sound perception (Gong et al., 2004; Liu et al., 2007; Zhang et al., 2013). Both alleles selectively impair the conversion of mechanical stimuli into electrical activity due to the fact that NOMPC and NAN calibrate resting and receptor currents in chordotonal cilia (Effertz et al., 2011; Gopfert et al., 2006; Lehnert et al., 2013; Yan et al., 2013). However, the molecular machinery of NOMPC/NAN/IAV in the mechanotransduction of chordotonal neurons remains elusive. The role of TRPA channels PAINLESS and PIEZO in mechanical nociception and sound detection have been identified in *Drosophila* (Kim et al., 2012; Tracey et al., 2003). Despite an increased molecular knowledge, the models and concepts of mechanotransduction are still very poorly understood. In this thesis, electrophysiological tools have been exploited in order to quantitatively *in vivo* analyse the mechanosensory roles of aGPCRs.

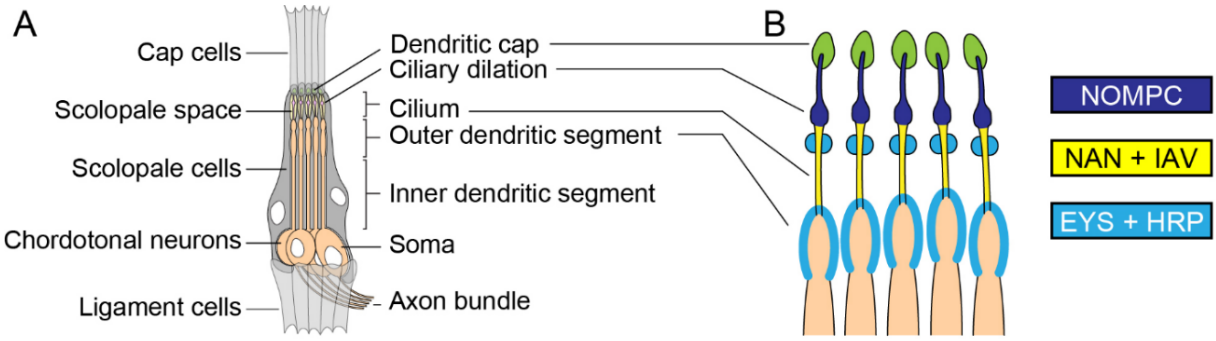

Figure 3. Localization of mechanically activated ion channels in lch5 cilia. Scholz *et al.*, 2015.

(A) Schematic representation of the anatomy of a third instar larval lch5**.**

(B) An enlarged illustration of lch5 ciliated dendrites and representation of antigen localization.

2.4 Adhesion GPCR

2.4.1 Background

Metabotropic receptors represent the biochemical signaling pathways initiated by trimeric guanine nucleotide-binding protein (G protein). Take the adenosine 3', 5'-cyclic monophosphate (cAMP) pathway as an example: following agonist binding to the receptor, guanosine diphosphate (GDP) is replaced by Guanosine triphosphate (GTP) of G_s (G-protein for stimulation of cAMP synthesis). This stimulates the α-subunit to dissociate from the G_s, which in turn activates an adenylyl cyclase to produce cAMP. This increase in cAMP activates protein kinase A (PKA), a serine/threonine kinase, to produce a cellular response (Figure 4). Due to their nature as major drug targets, GPCRs mediate various physiological processes in response to extracellular stimuli (Pierce et al., 2002). GPCRs serve as classical chemosensors and are essential for the translation of light, olfactory and gustatory stimuli into biochemical information by activating various signaling pathways. However, the physiological roles of mechanical modalities of GPCRs are largely unresolved.

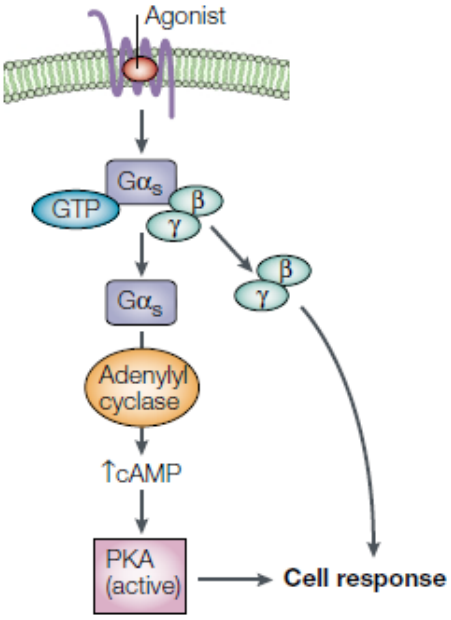

Figure 4. The classical cAMP pathway of GPCR signaling.

Modified from Pierce, 2002.

The activated receptor complex with G_s protein is formed following agonist binding. GDP is released from the G protein and is replaced by GTP. This causes the α-subunit and βγ dimers to dissociate from the G_s complex. The α-subunit ($G_{\alpha s}$) binds to and activates the adenylyl cyclase to produce cyclic AMP (cAMP) molecules, which in turn activate protein kinase A (PKA). This is a serine/threonine kinase that phosphorylates specific substrate proteins, thereby producing a cell response.

aGPCR stand out from other GPCR classes due to their structural properties. GPCRs are further divided into five classes based upon the canonical structure of the 7-transmembrane (7TM) domain: Glutamate, Rhodopsin, Adhesion, Frizzled/Taste 2, and Secretin (Fredriksson et al., 2003;

Lagerstrom and Schioth, 2008). The large aGPCR class presents unique architectural features that are distinguished from those of other GPCR families: large N and C termini (Bjarnadottir et al., 2004; McMillan et al., 2002) and a GPCR autoproteolysis-inducing domain (GAIN) (Arac et al., 2012). The GAIN domain contains a GPCR autoproteolysis site (GPS), which possesses the capacity to self-cleave nascent aGPCR pre-proteins into N- and C-terminal fragments (NTF and CTF, respectively, Figure 5)(Hamann et al., 2015; Langenhan et al., 2013). An extracellular domain (ECD) contains a unique combination of adhesive functional folds based upon its canonical topology; 7-transmembrane domain (7TM) and an intracellular domain (ICD, Figure 5) (Langenhan et al., 2013; Liebscher et al., 2013).

Different roles of aGPCR have been reported in developmental processes, including planar cell polarity, convergence/extension, migration and differentiation (Langenhan et al., 2009). Furthermore, aGPCRs may modulate synaptic transmission (O'Sullivan et al., 2012; Sudhof, 2001). Moreover, human mutations in aGPCR loci have been linked to disorders of the nervous and cardiovascular systems, as well as neoplasias of all major tissues (Langenhan et al., 2013). However, little is known regarding the physiological function, such as stimuli and signal transduction, of this receptor class.

A growing body of evidence places GPCRs in the context of mechanically mediated cellular functions. *In vitro* studies have shown that physical stimuli, such as membrane stretch, osmotic concentration, and viscosity, may lead to an agonist-independent activation of GPCRs (Chachisvilis et al., 2006; Mederos y Schnitzler et al., 2008; Zou et al., 2004), suggesting that the mechanisms linking mechanical stimuli to ion channel activation appear to rely critically on signaling cascades of GPCRs. *In vivo* findings on the mechanosensitive nature of aGPCRs have recently been reported, e.g. GPR56 regulates force-induced muscle hypertrophy in mice (White et al., 2014) and visual proteins (rhodopsins) serve *Drosophila* hearing (Senthilan et al., 2012). In addition to sensing forces, rhodopsins have also been found to function as thermosensors (Shen et al., 2011). However, the underlying molecular machinery and identity of GPCRs in mechanosensory neurons remains largely unknown. In contrast to physiological tasks, GPCRs are also involved in sensory cell development, e.g. VLGR1 partakes in the development of cochlear hair cells and retinal photoreceptors (McGee et al., 2006; Reiners et al., 2005; Skradski et al., 2001)

and its mutations have been linked to audiogenic seizures and to Usher syndrome (McMillan and White, 2004; Weston et al., 2004). Celsr1 knockout mice have demonstrated defects of the inner ear sensory epithelium due to a planar cell polarity disruption (Curtin et al., 2003). Furthermore, analysis of zebrafish gpr126 mutants have demonstrated an essential role in the development of myelinated axons in the peripheral nervous system (Monk et al., 2009). These findings add new facets to the multimodal activation spectrum of this ubiquitous protein superfamily.

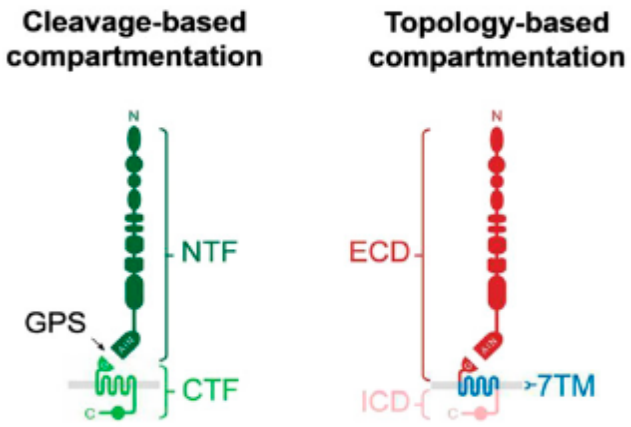

Figure 5. Schematic structural features of aGPCR

After autoproteolysis at the GPS within the GAIN domain, the two-portion receptor structure contains the NTF and the CTF (left). Based on topology, the receptor portions can be classified into an ECD, a 7TM domain and an ICD (right). After Hanmann, 2015

2.4.2 Latrophilin/dCIRL

A prototype aGPCP subgroup Latrophilins is present in invertebrate and vertebrate genomes, which suggests that they have a long evolutionary history (Figure 6A) (Fredriksson and Schioth, 2005) and that their architecture is highly conserved across the large phylogenetic distance (Figure 6B).

Latrophilin (The mammalian Latrophilin 1 homolog), alternatively named calcium-independent receptor of α-latrotoxin (CIRL), was first identified as a neuronal receptor for the black widow spider venom component alpha-latrotoxin (α-LTX) (Davletov et al., 1996; Krasnoperov et al., 1996). It triggers strong presynaptic exocytosis through formation of membrane pores (Orlova et al., 2000; Rosenthal and Meldolesi, 1989). For humans, black widow spider stings cause several health problems including muscle pain, abdominal cramps, profuse sweating, raised blood pressure and tachycardia (Muller, 1993; Zukowski, 1993).

When latrophilin receptors were tested for their role in synaptic transmission, it was found that, latrophilin knockout mice presented impairments in glutamate release from synaptosomes when applied with α-LTX; however, synaptic phenotypes of the mutant remain unclear (Tobaben et al., 2002). Latrophilins contain the "sticky" ECD with several protein domains, indicating roles of ligand binding, cell-matrix and cell-cell interaction in the nervous system. Recent work with latrophilin 1/ADGRL1 has suggested that it takes part in both presynaptic calcium homeostasis through interaction with a teneurin ligand (Silva et al., 2011) and in trans-cellular adhesion through interaction with neurexins 1b and 2b (Boucard et al., 2012). Furthermore, engagement of Latrophilin 3/ADGRL3 with FLRT proteins may contribute to synapse development (O'Sullivan et al., 2014). Latrophilin thus has become one of the prime receptors to study aGPCR roles in the nervous system.

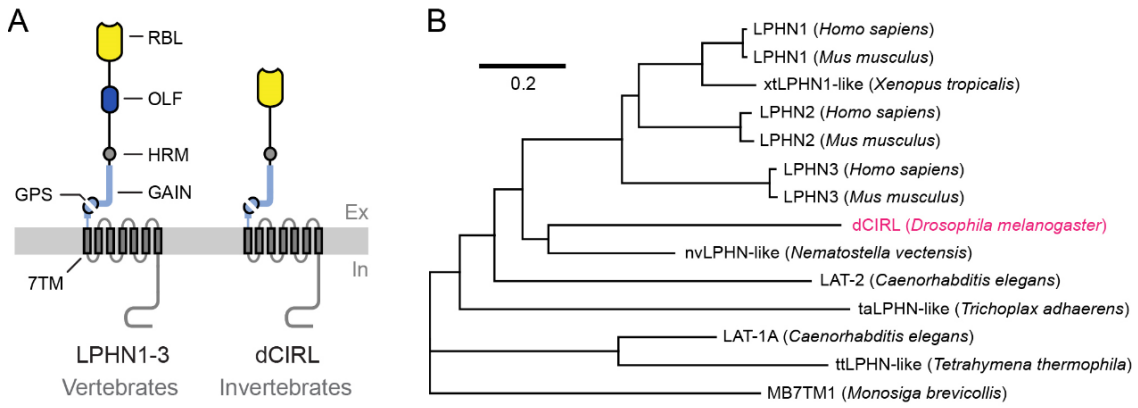

Figure 6. Prototype aGPCP – Latrophilin/CIRL. Scholz *et al.*, 2015.

(A) Conserved domain structure of the Latrophilin subfamily of aGPCR containing Rhamnose-binding lectin (RBL), Olfactomedin (OLF) (present only in vertebrates), Hormone receptor motif (HRM), GAIN, and 7TM domains (N/C order). (B) Phylogenetic analysis of dCIRL shows ancient conservation of Latrophilins from ciliates to humans.

2.5 Model organism: *Drosophila melanogaster*

The fruit fly *Drosophila melanogaster* belongs to the family of Drosophilidae of the dipteran insects. Since its introduction to the laboratory by Thomas Hunt Morgan in the early 20th century *Drosophila* has been a versatile model organism in biomedical research. During the last decades many genetic techniques have been used to manipulate the fruit fly's genome (Adams et al., 2000).

For example, the balancer chromosomes with dominant markers can prevent heterozygous mutations from recombining with their homologs (Hochman, 1971). Another invention of GAL4/UAS system allows for the expresses of proteins of interest in selective cells (Brand and Perrimon, 1993).

Powerful genetics aside, *Drosophila* offers great experimental accessibilities in the fields of development, physiology and behavior. Furthermore, the fruit fly as laboratory animal has practical advantages over vertebrate models: it is a small and inexpensive animal and it has high fertility with a short life cycle of 10 – 20 days which therefore allows for large-scale handling. The animals are kept in the laboratory (25 °C) in transparent plastic vials filled with a yeast-glucose culture medium supplying nutrition for adults and larvae (Figure 7B).

Females lay eggs on the surface of the culture medium after fertilization. It takes 1 day to reach the embryo stage from the larva stage. It takes three days for the larvae to mature in the medium (25 °C) from the first instar the third instar. The mature third instar larvae then leave the food medium to form a pupal case on the 6th day. Eclosion of the adult fly from the pupal stages requires another 3-4 days(Figure 7A) (Ashburner and Roote, 2007).

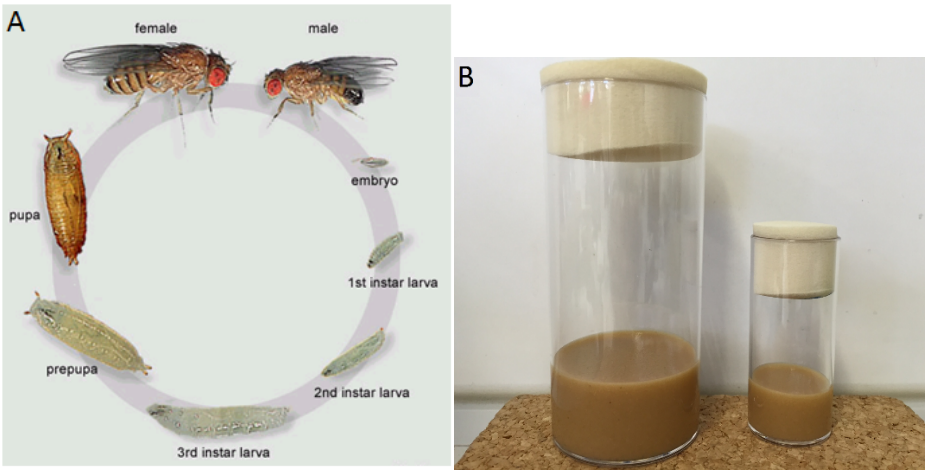

Figure 7. Maintenance of *Drosophila in* a laboratory

(A) The life cycle of *Drosophila melanogaster* (FlyMove). (B) Culture vials (68 ml, 10 ml).

2.6 Aim of this study

(i) Assays of Mechanosensation

Drosophila, similar to many insects, use their chordotonal neurons to modulate behavior through their responsiveness to acoustic vibration and gentle touch (Caldwell et al., 2003; Fushiki et al., 2013; Hughes and Thomas, 2007; Ohyama et al., 2013; Wu et al., 2011; Yan et al., 2013). Mechanosensory disturbance as a punishment in larval *Drosophila* has been implemented in associative learning assays (Eschbach et al., 2011; Saumweber et al., 2014). Moreover, the mechanosensory pathways of the fly´s chos may play a crucial role in entraining circadian clock of *Drosophila* (Simoni et al., 2014). Genetic and behavioral experiments have implied that *dCirl* affects coordinated larval locomotion through its function in chos (Scholz et al., 2015). When the behavioral phenotypes are caused by a defect in sensory transduction, a crucial step is to identify mechanosensory mutants. To obtain information on dCIRL, I set out to apply electrophysiological recording techniques to investigate the physiological roles in mechanosensory inputs of neuronal circuit.

In the past two decades, the *Drosophila* auditory system has presented a powerful genetic model system for studying the molecular aspects of the physiology of mechanosensory organs *in vivo* (Eberl et al., 2000; Kernan, 2007; Robert and Gopfert, 2004). During the course of this PhD project I aimed to establish an experimental platform in order to measure the activity of chordotonal neurons in response to mechanical stimulation in order to elucidate the link between neural activity and sensory modality (Figure 8). The larval chordotonal neurons are not easily accessible for whole-cell patch clamp recording due to anatomical limitations, e.g. the cluster of cell bodies (~ 5 µm in diameter) is covered by scolopale cells (Figure 3A). Therefore, the assay was based on extracellular recording from lch5 nerve fibers in semi-intact tissue preparation. In the extracellular recording configuration, the signals from the flow of ionic current through the extracellular fluid are very small and these are amplified by the amplifier to levels that are suitable for quantification. To deliver defined sound stimuli (vibration energy) to the sensory neurons, a fired-sealed electrode coupled to a piezo element was used.

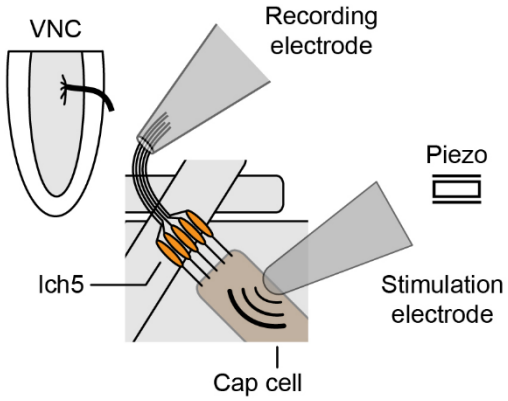

Figure 8. Mechanical probe for lch5. From Scholz et al., 2015

Schematic electrophysiological recording of lch5. A stimulation electrode applies sound frequencies to the lch5 while a suction electrode records neuronal activities from the axon bundle.

(ii) Motor neuron recordings

Larval crawling is a complex behavior that requires coordinated output from central pattern generator neurons to muscles through the firing of efferent motor neurons located in the ventral nerve cord (VNC) (Jan and Jan, 1976). In turn, the output can be adjusted through sensory feedback from afferent neurons of the PNS (Caldwell et al., 2003; Cheng et al., 2010; Suster and Bate, 2002). Type I motor-innervation is directly required for a full motor response. Thus, the functional consequences of *dCirl* removal from these neurons might account for the locomotion deficits observed in $dCirl^{KO}$ larvae. Previous two-electrode voltage clamp (TEVC) recordings from the NMJ have illustrated that synaptic neurotransmission was not affected by *dCirl* removal (data not shown). However, a functional requirement for *dCirl* might not be limited to synaptic properties at the NMJ. Instead, *dCirl* function may pertain to the excitability of the motor neurons in the VNC. To assess this possibility, I employed whole-cell patch clamp recordings of type Ib motor neurons. Previous electrophysiological measurements of *Drosophila* motor neurons have shown that it is feasible to access the ventral ganglion of *Drosophila* embryo (Baines and Bate, 1998) and larva (Rohrbough and Broadie, 2002). Whole-cell mode would be appropriate to determine properties of *Drosophila* central neurons, e.g. current densities, thresholds for excitability, and patterns of activity, which are essential to understand their coordinated functions in the nervous system (Choi et al., 2004).

3 MATERIALS & METHODS

3.1 Fly stocks

In collaboration with other members of the lab, the following strains were used for experiments:

w^{1118} (wildtype)

LAT163, $dCirl^{Rescue}$ (controls, Uta Strobel)

LAT26, $dCirl^{KO}$ (T. Langenhan)

LAT174, $dCirl^{T726A}$ (M. Nieberler)

LAT280, $dCirl^{H724A}$ (M. Nieberler)

LAT207, $dCirl^{BTX::HA::Flag}$ (N. Scholz)

LAT206, $dCirl^{BTX::HA::6xlg::Flag}$ (N. Scholz)

LAT111, *$dCirl^{KO}$/CyoGPFw-; 20xUAS-dCirl/TM6B,Tb* (J. Gehring)

LAT112, *+/CyoGFPw-; iav-Gal4/TM6b,Tb* (GAL4; J. Gehring)

LAT113, *$dCirl^{KO}$/CyOGFPw-; 20XUAS-IVS-mCD8::GFP/TM6B, Tb* (UAS-marker; J. Gehring)

LAT116, *$dCirl^{KO}$/CyoGFPw-; iav-Gal4/TM6B,Tb* (GAL4; J. Gehring)

LAT157, $dCirl^{C-Flag}$ (U. Strobel)

LAT159, $dCirl^{N-RFP}$ (U. Strobel)

LAT193, *$dCirl^{KO}$; ChR-XXM/CyoGFPw-* (U. Strobel)

LAT194, *$dCirl^{KO}$; UAS-bPAC/CyoGFPw-* (U. Strobel)

RJK300, *UAS-ChR2-XXM/CyoGFPw-*

Data were obtained from male 3rd instar larvae raised at 25°C.

3.2 Reagents

For optogenetic stimulation with Channelrhodopsin-2 (ChR2), 100 µM all-trans-retinal (RAL) supplementation was added to the laying medium, so that RAL is taken up by larvae to express

functional ChR2 (Figure 23) (Schroll et al., 2006). In order to identify the chordotonal neurons, green fluorescent protein (GFP) was used to label the target cells (Figure 20C).

- NaCl (cat. no. 1.06404, Merck)
- KCl (cat. no. 1.04933, Merck)
- $MgCl_2$ (cat. no. 1.05833, Merck)
- $NaHCO_3$ (cat. no. S6297, Sigma–Aldrich)
- NaH_2PO_4 (cat. no. 7558, Sigma–Aldrich)
- D-(+)-Trehalose dihydrate (cat. no. T5251, Sigma–Aldrich)
- D-(+)-Glucose (cat. no. G5400, Sigma–Aldrich)
- Sucrose (cat. no. S9378, Sigma–Aldrich)
- HEPES (cat. no. 54457, Sigma–Aldrich)
- $CaCl_2$ (cat. no. 21097, Fluka Analytics)
- TES (cat. no. T1375, Sigma–Aldrich)
- EGTA (cat. no. 03779-10G, Sigma–Aldrich)

3.3 Equipment

- Forceps (Dumont #5, type 11253-20; Dumont #55, type 11255-20, Fine Science Tools)
- Scissors (type 15005-08; type 15000-04, Fine Science Tools)
- Tissue adhesive (3M Vetbond, World Precision Instruments)
- Protease (type XIV, Sigma)
- Culture tubes (height 10.5 cm, diameter 4.6 cm)
- Petri dishes (diameter 55 mm)
- Piezo element (KEPO FT-15T-6.0A1-464; Conrad Electronic)
- Thick-walled borosilicate glass tubing (GB150-8P, inner diameter 0.86, outer diameter 1.5 mm, Science Products)
- DMZ-Universal puller (Zeitz Instruments)
- Patch-pipette fillers (20 µl, Eppendorf)
- Upright microscope (Nikon Eclipse-FN-1)
- Dissecting microscope (Stemi 2000, Carl Zeiss)

- Mercury lamp (Nikon intensilight C-HGFI)
- Micromanipulator and stimulation electrode holder (Sutter Instrument Company and Narishige)
- Patch-clamp amplifier (EPC 10 USB, HEKA Instruments)
- Software and data acquisition interface (Patchmaster, HEKA Instruments; Clampfit, Axon Instruments, Molecular Devices; ABF Utility, Synaptosoft; SigmaPlot (Systat Software Inc.)
- Vibration table (Newport)

Solution for whole-cell patch clamp recordings

For current clamp experiments, the *Drosophila* external saline was prepared using 135 mM NaCl, 5 mM KCl, 4 mM $MgCl_2$, 5 mM TES, 36 mM Sucrose. Adjust pH to 7.15 with NaOH. The intracellular recording solution was prepared using 140 mM KCH_3SO_3, 20 mM HEPES, 5 mM KCl, 2 mM EGTA, 2 mM MgCl, adjusted to pH 7.4 with NaOH. The Drosophila external saline can be stored at 4°C for a week and added 2 mM $CaCl_2$ on the day of experiment. Stock intracellular recording solution was aliquoted and stored at – 20°C.

Solution for lch5 neuron recordings

For larval dissection, the hemolymph-like saline was prepared using 103 mM NaCl, 3 mM KCl, 4 mM $MgCl_2$, 5 mM TES, 7 mM sucrose, 10 mM glucose, 10 mM trehalose, 26 mM $NaHCO_3$, 1 mM NaH_2PO_4, adjusted to pH 7.25 with HCl. For recording (extracellular and internal solution), 2 mM $CaCl_2$ was added to the saline. To isolate receptor currents, 12 µl (1 mM) TTX was added to the 3 ml bath solution (final concentration: 4 µM). The hemolymph-like saline can be stored at 4°C for a week and added to recording solution on the day of experiment.

3.4 Chordotonal neuron recordings

3.4.1 Preparation of mechanical stimulation

The recording glass electrodes pulled and fire-polished on every day of experiment using a DMZ-Universal puller to a tip diameter of 5-9 µm. The tip size of recording pipettes should be suited for the individual nerve cutting site in order to avoid damage of the nerve bundle during suction.

The piezo element was fixed on a three-axis micromanipulator. The fired-sealed mechanical probe screwed to the plastic pipette holder. The pipette holder was mounted on the ceramic part of piezo. The probe was positioned at an angle of 30–45° from the horizontal plane and moved downward toward the selected organ. The sine wave frequencies and displacement of the mechanical probe were controlled by the Patchmaster sftware program (HEKA Instruments). The mechanical stimulation protocol can be edited by using Pulse Generator (Patchmaster) consisting of a series of increasing sine frequencies (100, 300, 500, 700, 900, 1100, 1300, 1500 Hz,) and 8 V amplitude (peak to peak; Figure 9).

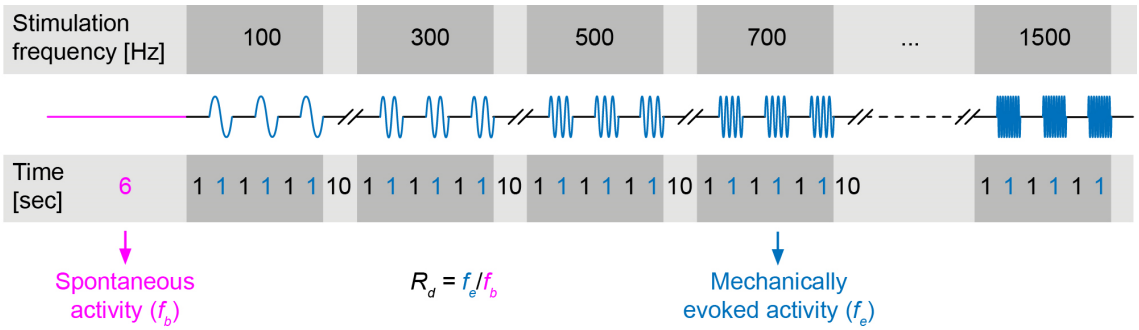

Figure 9. Stimulation protocol to probe electrical responses of lch5 upon mechanical stimuli.

3.4.2 Caculation of discriminability of lch5

Sensory perception and encoding rely on the ability to contrast evoked from spontaneous activity in the principal sensory neuron. Thus, I quantified the proportional chordotonal response towards mechanical stimulation, namely, the ratio between evoked and spontaneous spiking activity (R_d; Figure 9), as a measure of the chordotonal neurons' facility to distinguish signal from noise. All discrimination ratios R_d for each stimulation frequency were calculated:

$$R_d = f_e/f_b$$

where f_e is the average evoked response frequency and f_b the average spontaneous (background) spiking frequency of an individual lch5 recording. To establish the discrimination matrix, I then compared R_d values for each specific stimulation frequency with R_d values for every other stimulation frequency obtained for the same genotype through a nonparametric Mann- Whitney U test. Pairwise comparisons tested the null hypothesis that both samples were identical. The *P*

values for each comparison were color coded and entered into a rectangular array deriving a discrimination matrix for each genotype tested (Figure 21G).

3.4.3 Chordotonal receptor current recordings

For receptor current recording, 4 µM of TTX was added to the saline solution to block the spontaneous activity of lch5 neurons before mechanical stimulation. The obtained current traces were extracted by applying an offline low-pass filter (Gaussian; cutoff: 30 Hz). Phasic amplitude was measured between the onset of receptor current and its maximal peak. Tonic amplitude was determined by averaging the start and end points of the last 200 ms of mechanical stimulation.

3.4.4 Pharmacological inhibition with SQ

After a series of mechanical stimulation, 100 µM SQ22536 (Merck) was added to the saline solution to inhibit adenylyl cyclase activity. Chos were incubated for 10 min in the presence of SQ22536 before application of a second series of mechanical stimulation. After the second series of stimulation, the preparation was washed with fresh saline and a third series of stimulation was applied subsequently.

Optogenetic methods

3.4.5 *ChR2-XXM* stimulation of lch5

Blue light (0.4 s) was supplied by a mercury lamp (Nikon intensilight C-HGFI) and filtered by a 460–500 nm filter. The light-stimulation protocol consisted of a series of increasing light intensities (0.04, 0.08, 0.17, 0.34, 0.68, 1.35, 2.71 and 5.42 mW/mm^2) with intermittent breaks of 10 s.

3.4.6 *bPAC* stimulation

Three blocks of stimulation were applied subsequently with intermittent breaks of 3 s: *1. Sound; 2. Sound + Light; 3. Sound*. Chos were stimulated by a mechanical challenge at 900 Hz before, during and after light stimulation, where ten 1-s cycles of stimulation preceded by 1 s of rest were applied. Photoactivation (460–500 nm; 7–9 mW/mm^2) was applied continuously for 20 s by using the mercury lamp.

3.5 Motor neuron recordings

3.5.1 Background

The biological membrane of a cell, the lipid bilayer, is impermeant to ions. However, an action potential (AP) is induced by voltage-gated channels that allow ionic current to flow across the membrane. Sodium (Na^+) or calcium (Ca^{2+}) influx initialises membrane depolarization and subsequent potassium (K^+) efflux leads to membrane repolarization. To directly measure neuronal activities, intracellular electrode(s) can be inserted into cells. In the voltage clamp technique, membrane potential (V_m) is maintained constant (command potential, V_{cmd}). When V_m is different from V_{cmd} because of, for instance, a current flowing through the ion channels, a clamp amplifier applies a proportional current of inverted polarity to the cell. The feedback of this compensation current can be measured. In the current clamp technique (also known as the bridge mode), where the injection current into the cell is 'clamped', V_m can be changed freely.

In the patch-clamp technique, a low-resistance glass microelectrode is sealed onto the cell membrane to obtain a giga ohm (GΩ) seal (Neher, 1981). In the whole-cell configuration, an isolated membrane patch is ruptured by applying a short pulse of negative pressure. The electrolyte solution in the pipette then forms electrical continuity with the interior of the cell (Hamill et al., 1981).

In general, the same electrode is used record voltage and current passage simultaneously. The voltage at the top of the pipette (V_p) is controlled by the command voltage (V_{cmd}). The current passing through the series resistance (R_s; sum of pipette resistance and residual resistance of the ruptured patch) can lead to significant errors. Consequently, the time constant for resolving currents in the whole-cell patch clamp method is affected by R_s and membrane capacitance ($\tau = R_s \times C_m$). This induces both a transient and a steady-state increase in V_p compared with V_{cmd} (Figure 10), thus limiting the application of a single-electrode voltage-clamp to large cells. However, the technique delivers excellent results when recording, for instance, small central neurons in *Drosophila* embryos or larvae (Baines and Bate, 1998; Rohrbough and Broadie, 2002).

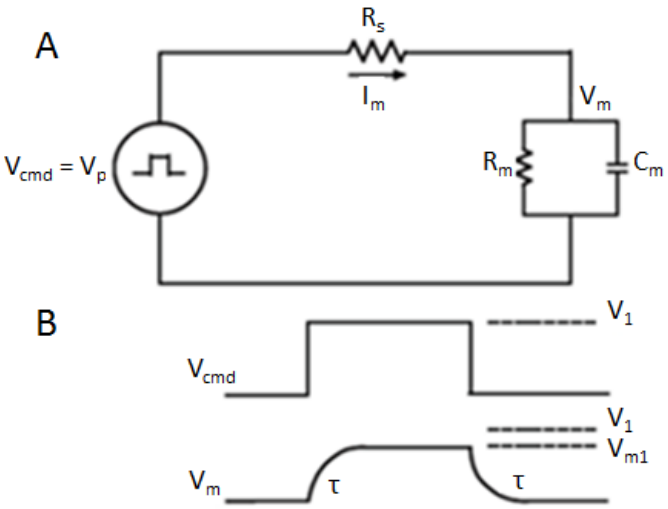

Figure 10. Voltage and temporal errors caused by access resistance Ra. Modified from (The Axon-Guide, 2008).

(A) The patch clamp circuit is simply illustrated as a voltage source (V_{cmd}) in series with the series resistance (R_s) of the recording pipette and the membrane (R_m, C_m). The circuit ensures that the pipette potential (V_p) is equal to V_{cmd}.

(B) After a step change in the command potential from V_{cmd} to V_1, a steady-state current I_m flows in the circuit to ensure that membrane potential (V_{m1}) is equal to $V_1 - I_m R_s$. In the meanwhile, V_m settles exponentially to its steady-state values with $\tau = [R_s R_m/(R_s + R_m)]C_m$, because $R_m >> R_s$ and τ is approximately equal to $R_s C_m$.

3.5.2 Whole-cell patch clamp recordings of somata in VNC

Whole-cell patch clamp recordings of glutamatergic motor neurons in the larval CNS (Figure 12) followed an established protocol (Baines and Bate, 1998). A pair of forceps was used to tear larval bodies and remove excess the tissue and cuticle attached to the CNS. The isolated CNS was secured on silicone elastomer (Sylgard)–coated coverslips by using tissue adhesive (Figure 11A). To expose motor neuron somata for recording, a glass pipette (tip diameter 5–10 µm) containing 1% (w/v) protease diluted in extracellular solution was positioned above the VNC. Gentle positive and negative pressure was applied in an alternating fashion under visual control to rupture the VNC sheath, and debris was cleared away by suction into the pipette. This procedure was repeated until several cell bodies could be seen clearly (Figure 11B, top). The motor neurons were visualised in the VNC through GFP expression by crossing *ok6-GAL4* flies with UAS-GFP flies (Figure 11B, bottom).

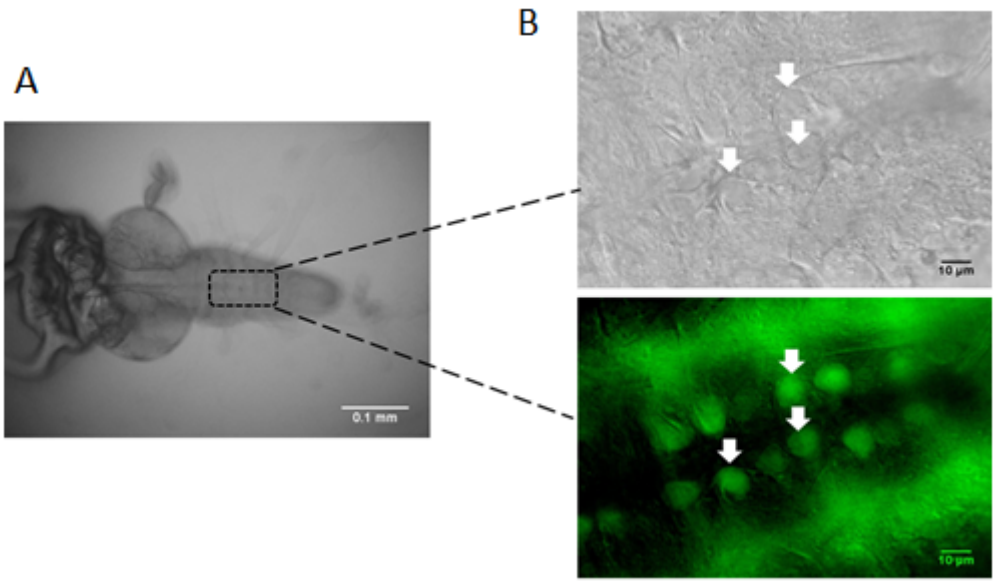

Figure 11. Technique to reveal larval motor neurons in VNC.

(A) An isolated larval CNS secured on Sylgard-coated coverslip, where the anterior side of the CNS is fixed by tissue adhesive, while the posterior end of the VNC is slightly attached to the Sylgard by using the posterior nerve roots. A magnified version of the dashed rectangular inset is shown in (B), which is the area selected for enzyme application.

(B) After enzymatic treatment, motor neuron somata are exposed for patch clamp recording (arrows). *Upper*: bright field; *lower*: fluorescence microscopy.

After revealing motor neurons in the VNC, the preparation was washed with fresh recording solution before obtaining GΩ seals. Thin-walled borosilicate glass electrodes were pulled, fire-polished to final resistances of 7–14 MΩ and filled with intracellular recording solution.

An EPC 10 USB Amplifier was used for whole-cell patch clamp recordings. Cells with a resting membrane potential of at least -55 mV and series resistance below 73 MΩ were used for further analysis (Marley and Baines, 2010). Firing delay was used to distinguish type Is and Ib motor neurons (Choi et al., 2004). For current-clamp experiments, a series of current pulses ranging from

-4 pA to 86 pA (10 pA, 500 ms steps) was injected into the cell, and the resulting action potential firing frequency was analyzed.

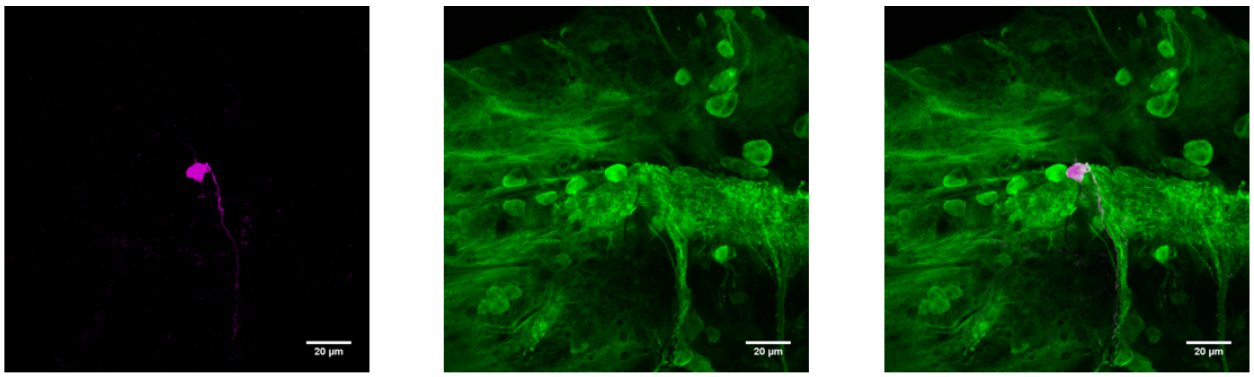

Figure 12. Confocal micrographs showing the target cell highlighted by staining.

To confirm the patch clamp configuration, 0.1% biocytin was added to the intracellular solution (Hefft and Jonas, 2005). After recording, the preparation was fixed with 4% paraformaldehyde in phosphate-buffered saline (PBS) with 0.2% triton (PBT). After a wash with PBT, the preparation was incubated with 5% normal goat serum (NGS) for 30 min and washed with PBT for 5 min again. Subsequently, primary antibody against GFP (rabbit, 1:300) in PBT containing 5% goat serum was applied overnight at 4°C. After washing for 60 min (2 times short, 3 washing steps each for 20 min) the preparation was stained with secondary antibodies (anti-rabbit-Alexa 488, 1:250; Neutravidin-Tetramethylrhodamine (recognizes Biocytin), 1:250) in PBT containing 5% NGS for 2 h at room temperature. After washing 2 times short, 3 x 20 min, the preparation was mounted in vectashield.

Left, Tetramethylrhodamine–conjugated avidin; *middle*, Alexa 488; *right,* merge.

3.6 Data analysis

Two-tailed Mann–Whitney tests of datasets were performed using SigmaPlot. In cases where the data was distributed normally within the compared groups, a t-test was used. In the figures, asterisks denote the level of significance: *$p \leq 0.05$, **$p \leq 0.01$ and ***$p \leq 0.001$. The data are presented as mean ± SEM.

4 Results

4.1 Development of protocol for chordotonal neuron recording

The larval PNS is composed of segmentally repeated chos, and each abdominal hemisegment includes three singlets of chordotonal neurons on the lateral and the ventral sides (lch1, vchA and vchB) and a cluster of five neurons (lch5) (Orgogozo and Grueber, 2005).

The scheme (Figure 13B) describes the recording strategy from lch5. Neuronal signals were recorded by sucking the axon bundle into the recording electrode while mechanical stimulation was applied simultaneously using a piezo element–coupled electrode. The probe tip was placed at the cap cells of the lch5, which are linked mechanically to the apical portions of chordotonal neurons and scolopale cells through an extracellular matrix (dendritic cap) (Chung et al., 2001) and septate junctions (Carlson et al., 1997), respectively (Figure 13A). Details of the experimental procedures are described below.

4.1.1 Animal dissection

1. At the outset, a male third-instar larva was pinned on a Sylgard block. A larval fillet was cut in hemolymph-like saline within a Petri dish.
2. Hemi-segments 2–6 of the larval fillet were selected for further dissection. The major muscles covering the body wall were crosscut along the centre of their length (Figure 13A1).
3. The axon bundle was severed from the VNC after its exit from the lch5 with a fine scissor (Figure 13A2).
4. Extra muscles were removed gently with a fine scissor to expose the cut position of the axon bundle (Figure 13A3).
5. The preparation was then transferred to an electrophysiological rig.

4.1.2 Extracellular recording

6. An upright microscope equipped with a 40x objective was used to visualize lch5 in a bright field (For beginners, cell-specific expression of the GFP transgene driven by the *iav-GAL4* enhancer will help identify single neurons).

7. The recording glass electrode was moved to the distal end of a nerve bundle by using the micromanipulator
8. The entire length of the nerve bundle was sucked into the electrode.
9. Neurons with robust spontaneous activity were selected for further stimulation and a stimulation electrode coupled to a piezo element was placed on the selected lch5 cap cells (Figure 13A4).
10. An electrophysiological amplifier was used to control the piezo device for mechanical stimulation and/or to trigger the mercury lamp for optogenetic stimulation (to adjust the light intensities by using neutral density filters). Simultaneously, an amplifier with low instrumentation noise was used to record neuronal activity extracellularly at a sample rate of 10 kHz and then low-pass-filtered at 2.9 kHz. Data were acquired and processed with Patchmaster software.

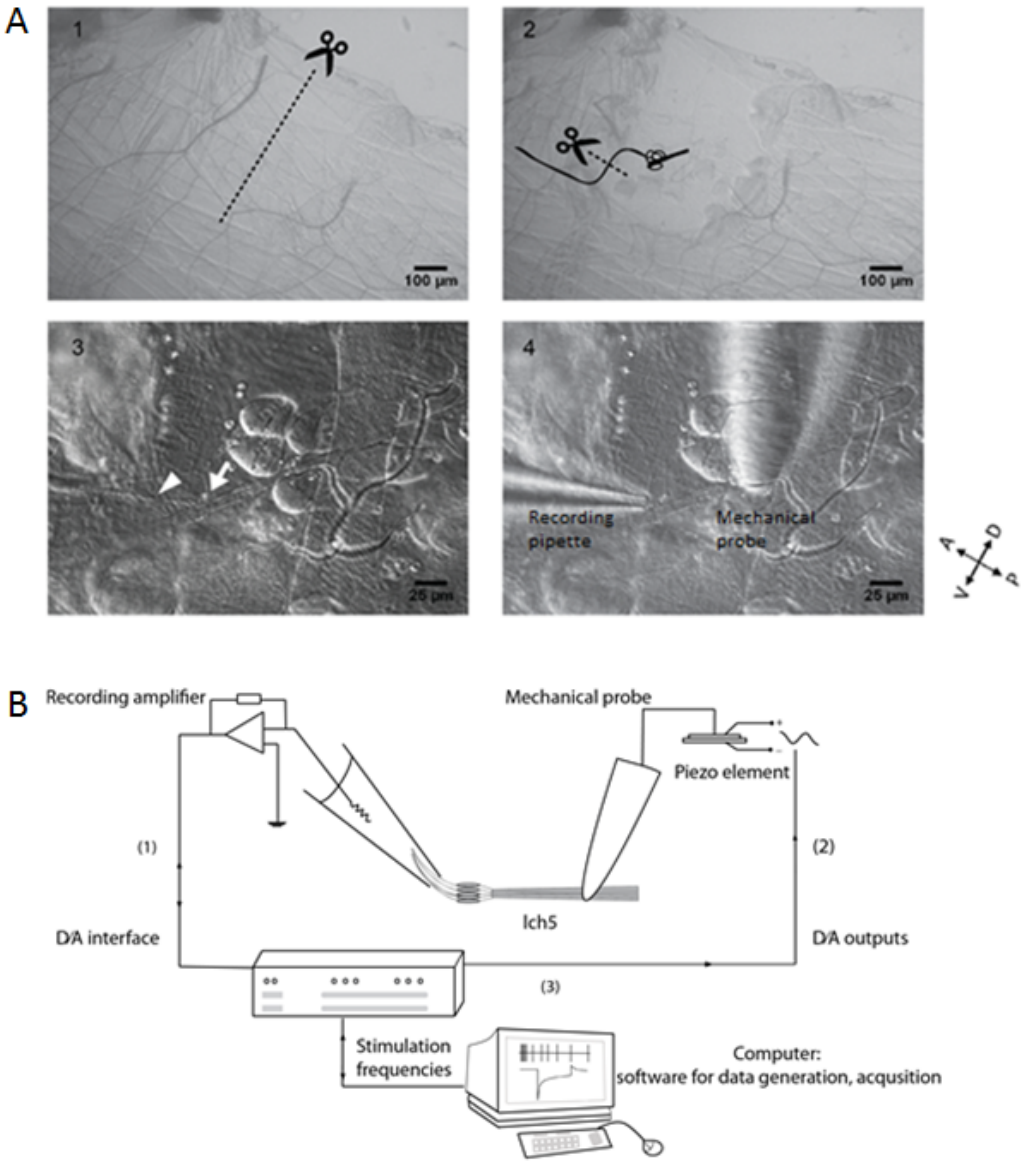

Figure 13. Preparation for probing lch5 responses to mechanical stimulation

(**A**) Panels 1–4 show the procedure of the preparation, as visualized under a bright field: (1) Major muscles covering the body wall were cut away gently with fine scissors. (2) The axon bundle was severed directly after its exit from the lch5. (3) Extra muscles covering the lch5 were removed to expose the axons (arrowhead) of the chordotonal neurons (arrow). (4) The axon bundle was sucked into a recording glass electrode (from left), and a fire-sealed glass electrode (from top) coupled to a piezo element was placed on the lch5 cap cells.

(**B**) Schematic representation of experimental circuit. (1) lch5 neurons were recorded using the extracellular recording; a glass pipette was filled with a hemolymph-like saline, and an Ag/AgCl wire was used to connect the cell to the headstage, a sensitive current-to-voltage converter. (2) The recording amplifier was connected to a computer through an analogue–digital interface to facilitate data acquisition. (3) The mechanical probe was connected to a piezo element, which was connected to the recording amplifier as well, and stimulus parameters such as duration and frequency of stimuli were set to be user configurable by using Patchmaster software.

4.1.3 Mechanical stimulation

Piezo devices provide precision motions by converting an electrical signal into a controlled physical displacement. They have been used to investigate mechanosensation at the cellular level in the flies and mammals(Hao et al., 2013; Yan et al., 2013). When a piezoelectric ceramic element is exposed to an alternating current electric field, it changes dimensions cyclically to produce a reliable cycling frequency of the field, meaning piezoelectric ceramic elements can be used as audible sound transducers (piezo buzzer) with a variety of advantages such as compact size, good reliability and ease of control (Figure 14).

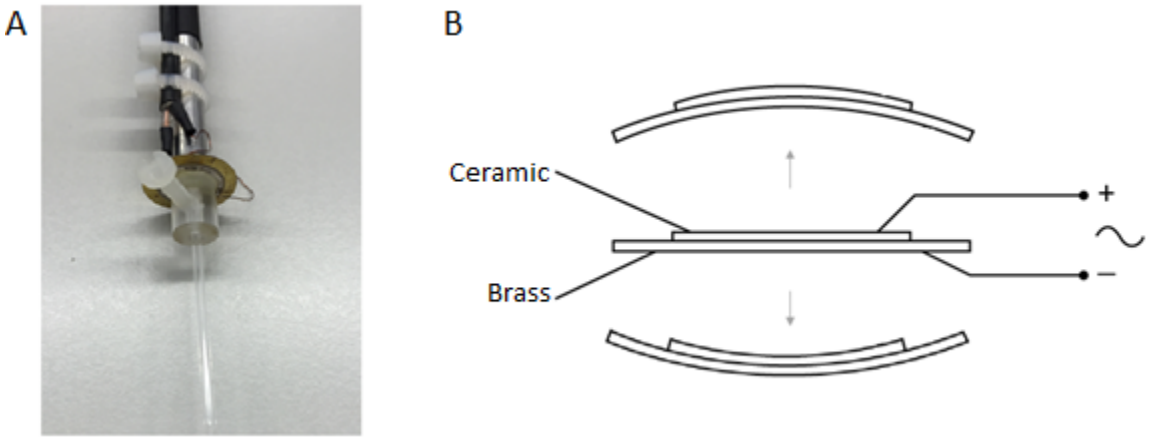

Figure 14. Structure of piezo device

(A) Experimental mechanical stimulator with a piezo buzzer element coupled to a fire-sealed glass electrode.

(B) Piezo buzzer element has a simple structure including two compartments: ceramic and brass. When an alternating voltage is applied to the ceramic element, it expands or shrinks diametrically, which generates vibration and, consequently, sound.

4.1.4 Statistical methods

Electrophysiological measurements obtained with Patchmaster were transferred to Clampfit (Axon Instruments) by using ABF Utility software. The stimulation frequencies were confirmed by fast Fourier transform (Figure 15A), and a notch filter was used subsequently to extract specific stimulation frequencies from the recordings (Figure 15B, C). Mechanically induced action currents

of the Ich5 neurons were detected by template-based search in Clampfit and plotted against the frequencies of the vibration generated by the ceramic element.

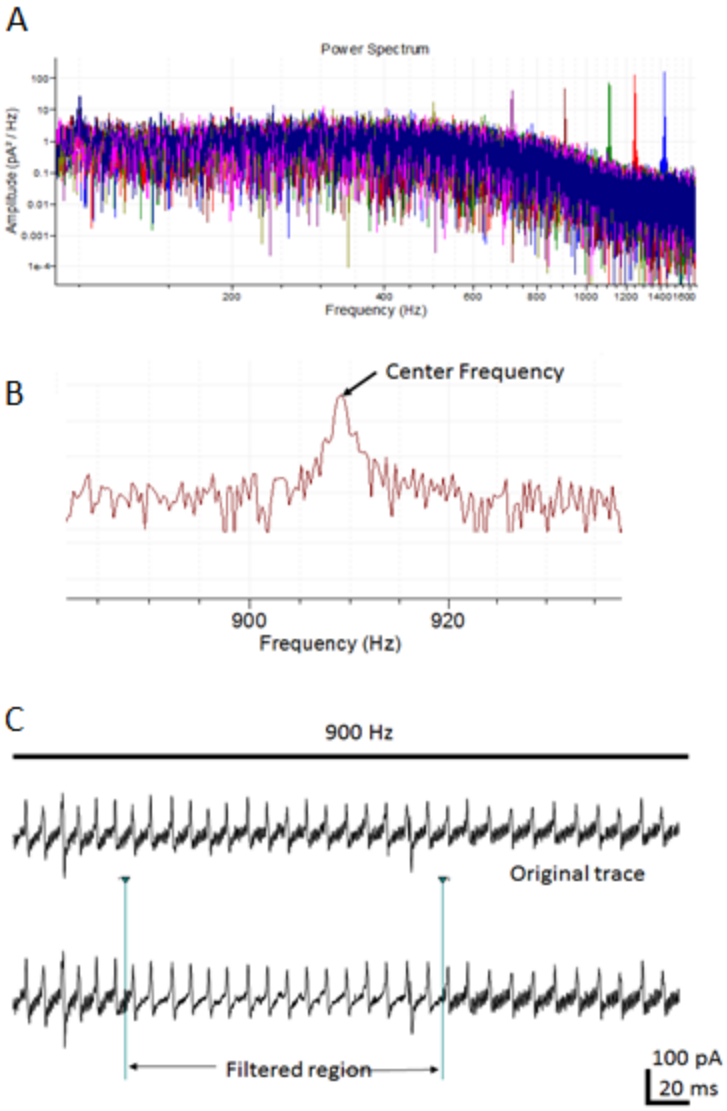

Figure 15. Confirmation of stimulation frequencies via Fast Fourier Transform

(A) The power spectrum represents detected stimulation frequencies from the piezo element (100, 300, 500, 700, 900, 1100, 1300 and 1500 Hz), and the arrow indicates the individual magnified peak in (B).

(B) A notch filter is used to reject a specific frequency of noise. The stimulation frequency (909 Hz) was measured accurately from the power spectrum and removed by the notch filter.

(C) Representative recording from Ich5 with specific stimulation frequency, which was removed by filtering.

Changes in the dimensions of a piezo element generate sound stimuli. To define the displacements of the mechanical probe (stimulation intensity), images were obtained using the stroboscopic method to demonstrate the oscillating pipette tip (Figure 16). In principle, when an oscillating object is illuminated with light of a frequency close to that of the oscillation frequency of the object and observed, the object appears to move at a frequency equal to the difference between the oscillation frequency of the object and frequency of the illumination light.

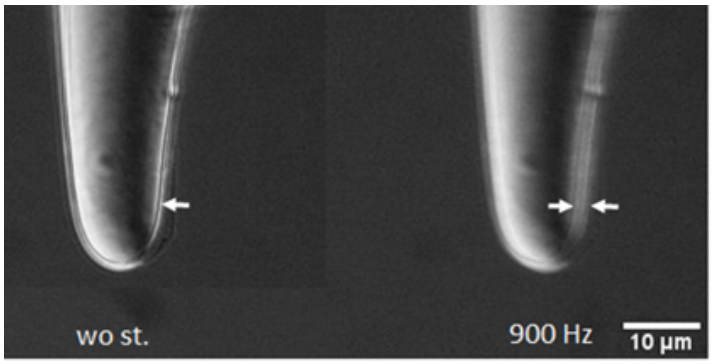

Figure 16. Visualization of vibrating stimulation electrode

A high-power LED was connected to a function generator via a transistor (MOSFET) driver circuit. The function generator was set to produce a rectangular pulse train at a frequency that was 1 Hz different from that applied to the pipette tip. When this LED light was used to visualize the tip, the tip appeared to oscillate at 1 Hz. The camera captured this and displayed it on a screen. The oscillation amplitude was measured directly in terms of pixels by using the cursors provided in the camera software.

Left: the edge line of the stimulation electrode is indicated by the arrow for the case in which a sinusoid analogue signal is not applied. *Right*: 'low motion' of the electrode is captured. The edge (or the area between the arrows) becomes blurred due to vibration, indicating approximate displacement of the oscillating pipette tip.

Although the piezo buzzer delivers amplitude displacements depending on increases in frequency (Figure 17), the device vibrated readily because its resonance frequency (f_r) was 6 ± 0.5 kHz >> 1.5 kHz (the largest stimulus frequency), suggesting that the decreased response of the chordotonal neurons at high frequencies reflects a decrease in the response of the nerve rather than a change in the stimulus. The power spectrum showed slightly increased amplitudes in proportion to stimulus frequencies, which is consistent with the impedance–frequency pattern of piezo materials (Figure 17).

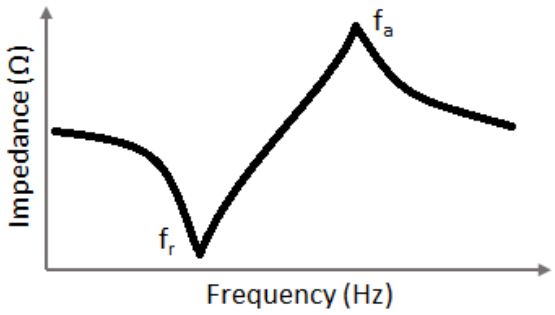

Figure 17. Response pattern of piezo ceramic material

The figure shows that a ceramic element's oscillations first approach resonance frequency (f_r, the minimum impedance frequency), where the element vibrates most readily and converts electrical energy into mechanical energy most efficiently. With any increase in the frequency, impedance increases to the anti-

resonance frequency (f_a, the maximum impedance frequency). Sourced from www.americanpiezo.com and modified.

4.2 Mechanosensitive characterization of lch5

Studies have suggested that aGPCRs govern cellular functions mechanically (Petersen et al., 2015; White et al., 2014), but mechanical perception through aGPCR activity impinging on cell responses has not been established yet. The research interest stems from the findings of a specific larval behavioural defect, which link dCIRL malfunction to the triggering of electrophysiological screens of chos of *Drosophila in vivo*. To examine how dCIRL is involved in sensory input, a tissue sample to record neuronal response to mechanical stimulation directly is required.

In order to test the tissue sample, I characterized two physiological properties of lch5 neurons. First, I assessed how long chos could be stimulated by vibration. To investigate this, I applied a 900 Hz stimulation train to the neurons for 4 min. A histogram plotted to determine the mean value of spikes in a time window of 10 s shows the response dynamics to the applied mechanical stimulus (Figure 18A). A statistical comparison between the evoked response frequency (f_e) and the spontaneous (background) spiking frequency (f_b) showed that lch5 neurons present highly significant mechanical responses only in the first 2 s (Figure 18B, Table 1).

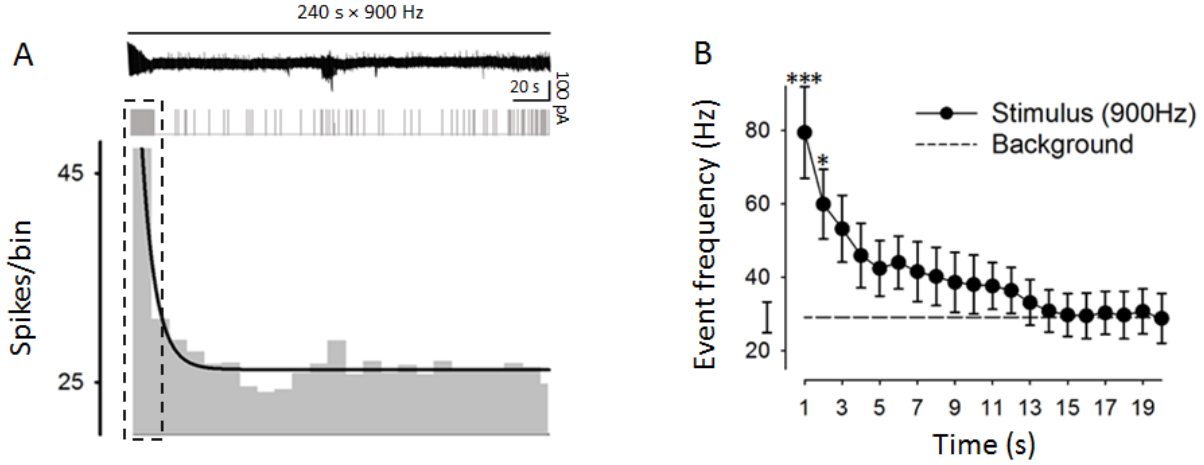

Figure 18. Time course of response during continuous mechanical stimulation

(A) Response dynamics of lch5 under 900 Hz stimulation for 4 min. Top: original trace; middle: raster plot; bottom: histogram plotted for mean values of spikes in a 10 s bin. The dashed rectangle is analysed further in (B).

(B) Statistical analysis of mechanically evoked event frequencies in the first 20 s indicating a highly significant difference between mechanically evoked and spontaneous event frequencies within 2 s.

Another property of interest is the break between two applications of stimulus within 1 s. To address this question, a series of pair-stimulations (1 s) with decreasing pause time from 10 to 0.25 s was applied to lch5 neurons (Figure 19A). In a statistical comparison between responses to the first ($f_{e1.sti}$) and the second ($f_{e2.sti}$) stimuli, we found no significant difference in terms of the number of generated spikes (Figure 19B, Table 2). These results suggest that the break of 1 s used in the stimulation protocol guarantees stable and reproducible results.

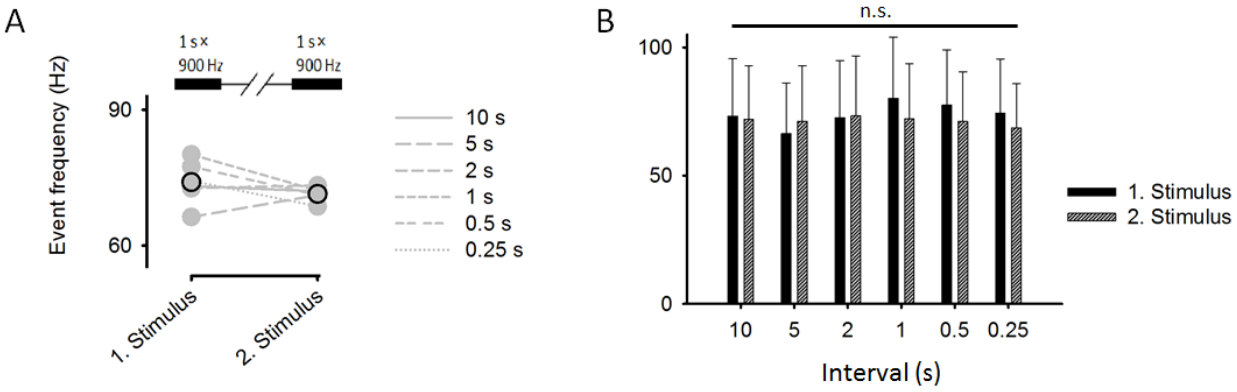

Figure 19. Recovery time between successive bouts of stimulation

(**A**) Top, pair-stimulation for a single cell with various break durations (10, 5, 2, 1, 0.5 and 0.25 s). Bottom, Quantification of response spikes for first and second stimulus.

(**B**) Statistical comparison of first and second response spikes indicates that the physiological recovery time of lch5 could be shorter than 0.25 s.

4.3 dCIRL modulation of absolute and relative electrical activity of chordotonal neurons in response to mechanical stimuli

Many diverse GPCRs pertaining to vision, olfaction and taste have been identified in terms of their transduction mechanisms. However, our ability to feel, touch and hear sounds based on response to mechanical stimulation is poorly understood owing to difficulties in studying the molecular mechanisms underlying mechanosensation.

Based on the obtained basal functional properties, I continued to study the function of dCIRL *in vivo*. Figure 20A shows the recordings of lch5 neurons from control and $dCirl^{KO}$ mutants. Without mechanical stimulation, lch5 neurons were active spontaneously. Any spontaneous neuronal

activity that occurs independently of sensory input is suggested to play a critical role in the development of a sensory system (Blankenship and Feller, 2010; Spitzer, 2006). In this work, vibration triggered an increase in action current frequencies, which is consistent with the findings in the literature (Zhang et al., 2013). The cells responded and adapted slowly, displaying phasic and tonic response components (Johansson and Vallbo, 1983). Both components were reduced significantly in *dCirl*^{KO} mutants (Figure 20B). When applying broad frequencies from 100–1500 Hz (Figure 9), the neuronal response activity peaked at stimulation frequencies of around 900 Hz. Most intriguingly, the mutant animals displayed significantly lower absolute action current frequencies across the entire stimulation spectrum (Figure20C, Table 3A), which was fully compensated for by the *dCirl*^{Rescue} allele (Figure 21A, Table 3B).

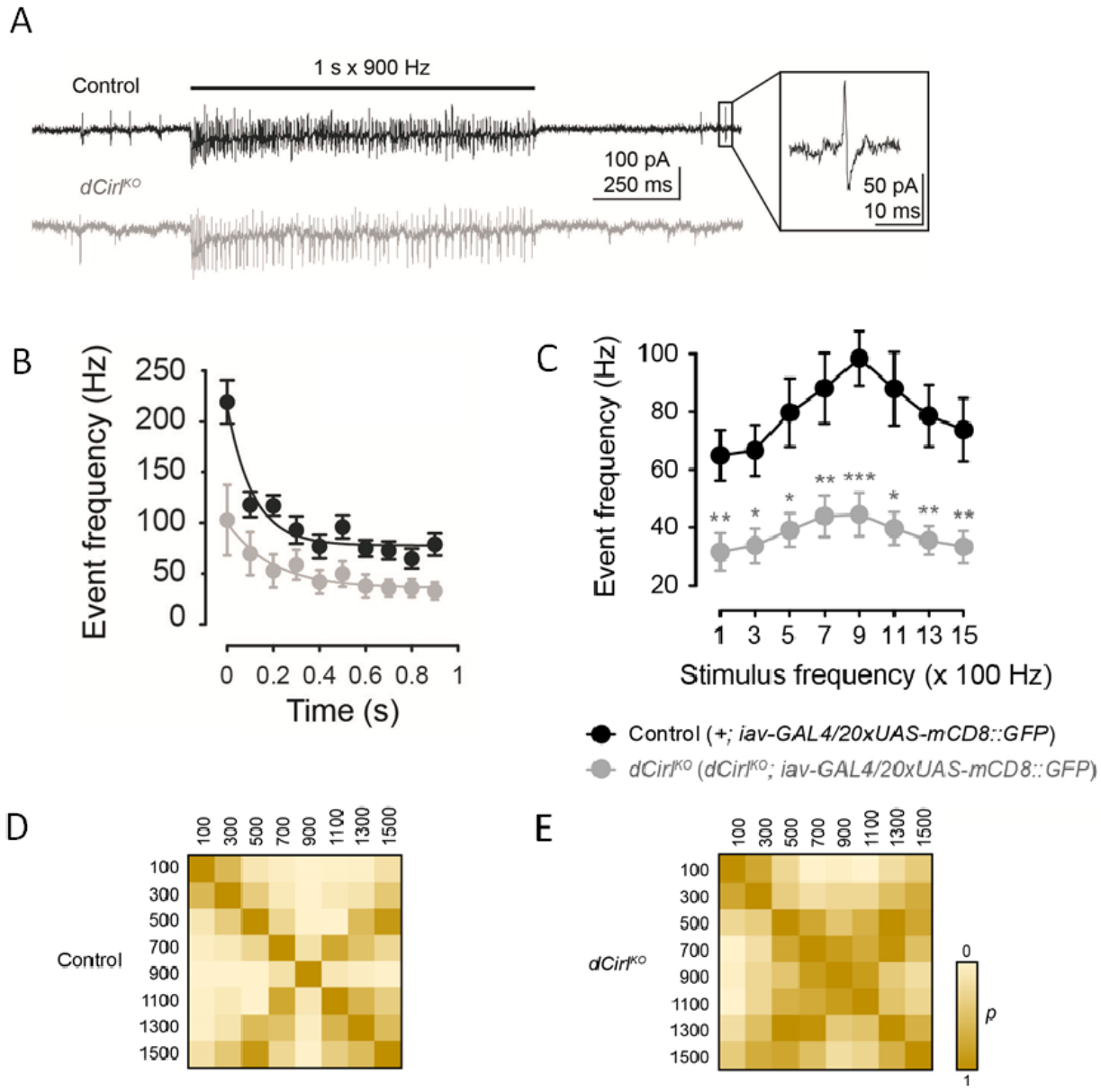

Figure 20. Essential role of dCIRL in physiological response to mechanical stimulation in lch5.

(**A**) Representative recordings from lch5 axons in control and *dCirl*^{KO} mutants. The boxed region shows a spontaneous event.

(**B**) Action current frequencies evoked by 900 Hz vibration (0.1 s sampling window) display an initial peak followed by a tonic response. Both components are reduced significantly in *dCirl*^{KO} mutants.

(C) Quantification of action current frequencies evoked by mechanical stimulation.

(**D** and **E**) Statistical comparisons of *Rd* values (colour-coded). Adjacent vibration stimuli elicit significantly different relative spiking responses in control lch5 (**D**), whereas dCIRL removal blurs mechanosignal discrimination.

The discrimination ratio R_d (ratio between evoked and spontaneous spiking activity) in control lch5 neurons peaked at around 900 Hz, suggesting that signal perception and/or encoding is most effective in this mechanostimulation range. In contrast, *dCirl*^{KO} lch5 neurons showed largely reduced R_d values for several vibration frequencies (Figure 21C; Table 3C). To depict how R_d values are distributed across the entire stimulation frequency spectrum, I statistically compared the R_d values for all pairs of stimulation frequencies and derived a discrimination matrix for each genotype, showing a general loss of mechanosignal discrimination in the absence of dCIRL (Figure20D, E and 21D, E, F). This demonstrates that besides modulating the absolute spiking activity of chordotonal neurons, dCIRL is necessary for their relative response to mechanical stimuli.

To test whether both absolute and relative spiking responses in lch5 rely on the function of dCIRL alone, dCIRL was cell-specifically re-expressed in mutant chordotonal neurons through the *iav-GAL4* driver. I found that the relative mechanosensory response was re-established partially (Figure21C, F), but the absolute firing frequencies were not recovered (Figure 21B).

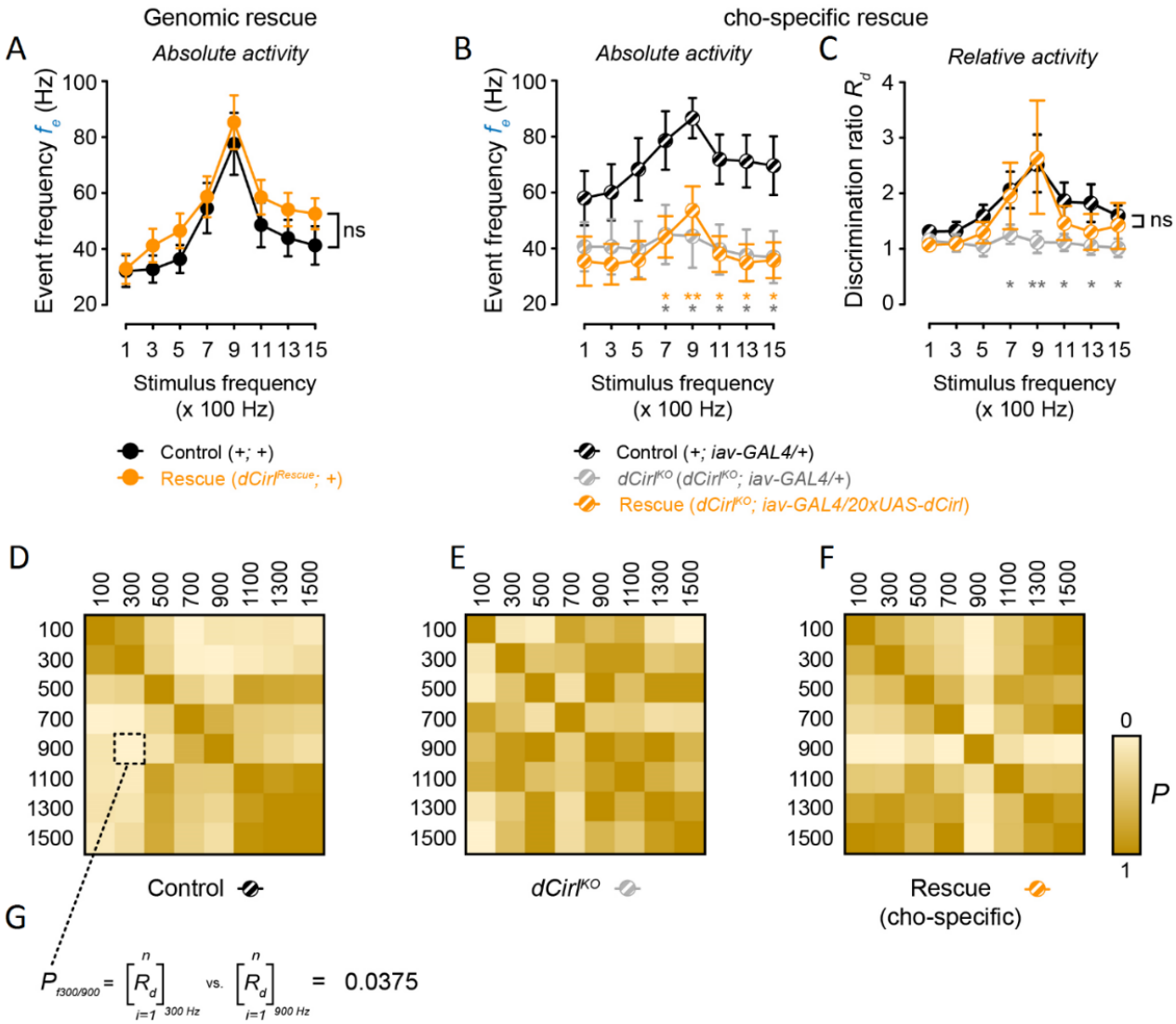

Figure 21. Essential role of dCIRL in eliciting relative response of larval chordotonal neurons to mechanical stimulation.

(**A**) Action current frequencies evoked by mechanical stimulation are completely restored in *dCirl*^{Rescue} larvae.

(**B**, **C**) Restricted re-expression of dCIRL in chordotonal neurons of *dCirl*^{KO} larvae does not rescue absolute action current frequency (**B**) but the relative spiking activity of lch5 (**C**), as evident from the discrimination ratio (R_d) plots.

(**D**-**F**) Discrimination matrices with plots of pairwise comparison of R_d values obtained for each stimulation frequency couple show that loss of discriminatory power due to dCIRL removal (**D**, **E**) is restored partially by chordotonal neuron-specific re-expression of dCIRL (**F**).

(**G**) Exemplified calculation used to compare each R_d pair for construction of discrimination matrix.

4.4 Characterization of molecular processes of dCIRL in mechanosensation

The experiments conducted herein provide direct functional evidence for the role of dCIRL in chordotonal dendrites, the site of mechanotransduction and receptor potential generation, or somata, where action potentials are likely initiated (Kernan, 2007). However, these results are consistent with two possible models: **1)** dCIRL is critical for mechanotransduction (receptor potential generation), or **2)** dCIRL is critical for signal transformation (action potential initiation and propagation; Figure 22).

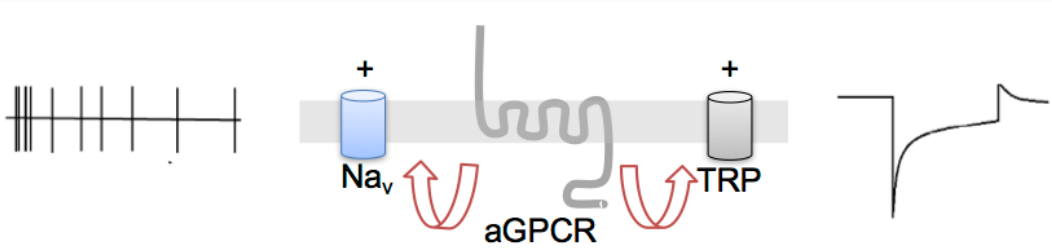

Figure 22. Hypothesis of two possible signalling pathway models of dCIRL

The metabotropic mechanoreceptor dCIRL could interact with TRP channels to modulate generation of receptor potential and/or interact with, e.g. sodium channels to regulate membrane excitability.

4.4.1 dCIRL does not impair spike propagation

Channelrhodopsin-2 (ChR2) is a powerful optogenetic tool, which has been identified as a directly light-activated cation-selective ion channel from the green algae *Chlamydomonasreinhardtii* (Nagel et al., 2003), and it was implemented successfully in living *Drosophila* larvae (Schroll et al., 2006). Kwon and colleagues (Kwon et al., 2010) showed that ChR2-based stimulation of the chos can lead to thermotaxis of larvae. Furthermore, optogenetic activation of chos has been reported in startle behavioural assay (Ohyama et al., 2013).

To test the first hypothesis that dCIRL is important for regulating membrane excitability, a novel ChR2 variant ChR2-XXM was employed. In collaboration with Georg Nagel (University of Würzburg), we had already developed ChR2-XXL (XXL stands for extra-high expression, extra-long open state time), a very efficient tool to activate neuronal cells *in vivo*. This was used successfully to elicit specific behaviours and to write memories through light (Dawydow et al., 2014). The recent improved XXM has advantages, for example, high photostimulation efficiency and faster

off-kinetics than those of ChR2-XXL. ChR2–XXM was expressed cell-specifically in chordotonal neurons through the *iav-GAL4* driver, so that the neurons could be activated artificially by blue light instead of mechanical stimulus. The representative recordings (Figure 23A) show that chordotonal neurons started firing upon the incidence of light. During a stimulation protocol with increasing light intensity (Figure 23B, top), we found no significant difference in light-evoked event frequencies between control and *dCirl*^{KO} background, meaning that dCIRL removal does not change membrane excitability, which is consistent with the specific role of dCIRL in modulating mechanically evoked receptor currents (Figure 24, bottom; Table 5).

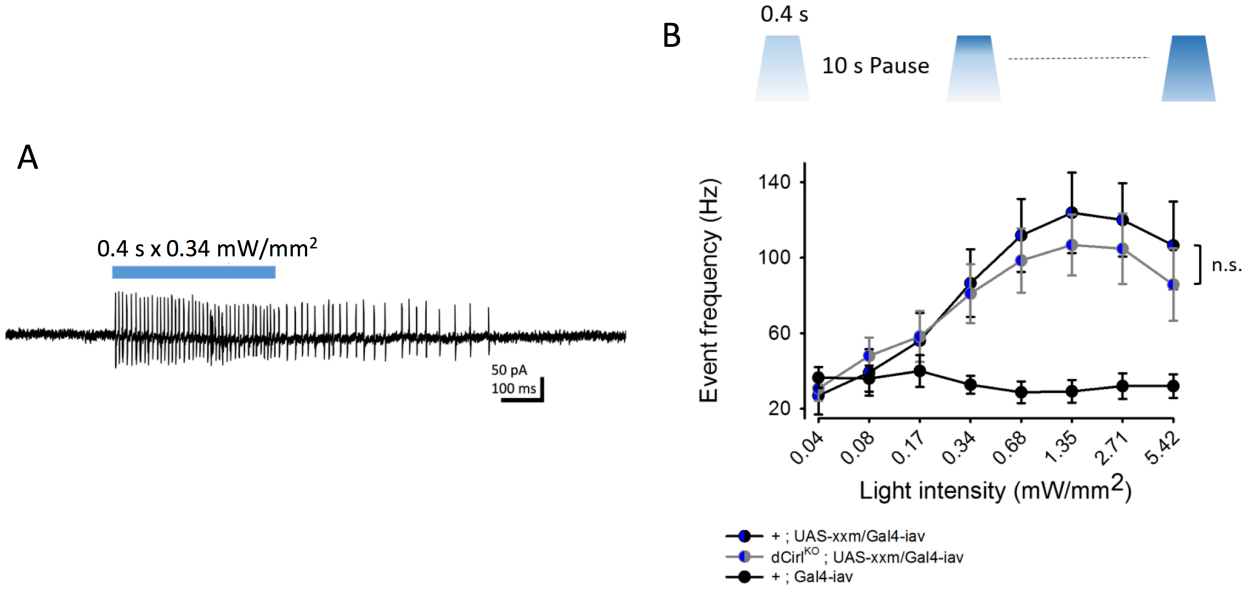

Figure 23. dCIRL does not impair spike propagation.

(A) Representative recording from lch5 expressing ChR2-XXM (a novel ChR2 variant) following activity induction *in vivo*.

(B) *Top*: scheme of light-stimulation protocol with increasing light intensity. *Bottom*: quantification of action current frequencies evoked by blue light (460 nm) indicates dCIRL removal does not change spike initiation. Wild-type animals lacking ChR2-XXM served as a control for unspecific light-induced effects.

4.4.2 dCIRL promotes receptor potential generation

Tetrodotoxin (TTX) can abolish the firing of nervous cells by binding to and blocking voltage-gated sodium channels in membranes (Lee and Ruben, 2008; Lewis and Raman, 2014). Therefore, action current responses in lch5 were suppressed, and only isolated receptor currents could be assessed.

To resolve whether dCIRL could modulate receptor potential, 4 µM TTX was used to inhibit the firing of neurons (Schmid et al., 2008) to record directly the receptor current of chordotonal neurons induced by mechanical stimulation. Consistent with the action current frequency recording (Figure20A, B), the cells started responding with the rising phase of receptor current upon mechanical stimulation and then adapted to display a tonic response component (Figure24A). Both components were reduced significantly in *dCirl*^{KO} mutants across all stimulation frequencies (100–1500 Hz) (Figure 24B; Table 5), supporting the notion that dCIRL may interact with mechanotransducers such as TRP channels to promote receptor currents.

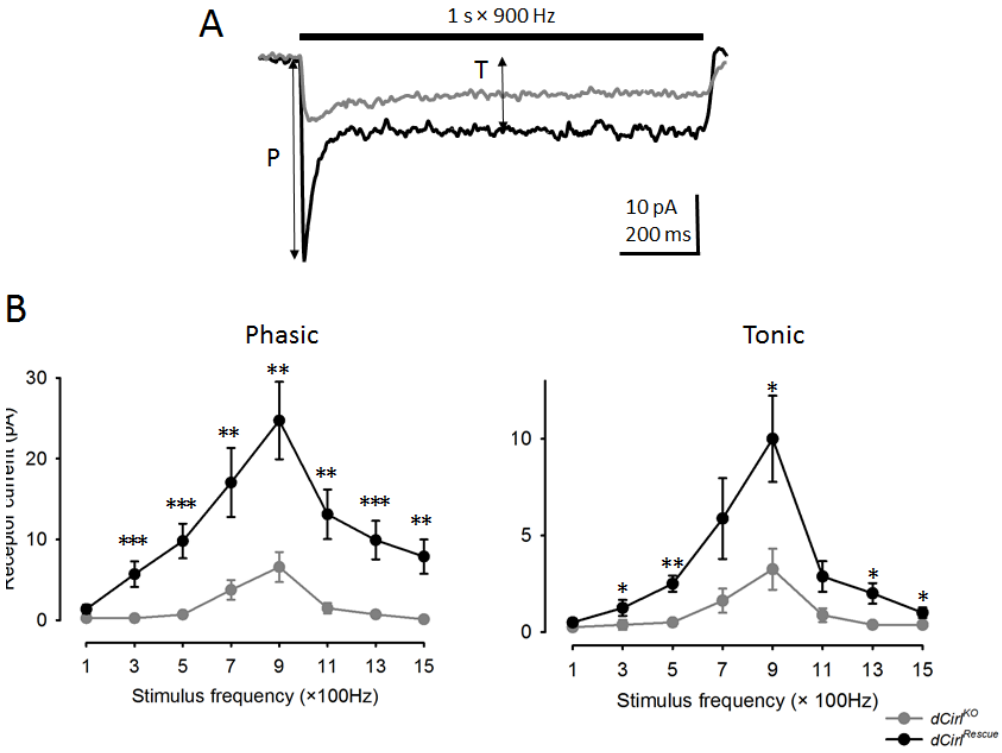

Figure 24. dCIRL promotes receptor current

(A) Representative receptor current recordings from lch5 of control and *dCirl*^{KO} mutants after bath application of TTX. P indicates the amplitude of the phasic component, whereas T denotes the amplitude of the tonic component.

(B) Quantification of current amplitudes of both components evoked by mechanical stimulation.

4.5 Role of cAMP in mechanosensation of lch5

We have shown that dCIRL can read out the mechanical sensitivity of chos. Nevertheless, the mechanism by which it transduces the signals into intracellular messages remains unclear. Optogenetic tools allow us to modulate the cellular cAMP in organisms through photoactivated adenylate cyclases (PAC) in order to demonstrate the signalling cascades of dCIRL (Schroder-Lang et al., 2007). In *Drosophila*, bPAC (identified in the genome of the bacterium *Beggiatoa*) mediates a light-dependent increase in cAMP, for example, in the central nervous system (Stierl et al., 2011) and in the *Drosophila* renal (Malpighian) tubules (Efetova et al., 2013) under the control of cell-type-specific promoters.

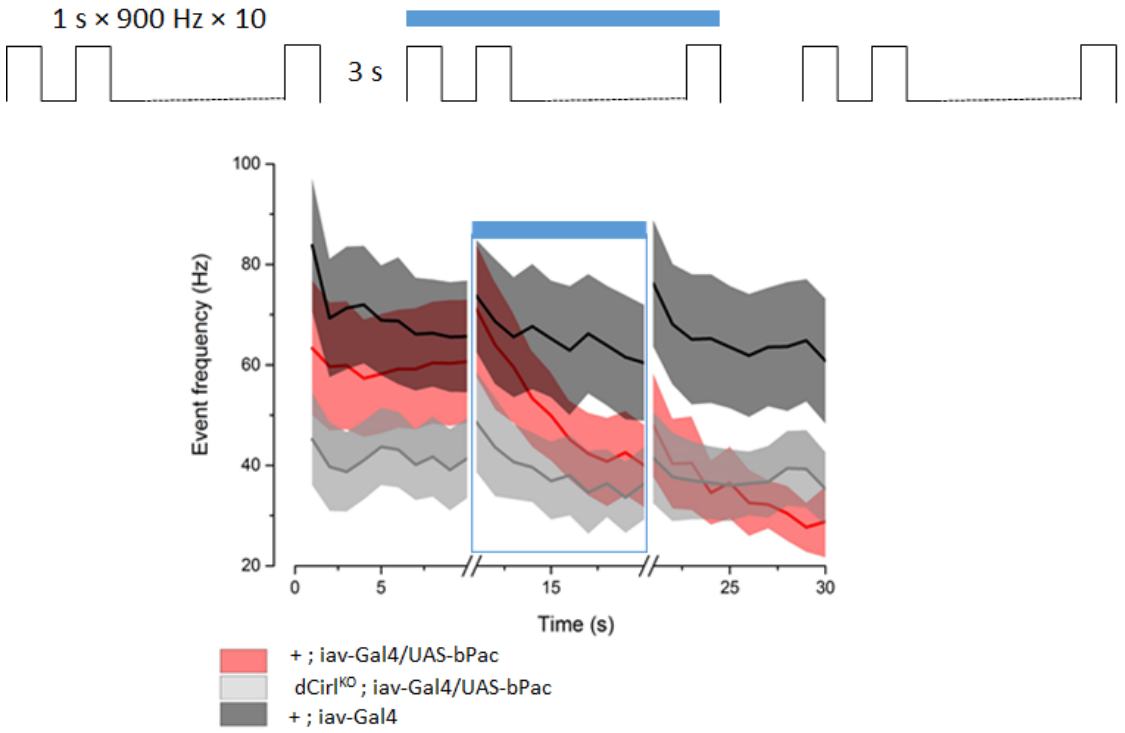

Figure 25. Effect of light-induced cAMP on mechanosensation.

Top: Protocol of combined mechano-light stimulation. *Bottom*: action current frequencies evoked by mechanical stimulation of lch5 expressing bPAC. Sound responses of bPAC-expressed controls (red) and *dCirl*^{KO} (gray) reach the same level during and after light stimulation, and error bar area was filled with colours.

To elucidate the role of cAMP in mechanosensation, bPAC was expressed cell-specifically in chordotonal neurons through the *iav-GAL4* driver, so that the intracellular cAMP could be elevated by using blue light. The cells were stimulated by sound (900 Hz) for the first 20 s, where ten 1-s cycles of stimulation preceded by 1 s of rest were applied. Then, the blue light (wavelength, 460 nm; light intensity, 7–9 mW/mm^2) was switched on, and the second series of mechanical stimuli were applied. Finally, for the last 20 s, only vibration was applied (Figure 25, top). As expected, the mechanically evoked event frequencies of WT control (not expressing bPAC) were unaffected by light. Intriguingly, the drop in evoked action current frequencies was not rescued by light-induced cAMP. In contrast, response frequency of the bPAC-expressed controls reduced dramatically to the mutant level during and after the onset of light incidence (Figure 25, bottom), indicating that cAMP elevation impinges on the receptor potential and, consequently, on the firing frequency of lch5. The $dCirl^{KO}$ animals were unaffected by light-induced cAMP, suggesting that dCIRL plays a role in decreasing the cAMP level of cells.

To support this finding, 100 µM SQ 22536 (Merck, in DMSO), an inhibitor of adenylyl cyclise, was use to decrease cAMP. After pharmacological treatment (10 min incubation in recording solution), the mechanical responsiveness of $dCirl^{KO}$ mutants was restored to the control level through SQ 22536-induced cAMP decrease (Figure 26A, B). After one wash with fresh recording solution, the evoked event frequencies of both genotypes remained comparable (Figure 26C), indicating that this restoration was caused only by the presence of SQ (not, e.g. DMSO).

Taken together, these findings suggest that dCIRL controls the mechanosensation of lch5 through downregulation of cAMP levels and, perhaps, through activation of the G_i-coupling pathway.

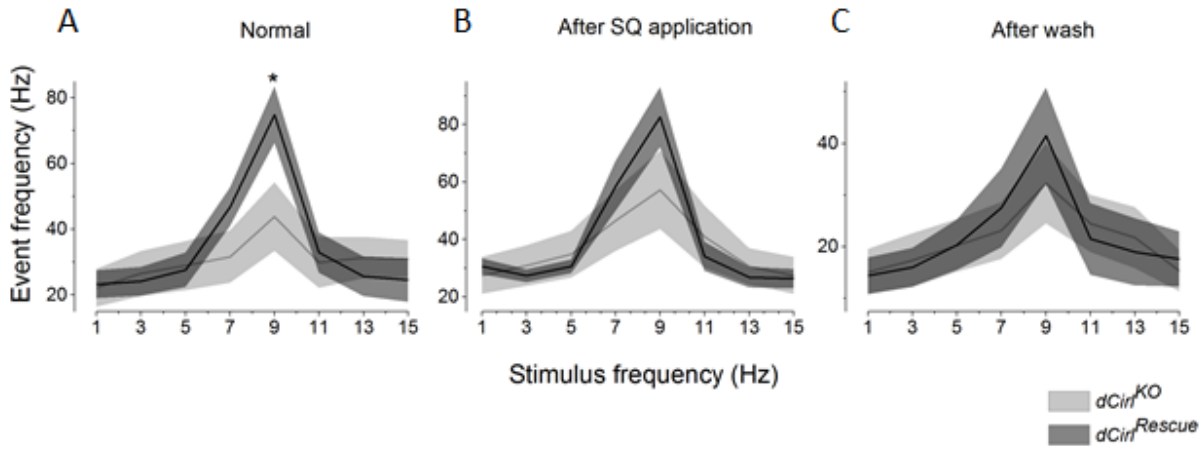

Figure 26. Inhibition of cAMP restores the evoked action current frequencies.

Treatment of dCIRL mutant with adenylyl cyclase inhibitor SQ led to decreased cAMP levels, where mechanosensivity was restored partially (A and B). After washing with fresh recording solution, the phenotypes remained comparable.

4.6 Structure-function analyses of dCIRL

As the structural properties of aGPCR (Figure 6) appear to be vital in the mechanical receptivity of chos, I measured distinct allelic versions of dCIRL to test these assumptions.

4.6.1 Effect of insertion of flag-tag in $dCIRL_{IC3}$ on mechanosensitivity of lch5

Along with the GAIN domain, another important structural feature of dCIRL is CTF. CTF consists of a residual part of the GAIN domain, 7 TM domain and ICD. The given intracellular part of the CTF is thought to mediate the signal transduction of aGPCR. A general question regarding structure-function of dCIRL concerns whether 7TM or ICD interacts with G-protein.

To test this, a *dCirl*$^{C\text{-}Flag}$ mutant was measured, in which a *3x flag*-tag sequence was fused into the third intracellular loop of the 7TM domain ($dCIRL_{IC3}$). The analysis showed that *dCirl*$^{C\text{-}Flag}$ larvae showed the same action current frequencies as those of *dCirl*^{Rescue} across the entire stimulation spectrum (Figure 27A; Table 6A). Moreover, this is an important control experiment for all constructs, which are used in the following results section. The results implied that the insertion of a flag-tag did not change the mechanical responsiveness of chordotonal neurons.

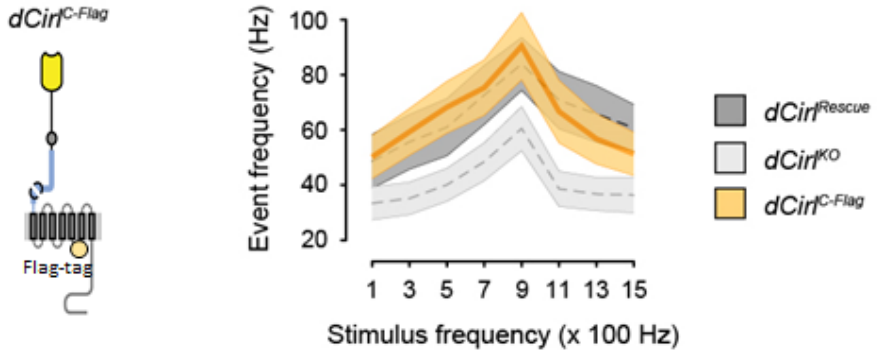

Figure 27. Functional analysis of C-flag-tag variant.

Left: construction of a *dCirl*$^{C\text{-}Flag}$; *right*: neuronal activities evoked by mechanical stimulation remain unaffected upon addition of flag-tag on the 7TM domain.

4.6.2 Mechanosensation of proteolysis-deficient mutants

A unique feature of the aGPCR class is the presence of a highly conserved cysteine-rich GPCR autoproteolysis site (GPS) comprising approximately 50 amino acids and located within the GPCR autoproteolysis-inducing (GAIN) domain (Lin et al., 2010; Stacey et al., 2000). The GPS self cleaves aGPCRs into a non-covalently attached NTF–CTF complex (Arac et al., 2012; Krasnoperov et al., 2009; Langenhan et al., 2013; Liebscher et al., 2013; Lin et al., 2004).

A recent study indicated that a short peptide sequence (termed *Stachel*) within the ectodomain of two aGPCRs (GPR126 and GPR133) functions as a tethered agonist. The cleavage event occurs to expose the *Stachel* to the seven transmembrane helix domain, which triggers activation of the receptors (Liebscher et al., 2014). This observation led to the assumption that the auto-cleavage capability of GPS plays a critical role in the receptors' signalling transduction. To validate the hypothesis, two proteolysis-deficient mutants (*dCirl*^{H724A} and *dCirl*^{T726A}), the amino acid of which was substituted at the auto-cleavage position (Figure 28A), were measured in the laboratory by using the mechanical stimulation setup. We found that the mechanosensory response profile of *dCirl*^{H724A} displayed a nearly wild-type pattern across the entire range of stimulation frequencies. In contrast, recordings from *dCirl*^{T726A} mutants (changing the first residue of the *Stachel* sequence, Figure 28A) were indistinguishable from those of null *dCirl*^{KO} mutants (Figure 28C; Table 7).

To further confirm these findings, I visualised the isolated receptor currents in the presence of TTX. I found that the trace components of both phasic and tonic currents are reduced significantly

in *dCirl*^{KO} and *dCirl*^{T726A} mutants. Intriguingly, the receptor current profile of *dCirl*^{H724A} mutants was at the same level as that of *dCirl*^{Rescue} (Figure 28B, D; Table 8). These results demonstrate that auto-cleavage is not required, but an intact *Stachel* is important to activate the receptors.

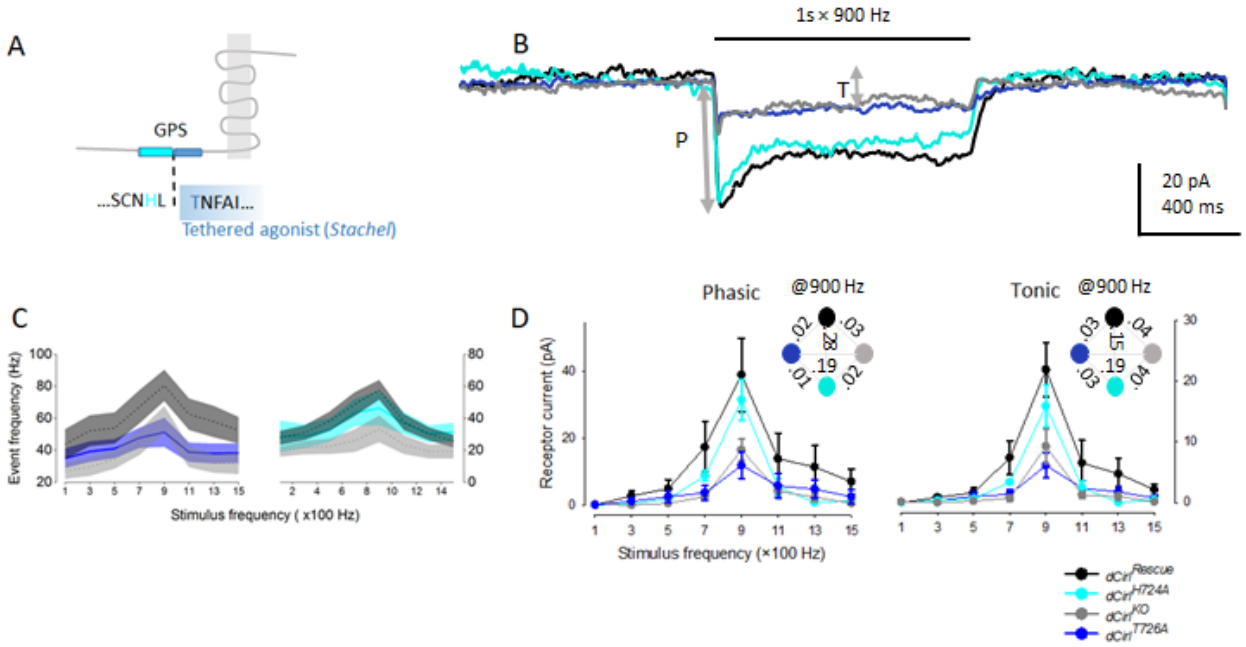

Figure 28. Functional analysis of proteolysis-deficient mutants

(A) Constructs of a *dCirl*^{H724A} and *dCirl*^{T726A}, where Histidine (H) and Threonine (T) were replaced by Alanine (A).

(B) Representative traces of receptor currents upon mechanical stimulation at 900 Hz.

(C) Quantification of action current frequencies evoked by mechanical stimulation.

(D) Quantification of phasic and tonic phases of receptor currents.

4.6.3 Length of dCIRL ECD regulates mechanosensation of Ich5

aGPCR receptors are characterized by their extracellular tails, which contain several adhesive motifs that attach ligands to mediate functions (Langenhan et al., 2013). I sought to test the hypothesis that ECD length plays a crucial role in tuning the mechanical perception of the receptor. Consider that distance-dependent relative ECD motion under mechanical stimuli will eventually reflect the subsequent modulation of metabotropic receptor activity. To interrogate this assumption, I first tested a model by relaxing distance and, consequently, tension on dCIRL ECD by inserting a red fluorescence protein (RFP) chromophore domain (~ 3 nm) between the N-

terminal adhesion folds and the GAIN domain. I found a tendency towards a reduced peak at 900 Hz but not across the entire stimulation range (Figure 29, Table 6B).

To further test the relationship between the increase in ECD length relative to tensile relaxation and receptor function, a spacer module spanning a larger distance was used. Each module included a doublet of two immunoglobulin (Ig) domains derived from the human CD4 receptor. This protein family appears to be inert and is therefore frequently expressed heterologously in *Drosophila* (Zito et al., 1999). Each distance spacer module contained a single HA (human influenza hemagglutinin) and adds ~6 nm to dCIRL ECD length (Figure 29, top, fly strains).

According to the recordings and quantitative analyses of the firing frequency of lch5 towards mechanical challenges, we found a gradual decline in mechanical response with increasing spacer number (Figure 29, bottom; Table 9). Taken together, the results indicate that the length-dependent tension of the ECD portion is required for the mechanical loading and signalling capacity of dCIRL.

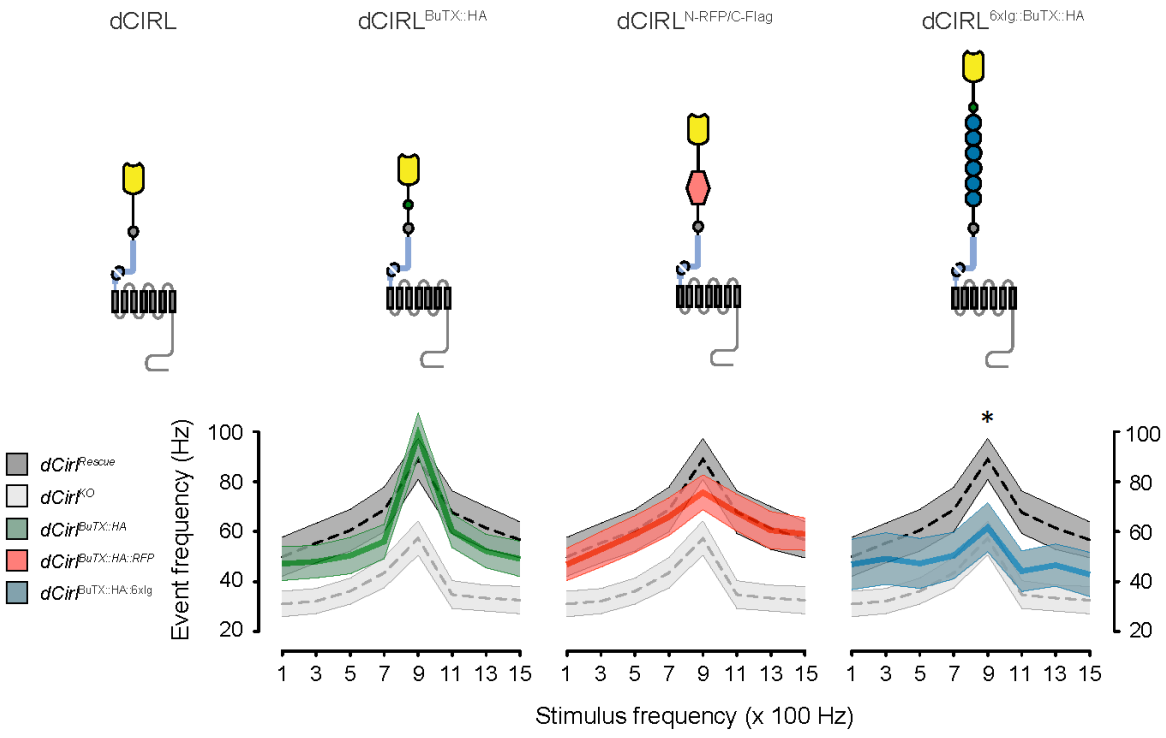

Figure 29. Effect of ECD length on mechanical loading of dCIRL.

Top: schematic of modifiable construction of dCIRL. *Bottom*: the mechanical responses are impacted by increasing ECD length.

4.7 Thermoresponses of lch5

Small animals such as fruit flies switch to a very different thermoregulation realm within seconds of fluctuation in environmental temperature or upon exposure to sunlight (Garrity et al., 2010). *Drosophila* larvae are able to detect cool temperatures (14–16°C) by activation of chos (Kwon et al., 2010), suggesting that in addition to acting as mechanosensory receptors, larval chordotonal neurons may function as thermoreceptors.

To systematically address the requirements of dCIRL in chos for sensing different temperatures, I examined the neuronal activity frequencies by increasing the temperature of the recording solution gradually (15, 20, 25, 30°C). The scheme shows that mechanical stimulus (900 Hz) and thermal stimulus occur simultaneously (Figure 30A). Quantitative analyses show that both mechanically evoked event frequencies increase in proportion to temperature and saturate at around 25°C (Figure 30B; Table 10), suggesting that the neuronal activities can be affected by temperature differences. The *dCirl*^{KO} mutants retained significantly lower evoked frequencies at around 20°C, indicating that dCIRL specifically affects the mechanosensory responses of chos. Similar spontaneous responses showed that thermosensation is independent of dCIRL.

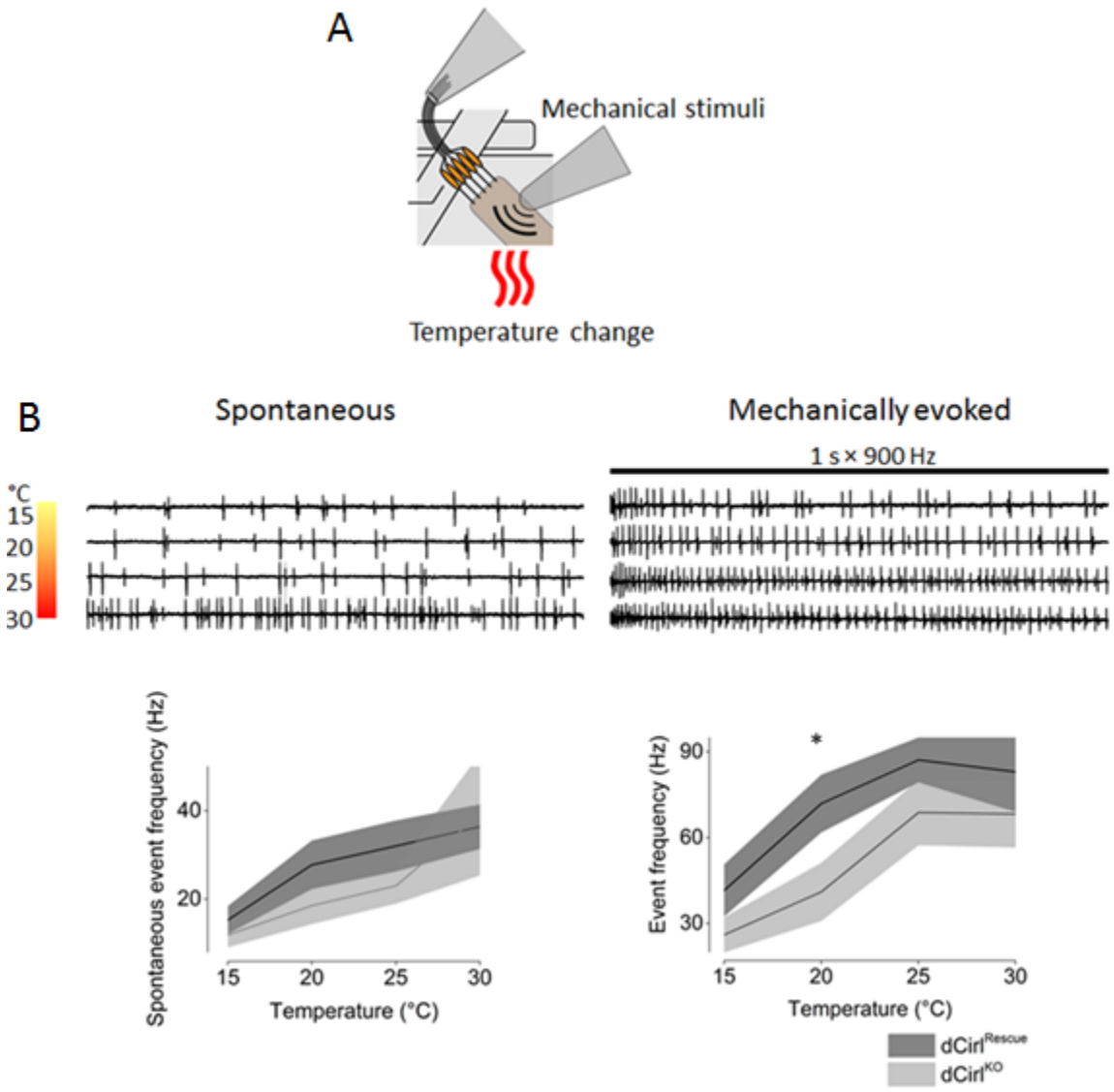

Figure 30. Mechano-thermosensation of lch5

(**A**) Schematic representation of multimodal setup. A stimulation electrode is used to apply a series of sound frequencies to lch5 under different temperatures, while a suction electrode records neuronal activities from axon bundle.

(**B**) *Top*: representative recording from lch5 as temperature of recording solution was increased gradually (15, 20, 25 and 30°C). *Bottom*: quantification of spontaneous and mechanically evoked action current frequencies of control and *dCirl*^{KO} mutants.

4.8 Effect of dCIRL removal on larval motor neuronal excitability

The introduction of whole-cell patch clamp recording (Neher, 1981) has facilitated researchers to determine the firing properties of neurons, for instance, frequency, amplitude and duration of action potentials, which are crucial for understanding coordinated nervous system functions and the development of neuronal signalling (Baines and Pym, 2006; Choi et al., 2004).

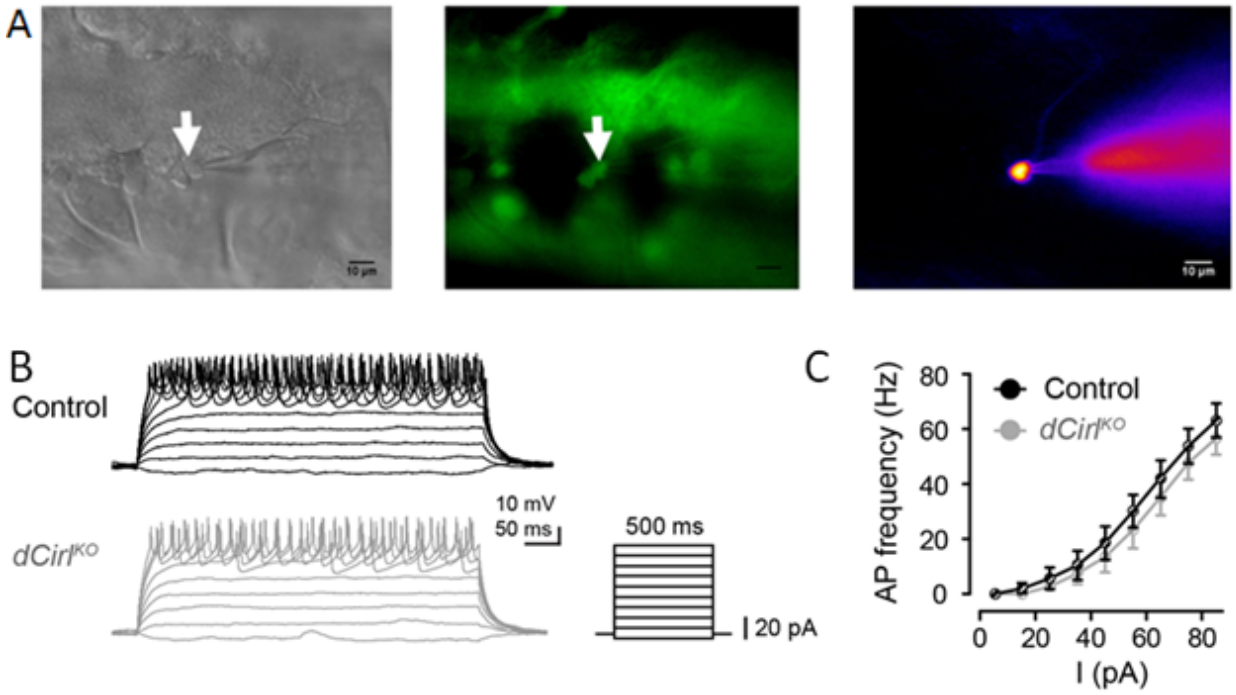

Figure 31. Removal of dCIRL does not change larval motor neuron excitability

(**A**) After establishment of the whole-cell patch clamp configuration, the target cell body (arrow) and its dendrite are loaded with µRuby fluorescent dye (1%, v/v) via a somatic recording pipette. To visualize the somata of motoneurons (middle), a GFP construct (UAS-mcD8::GFP) was expressed under the control of a motoneuron driver line (Ok6-Gal4); *Left*: brightfield; *middle*: GFP fluorescence; *right*: diffusion of µRuby fluorescent dye.

(**B**) Representative voltage traces of control and *dCirl*^{KO}-type Ib motor neurons. APs were triggered by injected current pulses across a range of -4 to +86 pA (in steps of 10 pA).

(**C**) Quantification of AP frequencies evoked by current injection showed that motor neuron excitability is not affected in *dCirl*^{KO} larvae.

Type I motor neurons are directly required for full motor response, and the functional consequences of dCIRL removal from these neurons might account for the locomotion deficits observed in *dCirl*^{KO} larvae. In two-electrode voltage clamp (TEVC) recordings, no change in synaptic transmission was observed at the NMJ in *dCirl*^{KO} larvae (data not shown). However, dCIRL

function may affect the excitability of motor neurons in the VNC. To assess this possibility, I conducted whole-cell patch clamp recordings of type-Ib motor neurons in wild-type and *dCirl*^{KO} backgrounds (Figure 31A). I found that action potential firing in *dCirl*^{KO} did not differ from that in the control samples across the entire spectrum of current pulses, indicating comparable membrane excitability (Figure 31B, C; Table 11).

5 Discussion

The focus of my doctoral research concerned unraveling the function of dCIRL, a member of a class of poorly characterized aGPCR homologs with elusive pharmacological and biological properties. To address these questions, I developed new technologies for *Drosophila* research including improved preparation strategies, electrophysiological techniques, and optogenetic assays. Through this work, I was able to show that dCIRL resides in mechanosensitive lch5, where they set the threshold for mechanical stimulus detection. Also, further evidence links basal functional lch5 properties to the downstream pathway and subcellular action of dCIRL upon mechanical challenge, which is critical step for grasping how aGPCR exerts physiological processes.

5.1 *Drosophila* model in mechanosensation

Physiological properties and profiles of endogenous mechanosensitive currents of sensory neurons, i.e. the mechanotransducer current from sensory nerve ending and the AP firing activity from nerve fibers, are crucial to understanding the mechanisms of mechanically activated receptors. In order to identify the molecules that regulate electrical activities of sensory neuron membrane and to detect environmental stimuli, numerous cell-based *in vitro* electrophysiological assays were achieved. Different techniques, such as fluid shear stress, membrane stretch and membrane indentation, have previously been used to apply mechanical forces in specific sensory somata (Bhattacharya et al., 2008; Maingret et al., 2000; McCarter et al., 1999; Olesen et al., 1988; Sukharev and Sachs, 2012) or intact tissue preparations (Reeh, 1986). Nevertheless, there is a limitation to the *in vitro* approaches as sensory neurons in culture may not retain all their native properties.

The the methods are already well established for recording sensory receptor potentials/currents (transepithelial potential) from the sensilla, e.g. sensory hairs in blowflies, for *in vivo* organisms (Wolbarsht and Dethier, 1958). The development of assays in the *Drosophila* model has played an important role in the identification and characterization of the elusive mechanotransducer modules. Albert et al. (2006) established a mechanics-based method in the ear using a laser beam in order to determine the mechanical properties (sound-induced displacement and the particle velocity) of the antennal arista-tip (Figure 32). This allows for a quantitative analysis of the specific roles of identified proteins in JO. Using this technique, the active mechanical processes in the fly

ear have been shown to be remarkably similar to those of the vertebrate hair cells (Nadrowski et al., 2008) and many genes have been identified that are involved in the hearing in the adult flies (Senthilan et al., 2012).

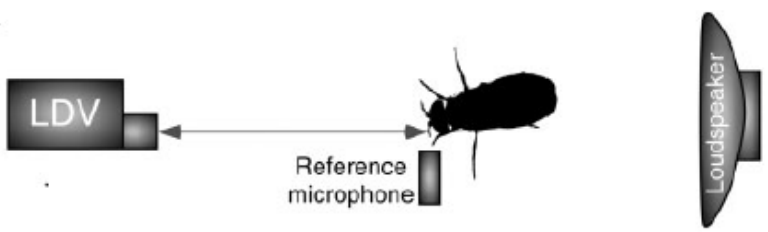

Figure 32. Experimental setup for analyzing vibrations of the sound receiver of flies

A laser-Doppler vibrometer (LDV) setup was used to measure the vibration of the antennal sound receiver (arista-tip), which is actively modulated by the motility of auditory neurons. From Lu et al. (2009)

The location of Johnston`s neurons (in the antennal ear) limits the application of electrophysiological recordings from a single neuron. However, the larval chordotonal neurons are accessible to recording, so that more precise neuronal physiological activities towards mechanical stimuli can be defined. Furthermore, live-imaging of the structure of chordotonal neurons can be applied simultaneously. In my preparation, the increased frequency sensitivity of lch5 to sinusoidal stimulation at its best frequency around 900 Hz, which differs from the best results (500 Hz) of previous study (Zhang et al., 2013). Nevertheless, given that the filet preparation and the introduction of mechanical forces could impact the response properties of chordotonal neurons, I cannot exclude that there are larval dissecting and instrumental differences between previous and current studies. Additionally, the findings showed larval best sense (approximately either 900 or 500 Hz) was higher than the adult`s sense range (100-300 Hz) and that this difference could mainly drive courtship behavior (Dickson, 2008; Greenspan and Ferveur, 2000; Yoon et al., 2013). The reason for such rearrangements could be that larvae are capable of sensation (through both touch and sound) (Kim et al., 2012; Tsubouchi et al., 2012; Yan et al., 2013) in order to escape from harmful mechanical stimuli for survival.

5.2 dCIRL modulates mechanosensory properties of chordotonal neurons

Primary sensory neurons such as the bipolar sensory nerve cells of chos process two qualitatively different changes of membrane excitability. Firstly, a direct stimulus leads to graded current flow through a stimulus-dependent modulation of sensory ion channels, producing a local signal referred to as the receptor potential. Secondly, receptor potentials carrying the sensory signal are translated into a “spike language” of nerve systems (trains of action potentials) by voltage-sensitive ion channels, primarily sodium channels. On the current larval model, evidence has been provided for the role of dCIRL in modulating the absolute firing rate of chordotonal neurons in response to mechanical stimuli. The further analyses demonstrated that the mechanosensory responses (relative to their background spike) were partially rescued (Figure 21C) while the absolute firing frequencies were not recovered through chordotonal-specific dCIRL expression (Figure 21B). This implies that, in addition to its cell-autonomous function for the relative response to mechanical stimulation, dCIRL may be required in other cells within or outside lch5, e.g. for an intercellular homodimeric interaction (Prömel et al., 2012a) in order to regulate the absolute spiking frequency. Alternatively, due to the fact that the production of the receptor through the GAL4/UAS system is unlikely to restore endogenous expression levels, this may preclude the generation of a physiologically evoked response frequency from the neurons.

Candidate gating modes in mechanosensation are achieved/composed through either the direct activation through the tension of elastic tethers (or membrane stretch) or the indirect activation via an intercellular downstream signaling pathway (Christensen and Corey, 2007). Given that the second-messenger cascades are slow, lasting typically tens of millisecond (Ranganathan et al., 1995), electrical responses mediated by the chordotonal neurons with short latencies (sub-millisecond) were caused by a direct gating paradigm (Albert et al., 2007; Nadrowski et al., 2008), where vibrations are coupled to the candidate channels and induce their gating (Corey and Hudspeth, 1983; Sukharev and Corey, 2004). Surely, the structural properties of dCIRL cannot support its function as an ionotropic mechanotransducer. The additional recordings provided direct evidence that dCIRL modulates mechano-dependent receptor currents, likely through its metabotropic activity (Figure 24). This is also consistent with the analyses of genetic interaction of dCIRL with TRP channels, in which dCIRL modulates gating properties of the mechanotransduction components (NOMPC/Nanchung) in chordotonal cilia (Scholz et al., 2015).

Similar to hair cells, the obtained receptor currents represented a decay despite the continuous mechanical stimulus and displayed two time scales: fast adaptation (milliseconds) and slow adaptation (10-fold slower) (Figure 31). These kinetics reflects the underlying mechanotransduction module at the molecular level (Crawford et al., 1989; Nadrowski et al., 2008; Ricci et al., 1998; Vollrath et al., 2007). This leads to further possible questions, such as how dCIRL shapes the gating mechanics of TRPs upon mechanical stimuli. This will provide new insights into the biomechanical study of mechanotransducer modules.

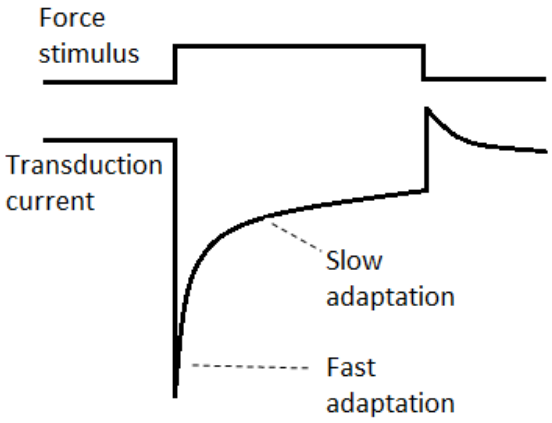

Figure 31. Kinetics of mechanically activated current of hair cells

Representation of fast and slow adaptation components by the current record in response to a force stimulus. Modified from LeMasurier and Gillespie (2005)

Chordotonal neurons responded with an increased action current frequencies upon mechanical stimulation and adapted slowly exhibiting a high dynamic sensitivity (Figure 20A, B), which are similar to the tactile sensory encoding of human skin (slow adapting unit I) (Johansson and Vallbo, 1983). The obtained basal functional lch5 parameters, including the adaptation and recovery mechanisms, demonstrate the classical sensory utility: while adapting to prolonged stimuli, the mechanotransducers remain active in order to respond to new stimuli so that no information is missed (LeMasurier and Gillespie, 2005).

Temperature is an essential physiological factor that influences the properties of neurons, e.g. the kinetics of the currents and the resting potential (Cao and Oertel, 2005). The recordings of chordotonal neurons demonstrated that the spontaneous- and vibration-triggered event frequencies increased with a saturation at high temperature (Figure 30), suggesting that the temperature could affect the excitability in regard to the threshold (resting potential) of APs.

Temperature affects many aspects of physiological processing, in which optimal temperatures for survival, both for growth and reproduction are selected and tissue-damaging thermal extremes are avoided (Dell et al., 2011). Vertebrates perceive and regulate environmental temperatures via innocuous- (warm or cool) and noxious (hot or cold) thermosensors in the peripheral nervous system that project to the skin. At the molecular level, findings have indicated that a subset of TRP proteins, the thermoTRPs, are involved in responding to distinct thermal thresholds (Cao et al., 2013a; Wu et al., 2010; Zakharian et al., 2010). *Drosophila* has emerged as a model organism for thermal sensory processing due to their sensitive and robust responses, triggering stable assayed behavior (Klein et al., 2015). Molecular thermoreceptors TRPA1 and PAINLESS were found to mediate thermotaxis (Rosenzweig et al., 2005; Rosenzweig et al., 2008) and escape responses (Sokabe et al., 2008). Importantly, previous study implicated that the *Drosophila* IAV mechanosensors (restricted in the cilium of chos) are involved in cool-responsive behavior, which is mediated through an increased activity of chordotonal neurons, suggesting that chos harbour parallel transduction pathways for mechanical and thermal stimuli (Sehadova et al., 2009). Although my recordings demonstrated that chos was able to sense temperature changes independent of dCIRL (Figure 30), the availability of electrophysiological readouts of lch5, together with a *Drosophila* genetic toolkit and the quantitative thermostimuli, provided an opportunity to investigate the putative polymodal characteristics of molecular receptors such as TRP channels in chos.

5.3 Molecular concepts of Latrophilin/dCIRL in mechanosensation

Previous studies of GPR126 have uncovered a crucial role of G_s coupled cAMP accumulation for the development of myelinated axons of zebrafish (Monk et al., 2009; Petersen et al., 2015). Other investigations have directly measured intracellular cAMP levels induced by basal activity of the aGPCRs GPR133 (Bohnekamp and Schoneberg, 2011) and GPR126 (Mogha et al., 2013), suggesting possible G_s-protein coupling. Interestingly, recent pharmacological studies of latrophilin homologs LAT-1 and a rat LPHN1 have demonstrated that the receptors elevated intracellular cAMP levels through interaction with a G_s protein (Muller et al., 2015). Coupling of aGPCR to more than one heterotrimeric G protein class is common in most GPCRs. For instance,

GPR126 and GPR133 can interact with both G_s and G_i proteins (Liebscher et al., 2013; Mogha et al., 2013). GPR64 can also couple to G_s and G_q proteins (Kirchhoff et al., 2006). Also, GPR56 interacts with $G_{q/11}$ (Little et al., 2004) and $G_{12/13}$ (Iguchi et al., 2008). Furthermore, VLGR1 can interact with G_i (Hu et al., 2014), G_q and G_s (Shin et al., 2013). Despite a wide variety of research efforts, G protein-mediated aGPCR signaling cascades have yet to be unambiguously defined. The present *in vivo* analyses have revealed that the decrease of cAMP level is a key signal for rescuing the phenotype of *dCirl*^{KO} (Figure 25, 26), suggesting that dCIRL acts as a regulator of cAMP modulated mechancial load via G_i recruiting. Further studies are required in order to elucidate mechanotransduction mechanisms of dCIRL. For example, live imaging techniques allow for the direct visualization and measurement of cAMP dynamics of chordotonal neurons following mechanical stimuli (Maiellaro et al., 2012).

dCIRL, such as many aGPCRs, possesses a long extracellular N-terminus with adhesive properties that anchor the receptor via cognate ligands to the extracellular matrix or to opposed cell surfaces. Mechanical tensile properties of the ECD of the receptor protein should facilitate the reliable transmission of mechanical deformation to the receptor (Krieg et al., 2015). In the current study, I have tested this assumption by relaxing distance and consequently tension of dCIRL´s ECD (Figure 29), perhaps through relieve of mechanical tension across the receptor's extracellular portion. In the presented experimental design, it makes sense to access the performance of the receptor with a shorter ECD by removing an estimated unstructured region IRH (inter-RBL-HRM) between RBL and HRM domains, where the IRH could be important for keeping a proper length of the ECD. However, there is such an ideal experiment is not possible. Given that there is no adhesive domain within IRH, we cannot conclude whether the IRH sequence is essential for the function of dCIRL or if the ECD is shortened through the missing IRH, regardless of the IRH sequence.

One hallmark feature of aGPCRs is the highly conserved, autoproteolytic GPS motif, which is also found in polycystic kidney disease gene products (PKD-1) (Li et al., 2008; Wei et al., 2007). Findings on some aGPCRs (e.g. EGF-TM7, BAI, and GPR56) have demonstrated that cleavage at the GPS may play a crucial role in receptor processing, trafficking and activation of the metabotropic signaling output (Jin et al., 2007; Okajima et al., 2010; Paavola et al., 2011; Yang et al., 2011),

while studies on other aGPCRs (e.g. polycystin-1, EMR2, LAT-1, GPR111 and GPR115) have suggested that proteolytic processing is dispensable for full receptor function (Chang et al., 2003; Prömel et al., 2012a; Prömel et al., 2012b; Qian et al., 2002). This is in accordance with my findings using a proteolysis-deficient mutation of *dCirl*^{H724A} (Figure 28) that autocleavage itself is not a general mechanism for all members of receptors and that autocleavage may differ for diverse aGPCRs or even for the same aGPCR in different developmental stage or cell population. Interestingly, mutation within the *Stachel* sequence (*dCirl*^{T726A}) was able to abolish dCIRL function in chordotonal neurons (Figure 28). In summary, my results consisted with a tethered agonist model of aGPCR (Langenhan et al., 2013; Liebscher et al., 2014; Liebscher et al., 2013), in which mechanical forces make structural changes of ECD in order to expose *Stachel* sequences that active the receptors (Figure 33).

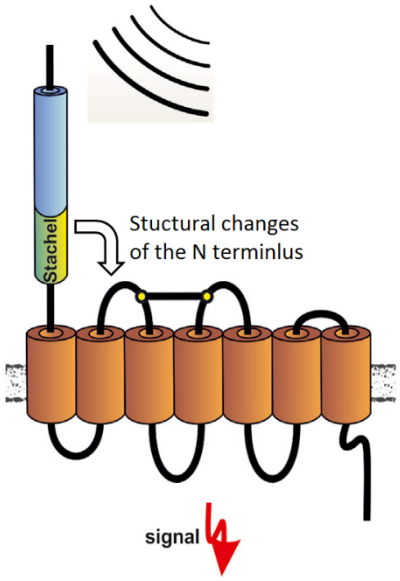

Figure 33. Tethered agonist model of aGPCR. Modified from Liebscher et al. (2014)

Through mechanical stimulation, the activating *Stachel* sequence could be exposed upon structural changes within the ECD, in order to mediate aGPCR activation.

5.4 Closing remarks

In order to assess the sensory effects, including the role of stimuli on receptors/sensors, quantitative methods are needed. In order to study the mechanosensory organ of *Drosophila* larvae, I developed a model that allowed for electrophysiological recording from chos and could subsequently correlate defined mechanical input to their electrical activity. This setup allowed for the characterization of basal functional properties and the receptor current profile of larval lch5

towards mechanical stimulation. The accountability of this method was enhanced through its repeatability and reproducibility and made it possible to probe polymodal properties of candidate proteins.

I was able to show that dCIRL shapes mechanosensation through chordontonal neurons and that dCIRL modulates lch5 neuron activity at the level of its receptor potential rather than its capacity to generate action potentials. Additionally, it was demonstrated that chos sense temperature changes independent of dCIRL. Further, it was shown that autoproteolytic processing is dispensable for dCIRL activity, but *Stachel* sequence is important. At the molecular scale, NTF length of dCIRL determines the mechanosensitivity of lch5. Finally, the results showed that dCIRL effects excitability of chordotonal neurons through the downregulation of cAMP levels upon mechanical stimulation, possibly through stimulation of a G_i pathway. These findings provide initial insights into the mechanosensory function of dCIRL and its role as a metabotropic mechanosensor.

In addition to analysing mechanosensory cells in *Drosophila*, I have employed electrophysiological measurements in order to probe the role of dCIRL in motor neuron excitability and synaptic transmission.

The current model in which dCIRL activities are studied provides an opportunity to study the functions of the mechanosensory organs and is potentially applicable in order to explore the characteristics and identities of mechanically activated receptors/channels.

6 References

Adams, M.D., Celniker, S.E., Holt, R.A., Evans, C.A., Gocayne, J.D., Amanatides, P.G., Scherer, S.E., Li, P.W., Hoskins, R.A., Galle, R.F.*, et al.* (2000). The genome sequence of Drosophila melanogaster. Science *287*, 2185-2195.

Albert, J.T., Nadrowski, B., and Gopfert, M.C. (2007). Mechanical signatures of transducer gating in the Drosophila ear. Curr Biol *17*, 1000-1006.

Albert, J.T., Nadrowski, B., Kamikouchi, A., and Göpfert, M.C. (2006). Mechanical tracing of protein function in the Drosophila ear. Nat Protoc.

Arac, D., Aust, G., Calebiro, D., Engel, F.B., Formstone, C., Goffinet, A., Hamann, J., Kittel, R.J., Liebscher, I., Lin, H.H.*, et al.* (2012). Dissecting signaling and functions of adhesion G protein-coupled receptors. Ann N Y Acad Sci *1276*, 1-25.

Arnadottir, J., and Chalfie, M. (2010). Eukaryotic mechanosensitive channels. Annu Rev Biophys *39*, 111-137.

Ashburner, M., and Roote, J. (2007). Culture of Drosophila: the laboratory setup. CSH Protoc *2007*, pdb ip34.

Baines, R.A., and Bate, M. (1998). Electrophysiological development of central neurons in the Drosophila embryo. J Neurosci *18*, 4673-4683.

Baines, R.A., and Pym, E.C. (2006). Determinants of electrical properties in developing neurons. Semin Cell Dev Biol *17*, 12-19.

Bhattacharya, M.R.C., Bautista, D.M., Wu, K., Haeberle, H., Lumpkin, E.A., and Julius, D. (2008). Radial stretch reveals distinct populations of mechanosensitive mammalian somatosensory neurons. P Natl Acad Sci USA *105*, 20015-20020.

Bjarnadottir, T.K., Fredriksson, R., Hoglund, P.J., Gloriam, D.E., Lagerstrom, M.C., and Schioth, H.B. (2004). The human and mouse repertoire of the adhesion family of G-protein-coupled receptors. Genomics *84*, 23-33.

Blankenship, A.G., and Feller, M.B. (2010). Mechanisms underlying spontaneous patterned activity in developing neural circuits. Nat Rev Neurosci *11*, 18-29.

Bodmer, R., Barbel, S., Sheperd, S., Jack, J.W., Jan, L.Y., and Jan, Y.N. (1987). Transformation of sensory organs by mutations of the cut locus of D. melanogaster. Cell *51*, 293-307.

Bohnekamp, J., and Schoneberg, T. (2011). Cell adhesion receptor GPR133 couples to Gs protein. J Biol Chem *286*, 41912-41916.

Boucard, A.A., Ko, J., and Sudhof, T.C. (2012). High affinity neurexin binding to cell adhesion G-protein-coupled receptor CIRL1/latrophilin-1 produces an intercellular adhesion complex. J Biol Chem *287*, 9399-9413.

Brand, A.H., and Perrimon, N. (1993). Targeted Gene-Expression as a Means of Altering Cell Fates and Generating Dominant Phenotypes. Development *118*, 401-415.

Caldwell, J.C., Miller, M.M., Wing, S., Soll, D.R., and Eberl, D.F. (2003). Dynamic analysis of larval locomotion in Drosophila chordotonal organ mutants. Proc Natl Acad Sci U S A *100*, 16053-16058.

Cao, E., Cordero-Morales, J.F., Liu, B., Qin, F., and Julius, D. (2013a). TRPV1 channels are intrinsically heat sensitive and negatively regulated by phosphoinositide lipids. Neuron *77*, 667-679.

Cao, E., Liao, M., Cheng, Y., and Julius, D. (2013b). TRPV1 structures in distinct conformations reveal activation mechanisms. Nature *504*, 113-118.

Cao, X.J., and Oertel, D. (2005). Temperature affects voltage-sensitive conductances differentially in octopus cells of the mammalian cochlear nucleus. J Neurophysiol *94*, 821-832.

Carlson, S.D., Hilgers, S.L., and Juang, J.L. (1997). Ultrastructure and blood-nerve barrier of chordotonal organs in the Drosophila embryo. J Neurocytol *26*, 377-388.

Chachisvilis, M., Zhang, Y.L., and Frangos, J.A. (2006). G protein-coupled receptors sense fluid shear stress in endothelial cells. Proc Natl Acad Sci U S A *103*, 15463-15468.

Chang, G.W., Stacey, M., Kwakkenbos, M.J., Hamann, J., Gordon, S., and Lin, H.H. (2003). Proteolytic cleavage of the EMR2 receptor requires both the extracellular stalk and the GPS motif. FEBS Lett *547*, 145-150.

Cheng, L.E., Song, W., Looger, L.L., Jan, L.Y., and Jan, Y.N. (2010). The role of the TRP channel NompC in Drosophila larval and adult locomotion. Neuron *67*, 373-380.

Choi, J.C., Park, D., and Griffith, L.C. (2004). Electrophysiological and morphological characterization of identified motor neurons in the Drosophila third instar larva central nervous system. J Neurophysiol *91*, 2353-2365.

Christensen, A.P., and Corey, D.P. (2007). TRP channels in mechanosensation: direct or indirect activation? Nat Rev Neurosci *8*, 510-521.

Chung, Y.D., Zhu, J., Han, Y., and Kernan, M.J. (2001). nompA encodes a PNS-specific, ZP domain protein required to connect mechanosensory dendrites to sensory structures. Neuron *29*, 415-428.

Clapham, D.E. (2003). TRP channels as cellular sensors. Nature *426*, 517-524.

Clapham, D.E., Runnels, L.W., and Strubing, C. (2001). The TRP ion channel family. Nat Rev Neurosci *2*, 387-396.

Corey, D.P., and Hudspeth, A.J. (1979). Response latency of vertebrate hair cells. Biophys J *26*, 499-506.

Corey, D.P., and Hudspeth, A.J. (1983). Kinetics of the receptor current in bullfrog saccular hair cells. J Neurosci *3*, 962-976.

Crawford, A.C., Evans, M.G., and Fettiplace, R. (1989). Activation and adaptation of transducer currents in turtle hair cells. J Physiol *419*, 405-434.

Curtin, J.A., Quint, E., Tsipouri, V., Arkell, R.M., Cattanach, B., Copp, A.J., Henderson, D.J., Spurr, N., Stanier, P., Fisher, E.M.*, et al.* (2003). Mutation of Celsr1 disrupts planar polarity of inner ear hair cells and causes severe neural tube defects in the mouse. Curr Biol *13*, 1129-1133.

Davletov, B.A., Shamotienko, O.G., Lelianova, V.G., Grishin, E.V., and Ushkaryov, Y.A. (1996). Isolation and biochemical characterization of a Ca2+-independent alpha-latrotoxin-binding protein. J Biol Chem *271*, 23239-23245.

Dawydow, A., Gueta, R., Ljaschenko, D., Ullrich, S., Hermann, M., Ehmann, N., Gao, S., Fiala, A., Langenhan, T., Nagel, G.*, et al.* (2014). Channelrhodopsin-2-XXL, a powerful optogenetic tool for low-light applications. Proc Natl Acad Sci U S A *111*, 13972-13977.

Dell, A.I., Pawar, S., and Savage, V.M. (2011). Systematic variation in the temperature dependence of physiological and ecological traits. Proc Natl Acad Sci U S A *108*, 10591-10596.

Delmas, P., and Coste, B. (2013). Mechano-gated ion channels in sensory systems. Cell *155*, 278-284.

Delmas, P., Hao, J., and Rodat-Despoix, L. (2011). Molecular mechanisms of mechanotransduction in mammalian sensory neurons. Nat Rev Neurosci *12*, 139-153.

Dhaka, A., Viswanath, V., and Patapoutian, A. (2006). Trp ion channels and temperature sensation. Annu Rev Neurosci *29*, 135-161.

Dickson, B.J. (2008). Wired for sex: the neurobiology of Drosophila mating decisions. Science *322*, 904-909.

Dubruille, R., Laurencon, A., Vandaele, C., Shishido, E., Coulon-Bublex, M., Swoboda, P., Couble, P., Kernan, M., and Durand, B. (2002). Drosophila regulatory factor X is necessary for ciliated sensory neuron differentiation. Development *129*, 5487-5498.

Eberl, D.F., Hardy, R.W., and Kernan, M.J. (2000). Genetically similar transduction mechanisms for touch and hearing in Drosophila. J Neurosci *20*, 5981-5988.

Efetova, M., Petereit, L., Rosiewicz, K., Overend, G., Haussig, F., Hovemann, B.T., Cabrero, P., Dow, J.A., and Schwarzel, M. (2013). Separate roles of PKA and EPAC in renal function unraveled by the optogenetic control of cAMP levels in vivo. J Cell Sci *126*, 778-788.

Effertz, T., Wiek, R., and Gopfert, M.C. (2011). NompC TRP Channel Is Essential for Drosophila Sound Receptor Function. Curr Biol *21*, 592-597.

Eschbach, C., Cano, C., Haberkern, H., Schraut, K., Guan, C.L., Triphan, T., and Gerber, B. (2011). Associative learning between odorants and mechanosensory punishment in larval Drosophila. Journal of Experimental Biology *214*, 3897-3905.

Fredriksson, R., Lagerstrom, M.C., Lundin, L.G., and Schioth, H.B. (2003). The G-protein-coupled receptors in the human genome form five main families. Phylogenetic analysis, paralogon groups, and fingerprints. Mol Pharmacol *63*, 1256-1272.

Fredriksson, R., and Schioth, H.B. (2005). The repertoire of G-protein-coupled receptors in fully sequenced genomes. Mol Pharmacol *67*, 1414-1425.

Fushiki, A., Kohsaka, H., and Nose, A. (2013). Role of sensory experience in functional development of Drosophila motor circuits. PLoS One *8*, e62199.

Garrity, P.A., Goodman, M.B., Samuel, A.D., and Sengupta, P. (2010). Running hot and cold: behavioral strategies, neural circuits, and the molecular machinery for thermotaxis in C. elegans and Drosophila. Genes Dev *24*, 2365-2382.

Gong, Z., Son, W., Chung, Y.D., Kim, J., Shin, D.W., McClung, C.A., Lee, Y., Lee, H.W., Chang, D.J., Kaang, B.K*., et al.* (2004). Two interdependent TRPV channel subunits, inactive and Nanchung, mediate hearing in Drosophila. J Neurosci *24*, 9059-9066.

Gopfert, M.C., Albert, J.T., Nadrowski, B., and Kamikouchi, A. (2006). Specification of auditory sensitivity by Drosophila TRP channels. Nat Neurosci *9*, 999-1000.

Gopfert, M.C., and Robert, D. (2001). Biomechanics. Turning the key on Drosophila audition. Nature *411*, 908.

Greenspan, R.J., and Ferveur, J.F. (2000). Courtship in Drosophila. Annu Rev Genet *34*, 205-232.

Hamann, J., Aust, G., Arac, D., Engel, F.B., Formstone, C., Fredriksson, R., Hall, R.A., Harty, B.L., Kirchhoff, C., Knapp, B*., et al.* (2015). International Union of Basic and Clinical Pharmacology. XCIV. Adhesion G protein-coupled receptors. Pharmacol Rev *67*, 338-367.

Hamill, O.P., Marty, A., Neher, E., Sakmann, B., and Sigworth, F.J. (1981). Improved patch-clamp techniques for high-resolution current recording from cells and cell-free membrane patches. Pflugers Arch *391*, 85-100.

Hao, J., Padilla, F., Dandonneau, M., Lavebratt, C., Lesage, F., Noel, J., and Delmas, P. (2013). Kv1.1 channels act as mechanical brake in the senses of touch and pain. Neuron *77*, 899-914.

Hefft, S., and Jonas, P. (2005). Asynchronous GABA release generates long-lasting inhibition at a hippocampal interneuron-principal neuron synapse. Nat Neurosci *8*, 1319-1328.

Hochman, B. (1971). Analysis of Chromosome-4 in Drosophila-Melanogaster .2. Ethyl Methanesulfonate Induced Lethals. Genetics *67*, 235-&.

Hu, Q.X., Dong, J.H., Du, H.B., Zhang, D.L., Ren, H.Z., Ma, M.L., Cai, Y., Zhao, T.C., Yin, X.L., Yu, X*., et al.* (2014). Constitutive Galphai coupling activity of very large G protein-coupled receptor 1 (VLGR1) and its regulation by PDZD7 protein. J Biol Chem *289*, 24215-24225.

Hughes, C.L., and Thomas, J.B. (2007). A sensory feedback circuit coordinates muscle activity in Drosophila. Mol Cell Neurosci *35*, 383-396.

Iguchi, T., Sakata, K., Yoshizaki, K., Tago, K., Mizuno, N., and Itoh, H. (2008). Orphan G protein-coupled receptor GPR56 regulates neural progenitor cell migration via a G alpha 12/13 and Rho pathway. J Biol Chem *283*, 14469-14478.

Jan, L.Y., and Jan, Y.N. (1976). Properties of the larval neuromuscular junction in Drosophila melanogaster. J Physiol *262*, 189-214.

Jin, Z., Tietjen, I., Bu, L., Liu-Yesucevitz, L., Gaur, S.K., Walsh, C.A., and Piao, X. (2007). Disease-associated mutations affect GPR56 protein trafficking and cell surface expression. Hum Mol Genet *16*, 1972-1985.

Johansson, R.S., and Vallbo, A.B. (1983). Tactile Sensory Coding in the Glabrous Skin of the Human Hand. Trends Neurosci *6*, 27-32.

Kamikouchi, A., Inagaki, H.K., Effertz, T., Hendrich, O., Fiala, A., Gopfert, M.C., and Ito, K. (2009). The neural basis of Drosophila gravity-sensing and hearing. Nature *458*, 165-171.

Kamikouchi, A., Shimada, T., and Ito, K. (2006). Comprehensive classification of the auditory sensory projections in the brain of the fruit fly Drosophila melanogaster. J Comp Neurol *499*, 317-356.

Keil, T.A. (1997). Functional morphology of insect mechanoreceptors. Microsc Res Tech *39*, 506-531.

Kernan, M.J. (2007). Mechanotransduction and auditory transduction in Drosophila. Pflugers Arch *454*, 703-720.

Kim, S.E., Coste, B., Chadha, A., Cook, B., and Patapoutian, A. (2012). The role of Drosophila Piezo in mechanical nociception. Nature *483*, 209-212.

Kirchhoff, C., Obermann, H., Behnen, M., and Davies, B. (2006). Role of epididymal receptor HE6 in the regulation of sperm microenvironment. Mol Cell Endocrinol *250*, 43-48.

Klein, M., Afonso, B., Vonner, A.J., Hernandez-Nunez, L., Berck, M., Tabone, C.J., Kane, E.A., Pieribone, V.A., Nitabach, M.N., Cardona, A*., et al.* (2015). Sensory determinants of behavioral dynamics in Drosophila thermotaxis. Proc Natl Acad Sci U S A *112*, E220-229.

Krasnoperov, V., Deyev, I.E., Serova, O.V., Xu, C., Lu, Y., Buryanovsky, L., Gabibov, A.G., Neubert, T.A., and Petrenko, A.G. (2009). Dissociation of the subunits of the calcium-independent receptor of alpha-latrotoxin as a result of two-step proteolysis. Biochemistry *48*, 3230-3238.

Krasnoperov, V.G., Beavis, R., Chepurny, O.G., Little, A.R., Plotnikov, A.N., and Petrenko, A.G. (1996). The calcium-independent receptor of alpha-latrotoxin is not a neurexin. Biochem Biophys Res Commun *227*, 868-875.

Krieg, M., Dunn, A.R., and Goodman, M.B. (2015). Mechanical systems biology of C. elegans touch sensation. BioEssays : news and reviews in molecular, cellular and developmental biology *37*, 335-344.

Kwon, Y., Shen, W.L., Shim, H.S., and Montell, C. (2010). Fine Thermotactic Discrimination between the Optimal and Slightly Cooler Temperatures via a TRPV Channel in Chordotonal Neurons. Journal of Neuroscience *30*, 10465-10471.

Lagerstrom, M.C., and Schioth, H.B. (2008). Structural diversity of G protein-coupled receptors and significance for drug discovery. Nat Rev Drug Discov *7*, 339-357.

Langenhan, T., Aust, G., and Hamann, J. (2013). Sticky signaling--adhesion class G protein-coupled receptors take the stage. Sci Signal *6*, re3.

Langenhan, T., Promel, S., Mestek, L., Esmaeili, B., Waller-Evans, H., Hennig, C., Kohara, Y., Avery, L., Vakonakis, I., Schnabel, R*., et al.* (2009). Latrophilin signaling links anterior-posterior tissue polarity and oriented cell divisions in the C. elegans embryo. Dev Cell *17*, 494-504.

Lee, C.H., and Ruben, P.C. (2008). Interaction between voltage-gated sodium channels and the neurotoxin, tetrodotoxin. Channels *2*, 407-412.

Lehnert, B.P., Baker, A.E., Gaudry, Q., Chiang, A.S., and Wilson, R.I. (2013). Distinct roles of TRP channels in auditory transduction and amplification in Drosophila. Neuron *77*, 115-128.

LeMasurier, M., and Gillespie, P.G. (2005). Hair-cell mechanotransduction and cochlear amplification. Neuron *48*, 403-415.

Lewis, A.H., and Raman, I.M. (2014). Resurgent current of voltage-gated Na+ channels. J Physiol-London *592*, 4825-4838.

Li, S., Jin, Z., Koirala, S., Bu, L., Xu, L., Hynes, R.O., Walsh, C.A., Corfas, G., and Piao, X. (2008). GPR56 regulates pial basement membrane integrity and cortical lamination. J Neurosci *28*, 5817-5826.

Liao, M., Cao, E., Julius, D., and Cheng, Y. (2013). Structure of the TRPV1 ion channel determined by electron cryo-microscopy. Nature *504*, 107-112.

Liebscher, I., Schon, J., Petersen, S.C., Fischer, L., Auerbach, N., Demberg, L.M., Mogha, A., Coster, M., Simon, K.U., Rothemund, S*., et al.* (2014). A Tethered Agonist within the Ectodomain Activates the Adhesion G Protein-Coupled Receptors GPR126 and GPR133. Cell Rep *9*, 2018-2026.

Liebscher, I., Schoneberg, T., and Promel, S. (2013). Progress in demystification of adhesion G protein-coupled receptors. Biol Chem *394*, 937-950.

Lin, H.H., Chang, G.W., Davies, J.Q., Stacey, M., Harris, J., and Gordon, S. (2004). Autocatalytic cleavage of the EMR2 receptor occurs at a conserved G protein-coupled receptor proteolytic site motif. Journal of Biological Chemistry *279*, 31823-31832.

Lin, H.H., Stacey, M., Yona, S., and Chang, G.W. (2010). GPS proteolytic cleavage of adhesion-GPCRs. Adv Exp Med Biol *706*, 49-58.

Little, K.D., Hemler, M.E., and Stipp, C.S. (2004). Dynamic regulation of a GPCR-tetraspanin-G protein complex on intact cells: central role of CD81 in facilitating GPR56-Galpha q/11 association. Mol Biol Cell *15*, 2375-2387.

Liu, L., Li, Y., Wang, R., Yin, C., Dong, Q., Hing, H., Kim, C., and Welsh, M.J. (2007). Drosophila hygrosensation requires the TRP channels water witch and nanchung. Nature *450*, 294-298.

Lu, Q.H., Senthilan, P.R., Effertz, T., Nadrowski, B., and Gopfert, M.C. (2009). Using Drosophila for studying fundamental processes in hearing. Integrative and Comparative Biology *49*, 674-680.

Lumpkin, E.A., Marquis, R.E., and Hudspeth, A.J. (1997). The selectivity of the hair cell's mechanoelectrical-transduction channel promotes Ca2+ flux at low Ca2+ concentrations. Proc Natl Acad Sci U S A *94*, 10997-11002.

Maiellaro, I., Lefkimmiatis, K., Moyer, M.P., Curci, S., and Hofer, A.M. (2012). Termination and activation of store-operated cyclic AMP production. J Cell Mol Med *16*, 2715-2725.

Maingret, F., Lauritzen, I., Patel, A.J., Heurteaux, C., Reyes, R., Lesage, F., Lazdunski, M., and Honore, E. (2000). TREK-1 is a heat-activated background K+ channel. Embo Journal *19*, 2483-2491.

Marley, R., and Baines, R.A. (2010). Electrophysiological Recording from Neurons in Drosophila Embryos and Larvae. In Drosophila neurobiology : a laboratory manual, B. Zhang, M.R. Freeman, and S. Waddell, eds. (N.Y.: Cold Spring Harbor).

McCarter, G.C., Reichling, D.B., and Levine, J.D. (1999). Mechanical transduction by rat dorsal root ganglion neurons in vitro. Neurosci Lett *273*, 179-182.

McGee, J., Goodyear, R.J., McMillan, D.R., Stauffer, E.A., Holt, J.R., Locke, K.G., Birch, D.G., Legan, P.K., White, P.C., Walsh, E.J*., et al.* (2006). The very large G-protein-coupled receptor VLGR1: a component of the ankle link complex required for the normal development of auditory hair bundles. J Neurosci *26*, 6543-6553.

McMillan, D.R., Kayes-Wandover, K.M., Richardson, J.A., and White, P.C. (2002). Very large G protein-coupled receptor-1, the largest known cell surface protein, is highly expressed in the developing central nervous system. Journal of Biological Chemistry *277*, 785-792.

McMillan, D.R., and White, P.C. (2004). Loss of the transmembrane and cytoplasmic domains of the very large G-protein-coupled receptor-1 (VLGR1 or Mass1) causes audiogenic seizures in mice. Mol Cell Neurosci *26*, 322-329.

Mederos y Schnitzler, M., Storch, U., Meibers, S., Nurwakagari, P., Breit, A., Essin, K., Gollasch, M., and Gudermann, T. (2008). Gq-coupled receptors as mechanosensors mediating myogenic vasoconstriction. EMBO J *27*, 3092-3103.

Meier, T., and Reichert, H. (1995). Developmental mechanisms, homology and evolution of the insect peripheral nervous system. In The Nervous Systems of Invertebrates: An Evolutionary and Comparative Approach, Breidbach, and Kutsch, eds. (Birkhäuser Basel: Birkhäuser Verlag Basel/Switzerland).

Minke, B., and Cook, B. (2002). TRP channel proteins and signal transduction. Physiol Rev *82*, 429-472.

Mogha, A., Benesh, A.E., Patra, C., Engel, F.B., Schoneberg, T., Liebscher, I., and Monk, K.R. (2013). Gpr126 functions in Schwann cells to control differentiation and myelination via G-protein activation. J Neurosci *33*, 17976-17985.

Molecular Device (2008). The axon guide: A guide to electrophysiology & biophysics laboratory techniques. In.

Monk, K.R., Naylor, S.G., Glenn, T.D., Mercurio, S., Perlin, J.R., Dominguez, C., Moens, C.B., and Talbot, W.S. (2009). A G Protein-Coupled Receptor Is Essential for Schwann Cells to Initiate Myelination. Science *325*, 1402-1405.

Muller, A., Winkler, J., Fiedler, F., Sastradihardja, T., Binder, C., Schnabel, R., Kungel, J., Rothemund, S., Hennig, C., Schoneberg, T.*, et al.* (2015). Oriented Cell Division in the C. elegans Embryo Is Coordinated by G-Protein Signaling Dependent on the Adhesion GPCR LAT-1. PLoS Genet *11*, e1005624.

Muller, G.J. (1993). Black and brown widow spider bites in South Africa. A series of 45 cases. S Afr Med J *83*, 399-405.

Nadrowski, B., Albert, J.T., and Gopfert, M.C. (2008). Transducer-based force generation explains active process in Drosophila hearing. Curr Biol *18*, 1365-1372.

Nagel, G., Szellas, T., Huhn, W., Kateriya, S., Adeishvili, N., Berthold, P., Ollig, D., Hegemann, P., and Bamberg, E. (2003). Channelrhodopsin-2, a directly light-gated cation-selective membrane channel. Proc Natl Acad Sci U S A *100*, 13940-13945.

Neher, E. (1981). Unit conductance studies in biological membranes. In Techniques in cellular physiology, P.F. Baker, ed. (Amsterdam, Holland: Elsevier/North).

O'Sullivan, M.L., de Wit, J., Savas, J.N., Comoletti, D., Otto-Hitt, S., Yates, J.R., 3rd, and Ghosh, A. (2012). FLRT proteins are endogenous latrophilin ligands and regulate excitatory synapse development. Neuron *73*, 903-910.

O'Sullivan, M.L., Martini, F., von Daake, S., Comoletti, D., and Ghosh, A. (2014). LPHN3, a presynaptic adhesion-GPCR implicated in ADHD, regulates the strength of neocortical layer 2/3 synaptic input to layer 5. Neural Dev *9*, 7.

Ohmori, H. (1985). Mechano-electrical transduction currents in isolated vestibular hair cells of the chick. J Physiol *359*, 189-217.

Ohyama, T., Jovanic, T., Denisov, G., Dang, T.C., Hoffmann, D., Kerr, R.A., and Zlatic, M. (2013). High-throughput analysis of stimulus-evoked behaviors in Drosophila larva reveals multiple modality-specific escape strategies. PLoS One *8*, e71706.

Okajima, D., Kudo, G., and Yokota, H. (2010). Brain-specific angiogenesis inhibitor 2 (BAI2) may be activated by proteolytic processing. J Recept Signal Transduct Res *30*, 143-153.

Olesen, S.P., Clapham, D.E., and Davies, P.F. (1988). Haemodynamic shear stress activates a K+ current in vascular endothelial cells. Nature *331*, 168-170.

Orgogozo, V., and Grueber, W.B. (2005). FlyPNS, a database of the Drosophila embryonic and larval peripheral nervous system. BMC Dev Biol *5*, 4.

Orlova, E.V., Rahman, M.A., Gowen, B., Volynski, K.E., Ashton, A.C., Manser, C., van Heel, M., and Ushkaryov, Y.A. (2000). Structure of alpha-latrotoxin oligomers reveals that divalent cation-dependent tetramers form membrane pores. Nat Struct Biol *7*, 48-53.

Paavola, K.J., Stephenson, J.R., Ritter, S.L., Alter, S.P., and Hall, R.A. (2011). The N terminus of the adhesion G protein-coupled receptor GPR56 controls receptor signaling activity. J Biol Chem *286*, 28914-28921.

Petersen, S.C., Luo, R., Liebscher, I., Giera, S., Jeong, S.J., Mogha, A., Ghidinelli, M., Feltri, M.L., Schoneberg, T., Piao, X.H.*, et al.* (2015). The Adhesion GPCR GPR126 Has Distinct, Domain-Dependent Functions in Schwann Cell Development Mediated by Interaction with Laminin-211. Neuron *85*, 755-769.

Pierce, K.L., Premont, R.T., and Lefkowitz, R.J. (2002). Seven-transmembrane receptors. Nat Rev Mol Cell Bio *3*, 639-650.

Prömel, S., Frickenhaus, M., Hughes, S., Mestek, L., Staunton, D., Woollard, A., Vakonakis, I., Schoneberg, T., Schnabel, R., Russ, A.P.*, et al.* (2012a). The GPS Motif Is a Molecular Switch for Bimodal Activities of Adhesion Class G Protein-Coupled Receptors. Cell Rep *2*, 321-331.

Prömel, S., Waller-Evans, H., Dixon, J., Zahn, D., Colledge, W.H., Doran, J., Carlton, M.B., Grosse, J., Schoneberg, T., Russ, A.P.*, et al.* (2012b). Characterization and functional study of a cluster of four highly conserved orphan adhesion-GPCR in mouse. Dev Dyn *241*, 1591-1602.

Qian, F., Boletta, A., Bhunia, A.K., Xu, H., Liu, L., Ahrabi, A.K., Watnick, T.J., Zhou, F., and Germino, G.G. (2002). Cleavage of polycystin-1 requires the receptor for egg jelly domain and is disrupted by human autosomal-dominant polycystic kidney disease 1-associated mutations. Proc Natl Acad Sci U S A *99*, 16981-16986.

Ranganathan, R., Malicki, D.M., and Zuker, C.S. (1995). Signal transduction in Drosophila photoreceptors. Annu Rev Neurosci *18*, 283-317.

Reeh, P.W. (1986). Sensory receptors in mammalian skin in an in vitro preparation. Neurosci Lett *66*, 141-146.

Reiners, J., van Wijk, E., Marker, T., Zimmermann, U., Jurgens, K., te Brinke, H., Overlack, N., Roepman, R., Knipper, M., Kremer, H.*, et al.* (2005). Scaffold protein harmonin (USH1C) provides molecular links between Usher syndrome type 1 and type 2. Hum Mol Genet *14*, 3933-3943.

Ricci, A.J., Wu, Y.C., and Fettiplace, R. (1998). The endogenous calcium buffer and the time course of transducer adaptation in auditory hair cells. J Neurosci *18*, 8261-8277.

Robert, D., and Gopfert, M.C. (2004). Introduction to the biology of insect audition: Diversity in forms and functions. Microsc Res Techniq *63*, 311-312.

Rohrbough, J., and Broadie, K. (2002). Electrophysiological analysis of synaptic transmission in central neurons of Drosophila larvae. J Neurophysiol *88*, 847-860.

Rosenthal, L., and Meldolesi, J. (1989). Alpha-latrotoxin and related toxins. Pharmacol Ther *42*, 115-134.

Rosenzweig, M., Brennan, K.M., Tayler, T.D., Phelps, P.O., Patapoutian, A., and Garrity, P.A. (2005). The Drosophila ortholog of vertebrate TRPA1 regulates thermotaxis. Genes Dev *19*, 419-424.

Rosenzweig, M., Kang, K., and Garrity, P.A. (2008). Distinct TRP channels are required for warm and cool avoidance in Drosophila melanogaster. Proc Natl Acad Sci U S A *105*, 14668-14673.

Saumweber, T., Cano, C., Klessen, J., Eichler, K., Fendt, M., and Gerber, B. (2014). Immediate and punitive impact of mechanosensory disturbance on olfactory behaviour of larval Drosophila. Biol Open *3*, 1005-1010.

Schmid, A., Hallermann, S., Kittel, R.J., Khorramshahi, O., Frolich, A.M.J., Quentin, C., Rasse, T.M., Mertel, S., Heckmann, M., and Sigrist, S.J. (2008). Activity-dependent site-specific changes of glutamate receptor composition in vivo. Nat Neurosci *11*, 659-666.

Scholz, N., Gehring, J., Guan, C., Ljaschenko, D., Fischer, R., Lakshmanan, V., Kittel, R.J., and Langenhan, T. (2015). The adhesion GPCR latrophilin/CIRL shapes mechanosensation. Cell reports *11*, 866-874.

Schroder-Lang, S., Schwarzel, M., Seifert, R., Strunker, T., Kateriya, S., Looser, J., Watanabe, M., Kaupp, U.B., Hegemann, P., and Nagel, G. (2007). Fast manipulation of cellular cAMP level by light in vivo. Nat Methods *4*, 39-42.

Schroll, C., Riemensperger, T., Bucher, D., Ehmer, J., Voller, T., Erbguth, K., Gerber, B., Hendel, T., Nagel, G., Buchner, E.*, et al.* (2006). Light-induced activation of distinct modulatory neurons triggers appetitive or aversive learning in Drosophila larvae. Curr Biol *16*, 1741-1747.

Schwander, M., Kachar, B., and Muller, U. (2010). Review series: The cell biology of hearing. J Cell Biol *190*, 9-20.

Sehadova, H., Glaser, F.T., Gentile, C., Simoni, A., Giesecke, A., Albert, J.T., and Stanewsky, R. (2009). Temperature entrainment of Drosophila's circadian clock involves the gene nocte and signaling from peripheral sensory tissues to the brain. Neuron *64*, 251-266.

Senthilan, P.R., Piepenbrock, D., Ovezmyradov, G., Nadrowski, B., Bechstedt, S., Pauls, S., Winkler, M., Mobius, W., Howard, J., and Gopfert, M.C. (2012). Drosophila auditory organ genes and genetic hearing defects. Cell *150*, 1042-1054.

Shen, W.L., Kwon, Y., Adegbola, A.A., Luo, J., Chess, A., and Montell, C. (2011). Function of rhodopsin in temperature discrimination in Drosophila. Science *331*, 1333-1336.

Shin, D., Lin, S.T., Fu, Y.H., and Ptacek, L.J. (2013). Very large G protein-coupled receptor 1 regulates myelin-associated glycoprotein via G(alpha s)/G(alpha q)-mediated protein kinases A/C. P Natl Acad Sci USA *110*, 19101-19106.

Silva, J.P., Lelianova, V.G., Ermolyuk, Y.S., Vysokov, N., Hitchen, P.G., Berninghausen, O., Rahman, M.A., Zangrandi, A., Fidalgo, S., Tonevitsky, A.G.*, et al.* (2011). Latrophilin 1 and its endogenous ligand Lasso/teneurin-2 form a high-affinity transsynaptic receptor pair with signaling capabilities. Proc Natl Acad Sci U S A *108*, 12113-12118.

Simoni, A., Wolfgang, W., Topping, M.P., Kavlie, R.G., Stanewsky, R., and Albert, J.T. (2014). A mechanosensory pathway to the Drosophila circadian clock. Science *343*, 525-528.

Skradski, S.L., Clark, A.M., Jiang, H., White, H.S., Fu, Y.H., and Ptacek, L.J. (2001). A novel gene causing a mendelian audiogenic mouse epilepsy. Neuron *31*, 537-544.

Sokabe, T., Tsujiuchi, S., Kadowaki, T., and Tominaga, M. (2008). Drosophila Painless is a Ca2+-requiring channel activated by noxious heat. Journal of Neuroscience *28*, 9929-9938.

Song, W., Onishi, M., Jan, L.Y., and Jan, Y.N. (2007). Peripheral multidendritic sensory neurons are necessary for rhythmic locomotion behavior in Drosophila larvae. Proc Natl Acad Sci U S A *104*, 5199-5204.

Spitzer, N.C. (2006). Electrical activity in early neuronal development. Nature *444*, 707-712.

Stacey, M., Lin, H.H., Gordon, S., and McKnight, A.J. (2000). LNB-TM7, a group of seven-transmembrane proteins related to family-B G-protein-coupled receptors. Trends Biochem Sci *25*, 284-289.

Stierl, M., Stumpf, P., Udwari, D., Gueta, R., Hagedorn, R., Losi, A., Gartner, W., Petereit, L., Efetova, M., Schwarzel, M.*, et al.* (2011). Light modulation of cellular cAMP by a small bacterial photoactivated adenylyl cyclase, bPAC, of the soil bacterium Beggiatoa. J Biol Chem *286*, 1181-1188.

Sudhof, T.C. (2001). alpha-Latrotoxin and its receptors: neurexins and CIRL/latrophilins. Annu Rev Neurosci *24*, 933-962.

Sukharev, S., and Corey, D.P. (2004). Mechanosensitive channels: multiplicity of families and gating paradigms. Sci STKE *2004*, re4.

Sukharev, S., and Sachs, F. (2012). Molecular force transduction by ion channels - diversity and unifying principles. Journal of Cell Science *125*, 3075-3083.

Suster, M.L., and Bate, M. (2002). Embryonic assembly of a central pattern generator without sensory input. Nature *416*, 174-178.

Tobaben, S., Sudhof, T.C., and Stahl, B. (2002). Genetic analysis of alpha-latrotoxin receptors reveals functional interdependence of CIRL/latrophilin 1 and neurexin 1 alpha. J Biol Chem *277*, 6359-6365.

Tracey, W.D., Jr., Wilson, R.I., Laurent, G., and Benzer, S. (2003). painless, a Drosophila gene essential for nociception. Cell *113*, 261-273.

Tsubouchi, A., Caldwell, J.C., and Tracey, W.D. (2012). Dendritic filopodia, Ripped Pocket, NOMPC, and NMDARs contribute to the sense of touch in Drosophila larvae. Curr Biol *22*, 2124-2134.

Venkatachalam, K., and Montell, C. (2007). TRP channels. Annu Rev Biochem *76*, 387-417.

Voets, T., Talavera, K., Owsianik, G., and Nilius, B. (2005). Sensing with TRP channels. Nat Chem Biol *1*, 85-92.

Vollrath, M.A., Kwan, K.Y., and Corey, D.P. (2007). The micromachinery of mechanotransduction in hair cells. Annual Review of Neuroscience *30*, 339-365.

Walker, R.G., Willingham, A.T., and Zuker, C.S. (2000). A Drosophila mechanosensory transduction channel. Science *287*, 2229-2234.

Wei, W., Hackmann, K., Xu, H., Germino, G., and Qian, F. (2007). Characterization of cis-autoproteolysis of polycystin-1, the product of human polycystic kidney disease 1 gene. J Biol Chem *282*, 21729-21737.

Weston, M.D., Luijendijk, M.W., Humphrey, K.D., Moller, C., and Kimberling, W.J. (2004). Mutations in the VLGR1 gene implicate G-protein signaling in the pathogenesis of Usher syndrome type II. Am J Hum Genet *74*, 357-366.

White, J.P., Wrann, C.D., Rao, R.R., Nair, S.K., Jedrychowski, M.P., You, J.S., Martinez-Redondo, V., Gygi, S.P., Ruas, J.L., Hornberger, T.A*., et al.* (2014). G protein-coupled receptor 56 regulates mechanical overload-induced muscle hypertrophy. Proc Natl Acad Sci U S A *111*, 15756-15761.

Wolbarsht, M.L., and Dethier, V.G. (1958). Electrical activity in the chemoreceptors of the blowfly. I. Responses to chemical and mechanical stimulation. J Gen Physiol *42*, 393-412.

Wu, L.J., Sweet, T.B., and Clapham, D.E. (2010). International Union of Basic and Clinical Pharmacology. LXXVI. Current progress in the mammalian TRP ion channel family. Pharmacol Rev *62*, 381-404.

Wu, Z., Sweeney, L.B., Ayoob, J.C., Chak, K., Andreone, B.J., Ohyama, T., Kerr, R., Luo, L., Zlatic, M., and Kolodkin, A.L. (2011). A combinatorial semaphorin code instructs the initial steps of sensory circuit assembly in the Drosophila CNS. Neuron *70*, 281-298.

Yan, Z.Q., Zhang, W., He, Y., Gorczyca, D., Xiang, Y., Cheng, L.E., Meltzer, S., Jan, L.Y., and Jan, Y.N. (2013). Drosophila NOMPC is a mechanotransduction channel subunit for gentle-touch sensation. Nature *493*, 221-225.

Yang, L., Chen, G., Mohanty, S., Scott, G., Fazal, F., Rahman, A., Begum, S., Hynes, R.O., and Xu, L. (2011). GPR56 Regulates VEGF production and angiogenesis during melanoma progression. Cancer Res *71*, 5558-5568.

Yoon, J., Matsuo, E., Yamada, D., Mizuno, H., Morimoto, T., Miyakawa, H., Kinoshita, S., Ishimoto, H., and Kamikouchi, A. (2013). Selectivity and plasticity in a sound-evoked male-male interaction in Drosophila. PLoS One *8*, e74289.

Yorozu, S., Wong, A., Fischer, B.J., Dankert, H., Kernan, M.J., Kamikouchi, A., Ito, K., and Anderson, D.J. (2009). Distinct sensory representations of wind and near-field sound in the Drosophila brain. Nature *458*, 201-205.

Zakharian, E., Cao, C., and Rohacs, T. (2010). Gating of transient receptor potential melastatin 8 (TRPM8) channels activated by cold and chemical agonists in planar lipid bilayers. J Neurosci *30*, 12526-12534.

Zhang, W., Yan, Z., Jan, L.Y., and Jan, Y.N. (2013). Sound response mediated by the TRP channels NOMPC, NANCHUNG, and INACTIVE in chordotonal organs of Drosophila larvae. Proc Natl Acad Sci U S A *110*, 13612-13617.

Zito, K., Parnas, D., Fetter, R.D., Isacoff, E.Y., and Goodman, C.S. (1999). Watching a synapse grow: noninvasive confocal imaging of synaptic growth in Drosophila. Neuron *22*, 719-729.

Zou, Y., Akazawa, H., Qin, Y., Sano, M., Takano, H., Minamino, T., Makita, N., Iwanaga, K., Zhu, W., Kudoh, S*., et al.* (2004). Mechanical stress activates angiotensin II type 1 receptor without the involvement of angiotensin II. Nat Cell Biol *6*, 499-506.

Zukowski, C.W. (1993). Black widow spider bite. J Am Board Fam Pract *6*, 279-281.

7 Supplemental data

Table 1. Characterization of the time course of lch5 neuron response. All values represent the mean ± SEM. f_s = stimulation frequency, f_e = mechanically evoked action current frequency.

Related to Figure 18B											
Time (s)	0-1	1-2	2-3	3-4	4-5	5-6	6-7	7-8	8-9	9-10	f_s (Hz)
f_e (Hz)	79 ±12	60 ±9	53 ±9	46 ±9	42 ±8	44 ±7	42 ±8	40 ±8	39 ±8	38 ±8	900
P	.001	.011	.054	.140	.070	.045	.096	.116	.156	.168	f_b (Hz)
Time (s)	10-11	11-12	12-13	13-14	14-15	15-16	16-17	17-18	18-19-	19-20	29 ± 4
f_e (Hz)	38 ±6	36 ±6	33 ±6	31 ±6	30 ±6	30 ±6	30 ±6	30 ±6	31 ±6	29 ±7	*n*
P	.139	.172	.300	.406	.467	.479	.435	.469	.416	.485	10

Table 2. Determination of recovery time. All values represent the mean ± SEM. f_s = stimulation frequency, $f_{e1.sti}$ = first mechanically evoked action current frequency, $f_{e2.sti}$ = second mechanically evoked action current frequency.

Related to Figure 19						
Pause time (s)	10	5	2	1	0.5	0.25
f_s (Hz)	900	900	900	900	900	900
$f_{e1.sti}$ (Hz)	73 ± 22	66 ± 20	72 ± 22	80 ± 24	78 ± 22	74 ± 21
$f_{e2.sti}$ (Hz)	72 ± 21	71 ± 22	73 ± 23	72 ± 21	71 ± 19	68 ± 17
P	.699	1.000	.492	.818	.699	.420

Table 3. Quantification of dCIRL roles in mechanosensation. Mechanically triggered action current frequency in lch5 neurons for initial mutant characterization (A), genomic rescue (B) and chordotonal neuron-specific rescue (C). Note the presence or absence of the *iav-GAL4* driver in the individual datasets. All values represent the mean ± SEM. f_s = stimulation frequency, f_e = mechanically evoked action current frequency. From Scholz et al. 2015

	(A) Related to Figure 20C			**(B) Related to Figure 21A**			**(C) Related to Figure 21B**				
Genotype	*w^-; +; iav-GAL4/UAS-20xUAS-IVS-mCD8::GFP;*	*w^-; dCirl^{KO}; iav-GAL4/UAS-20xUAS-IVS-mCD8::GFP;*		*w^-; +; +;*	*w^-; dCirl^{Rescue}; +;*		*w^-; +; iav-GAL4+;* (1)	*w^-; dCirl^{KO}; iav-GAL4/+;* (2)	*w^-; dCirl^{KO}; iav-GAL4/UAS-dCirl;* (3)	1 vs 2	1 vs 3
f_s (Hz)	f_e (Hz)	f_e (Hz)	*P*	f_e (Hz)	f_e (Hz)	*P*	f_e (Hz)	f_e (Hz)	f_e (Hz)	*P*	*P*
0	48 ± 5	28 ± 4	.005	28 ± 5	29 ± 5	.762	43 ± 5	34 ± 5	32 ± 6	.121	.130
100	65 ± 9	32 ± 6	.007	32 ± 6	33 ± 5	.880	58 ± 10	41 ± 9	36 ± 9	.199	.221
300	67 ± 9	34 ± 6	.016	33 ± 5	41 ± 6	.225	60 ± 10	41 ± 10	35 ± 7	.226	.072
500	80 ± 12	39 ± 6	.026	36 ± 5	47 ± 6	.289	69 ± 11	40 ± 10	36 ± 7	.059	.060
700	88 ± 12	44 ± 7	.009	55 ± 9	59 ± 7	.496	79 ± 10	45 ± 11	44 ± 7	.041	.013
900	98 ± 9	45 ± 8	<.001	78 ± 11	85 ± 10	.879	87 ± 7	45 ± 11	54 ± 9	.019	.002
1100	88 ± 13	40 ± 6	.010	49 ± 8	59 ± 6	.344	72 ± 9	40 ± 9	38 ± 6	.026	.016
1300	79 ± 11	36 ± 5	.006	44 ± 6	54 ± 6	.212	71 ± 9	38 ± 9	35 ± 6	.014	.013
1500	74 ± 11	33 ± 5	.007	41 ± 7	53 ± 6	.130	70 ± 11	37 ± 9	36 ± 6	.045	.030
n	10	10		10	10		10	10	9		

Table 4. Analyses of spike propagation through optogenetic stimuli. All values represent the mean ± SEM. *LI* = light intensity, f_{le} = light-evoked action current frequency.

Related to Figure 23				
Genotype	*+ ; iav-Gal4/UAS-XXM* (1)	*dCirl^{KO} ; iav-Gal4/UAS-XXM* (2)	*+ ; iav-Gal4*	1 vs 2
LI (mW/mm^2)	f_{le} (Hz)	f_{le} (Hz)	f_{le} (Hz)	*P*
0.04	11 ± 4	12 ± 3	15 ± 2	.384
0.08	16 ± 5	19 ± 4	14 ± 3	.151
0.17	22 ± 6	23 ± 5	16 ± 3	.705
0.34	35 ± 7	32 ± 6	13 ± 2	.410
0.68	45 ± 8	39 ± 7	12 ± 2	.306
1.35	50 ± 9	43 ± 6	12 ± 2	.266
2.71	48 ± 8	42 ± 7	13 ± 3	.288
5.42	43 ± 9	34 ± 8	13 ± 2	.250
n	10	10	10	

Table 5. Quantification and comparison of tonic and phasic components of mechanically evoked receptor current in lch5. All values represent the mean ± SEM. f_s = stimulation frequency, I_p = phasic receptor current, I_T = tonic receptor current.

Related to Figure 24						
Genotype	*dCirl*^{Rescue}		*dCirl*^{KO}		1 vs 3	2 vs 4
f_s (Hz)	I_P (pA) (1)	I_T (pA) (2)	I_P (pA) (3)	I_T (pA) (4)	*P*	*P*
100	1 ± 1	1 ± 0	0 ± 0	0± 0	.234	.380
300	6 ± 2	1 ± 0	0 ± 0	0 ± 0	<.001	.005
500	10 ± 2	3 ± 0	1 ± 0	1 ± 0	.001	.005
700	17 ± 4	6 ± 2	4 ± 1	2 ± 1	.007	.038
900	25 ± 5	10 ± 2	7 ± 2	3 ± 1	.002	.005
1100	13 ± 3	3 ± 1	1 ± 1	1 ± 0	.007	.007
1300	10 ± 2	2 ± 1	1 ± 0	0 ± 0	.001	<.001
1500	8 ± 2	1 ± 0	0 ± 0	0 ± 0	.002	.007
n	8		8			

Table 6. Functional analysis of C-Flagtag and N-RFP variants. All values represent the mean ± SEM. f_s = stimulation frequency, f_e = mechanically evoked action current frequency.

(A) Related to Figure 27						**(B) Related to Figure 29**				
C-Flagtag						N-RFP				
Genotype	*dCirl*$^{C\text{-}Flag}$ (1)	*dCirl*^{Rescue} (2)	*dCirl*^{KO} (3)	*P*		*dCirl*$^{N\text{-}RFP/C\text{-}Flag}$ (1)	*dCirl*^{Rescue} (2)	*dCirl*^{KO} (3)	*P*	
f_s (Hz)	f_e (Hz)	f_e (Hz)	f_e (Hz)	1 vs 2	1 vs 3	f_e (Hz)	f_e (Hz)	f_e (Hz)	1 vs 2	1 vs 3
100	50 ± 8	47 ± 7	30 ± 4	.442	.059	47 ± 6	50 ± 8	31 ± 5	.382	.030
300	59 ± 8	51 ± 7	32 ± 5	.256	.012	53 ± 7	55 ± 8	32 ± 5	.925	.026
500	68 ± 9	55 ± 7	36 ± 5	.158	.006	58 ± 7	60 ± 8	36 ± 5	1	.019
700	75 ± 10	66 ± 8	44 ± 6	.267	.005	66 ± 8	69 ± 9	44 ± 6	.914	.013
900	90 ± 12	83 ± 8	59 ± 6	.478	.012	76 ± 7	89 ± 8	57 ± 7	.113	.034
1100	67 ± 11	62 ± 8	36 ± 5	.307	.012	68 ± 7	68 ± 9	35 ± 6	.495	<.001
1300	57 ± 9	56 ± 8	33 ± 5	.391	.021	61 ± 7	61 ± 9	33 ± 5	.469	.002
1500	51 ± 8	52 ± 7	32 ± 5	.369	.030	59 ± 6	57 ± 7	33 ± 5	.407	.002
n	9	10	10			20	20	20		

Table 7. Event frequency analysis of autoproteolysis-deficient mutants. All values represent the mean ± SEM. f_s = stimulation frequency, f_e = mechanically evoked action current frequency.

Related to Figure 28C										
	dCirl$^{T>A}$					*dCirl*$^{H>A}$				
Genotype	*dCirl*^{T726A} (1)	*dCirl*^{Rescue} (2)	*dCirl*^{KO} (3)	1 vs 2	1 vs 3	*dCirl*^{H724A} (1)	*dCirl*^{Rescue} (2)	*dCirl*^{KO} (3)	1 vs 2	1 vs 3
f_s (Hz)	f_e (Hz)	f_e (Hz)	f_e (Hz)	*P*	*P*	f_e (Hz)	f_e (Hz)	f_e (Hz)	*P*	*P*
100	35 ± 6	44 ± 9	27 ± 5	.705	.509	29 ± 10	28 ± 4	19 ± 3	.475	.348
300	39 ± 6	52 ± 10	30 ± 6	.540	.265	29 ± 7	31 ± 5	22 ± 4	.419	.598
500	41 ± 6	54 ± 10	34 ± 6	.552	.439	33 ± 8	38 ± 6	22 ± 5	.283	.151
700	48 ± 6	67 ± 10	45 ± 8	.249	.598	44 ± 8	49 ± 7	26 ± 7	.495	.030
900	51 ± 9	81 ± 10	59 ± 9	.059	.531	46 ± 11	58 ± 6	33 ± 8	.163	.241
1100	39 ± 6	63 ± 10	36 ± 7	.097	.509	37 ± 7	38 ± 5	24 ± 6	.925	.060
1300	38 ± 6	58 ± 10	32 ± 6	.171	.475	30 ± 5	30 ± 4	19 ± 4	.494	.043
1500	38 ± 6	53 ± 7	32 ± 7	.296	.327	31 ± 6	26 ± 4	20 ± 5	.495	.026
n	16	17	16			10	13	14		

Table 8. Analyses of mechanically evoked receptor current between *dCirl* wildtype, GPS-defective and knockout recordings. All values represent the mean ± SEM. f_s = stimulation frequency, I_p = phasic receptor current, I_T = tonic receptor current.

Related to Figure 28D																
Genotype	*dCirl*^{Rescue}		*dCirl*^{KO}		*dCirl*^{H724A}		*dCirl*^{T726A}		*P*							
f_s (Hz)	I_P (pA) (1)	I_T (pA) (2)	I_P (pA) (3)	I_T (pA) (4)	I_P (pA) (5)	I_T (pA) (6)	I_P (pA) (7)	I_T (pA) (8)	1 vs 5	1 vs 7	2 vs 6	2 vs 8	3 vs 5	3 vs 7	4 vs 6	4 vs 8
100	0 ± 0	0 ± 0	0 ± 0	0 ± 0	0 ± 0	0 ± 0	0 ± 0	0 ± 0	1	1	1	1	.721	.721	.721	.721
300	3 ± 1	1 ± 0	0 ± 0	0 ± 0	0 ± 0	0 ± 0	1 ± 1	0 ± 0	.279	.279	.574	.505	.442	.721	.442	.721
500	5 ± 3	2 ± 0	1 ± 1	0 ± 0	2 ± 1	1 ± 0	3 ± 2	0 ± 0	.798	.505	.645	.505	.279	.645	.442	.645
700	17 ± 8	6 ± 2	3 ± 1	1 ± 0	9 ± 2	3 ± 0	4 ± 2	1 ± 0	1	.065	.798	.105	.005	.878	.005	.645
900	39 ± 11	17 ± 2	17 ± 3	7 ± 2	32 ± 6	13 ± 3	12 ± 4	7 ± 2	.280	.018	.150	.015	.024	.190	.080	.193
1100	14 ± 8	5 ± 3	4 ± 2	1 ± 1	5 ± 2	3 ± 1	6 ± 4	1 ± 1	.798	.645	.959	.798	.959	.505	.721	.959
1300	11 ± 6	3 ± 1	2 ± 1	1 ± 1	1 ± 0	0 ± 0	5 ± 3	1 ± 1	.505	1	.234	.645	.505	.721	.234	.798
1500	7 ± 4	2 ± 1	1 ± 1	0 ± 0	1 ± 1	1 ± 0	3 ± 2	0 ± 0	.382	.382	.279	.328	.442	.721	.645	.645
n	8		8		8		8									

Table 9. Function analyses of lengthsensors. All values represent the mean ± SEM. f_s = stimulation frequency, f_e = mechanically evoked action current frequency.

Related to Figure 29								
Genotype	*dCirl*$^{BuTX::HA}$ (1)	*dCirl*$^{BuTX::HA::6xIg}$ (2)	*dCirl*^{Rescue} (3)	*dCirl*^{KO} (4)	*P*			
f_s (Hz)	f_e (Hz)	f_e (Hz)	f_e (Hz)	f_e (Hz)	1 vs 3	1 vs 4	2 vs 3	2 vs 4
100	47 ± 7	47 ± 10	53 ± 5	37 ± 9	.411	.058	.409	.217
300	48 ± 7	49 ± 10	49 ± 6	36 ± 8	.947	.099	.860	.053
500	50 ± 7	47 ± 10	58 ± 7	38 ± 9	.725	.067	.403	.148
700	56 ± 7	50 ± 9	62 ± 12	42 ± 10	.495	.109	.291	.265
900	99 ± 9	62 ± 10	90 ± 11	58 ± 10	.232	<.001	.027	.359
1100	60 ± 7	44 ± 8	61 ± 11	38 ± 10	.286	.015	.045	.172
1300	52 ± 7	47 ± 8	52 ± 11	33 ± 5	.242	.020	.141	.194
1500	49 ± 7	43 ± 9	49 ± 11	32 ± 5	.253	.042	.128	.344
n	10	10	20	20				

Table 10. Ich5 activities upon mechanical-thermal stimuli. All values represent the mean ± SEM. f_s = stimulation frequency, f_b = average spontaneous frequency, f_e = mechanically evoked action current frequency.

Related to Figure 30					
Genotype	*dCirl*^{Rescue}		*dCirl*^{KO}		*P*
f_s (Hz)		900		900	
Temperature (°C)	f_b (Hz) (1)	f_e (Hz) (2)	f_b (Hz) (3)	f_e (Hz) (4)	(2) vs (4)
15	15 ± 3	42 ± 9	12 ± 3	26 ± 6	0.09
20	28 ± 6	72 ± 10	19 ± 4	41 ± 10	0.025
25	32 ± 6	87 ± 8	23 ± 4	69 ± 11	0.103
30	36 ± 5	83 ± 14	39 ± 14	68 ± 12	0.217
n	8		8		

Table 11. Patch clamp recordings from motor neurons. All values represent the mean ± SEM.

Related to Figure 31			
	w⁻; ok6-GAL4 +/+; UAS-20xUAS-IVS-mCD8::GFP/+;	*w⁻; ok6-GAL4 dCirl^{KO}/dCirl^{KO}; UAS-20xUAS-IVS-mCD8::GFP/+;*	*P*
Input (pA)	AP frequency [Hz]	AP frequency [Hz]	
-4	0	0	NA
6	0	0	NA
16	2 ± 2	0	NA
26	6 ± 4	3 ± 2	.839
36	11 ± 5	8 ± 4	.693
46	19 ± 6	14 ± 6	.379
56	30 ± 6	23 ± 7	.353
66	42 ± 6	35 ± 7	.386
76	54 ± 6	48 ± 6	.402
86	63 ± 6	57 ± 6	.311
n	12	12	

8 Abbreviations

aGPCR	adhesion GPCR
AP	action potential
PAC	photoactivated adenylyl cyclase
cAMP	cyclic adenosine monophosphate
CD8	Cluster of differentiation 8 or cluster of designation 8
chos	chordotonal organs
ChR2	Channelrhodopsin-2
C_m	membrane capacitance
CIRL	calcium-independent receptor of α-latrotoxin
CNS	central nervous system
CTF	C-terminal fragment
da	dendritic arborization
ECD	Extracellular domain
e.g.	for example, Latin exempli gratia
EGTA	Ethyleneglycol-bis(β-aminoethyl)-N,N,N′,N′-tetraacetic Acid
es	external campaniform sensilla
f_a	the maximum impedance frequency
f_b	average spontaneous frequency
f_e	average evoked response frequency
f_r,	the minimum impedance frequency
GAIN	GPCR autoproteolysis-inducing domain
GΩ	giga Ohm
GFP	green fluorescent protein
GPCR	G-protein coupled receptor
GPS	GPCR proteolysis site
HA	human influenza hemagglutinin
IAV	INACTIVE
ICD	Intracellular domain

i.e.	that is, latin id est
Ib	type I big boutons
Is	type I small boutons
Ig	immunoglobulin
JO	Johnston´s organ
lch5	lateral pentascolopidial organ
MD	multidendritic
min	minutes
Nan	NANCHUNG
ND	neutral density
NGS	normal goat serum
NOMPC	No mechanoreceptor potential C
NTF	N-terminal domain
PBS	phosphate buffer saline
PNS	peripheral nervous system
RAL	All-trans-retinal
R_d	discrimination ratio
RFP	red florescence protein
R_s	series resistance
R_m	membrane resistance
s	second
td	tracheal dendrite
TRP	transient receptor potential
TTX	Tetrodotoxin
7TM	7-transmembrane
UAS	upstream activating sequence
V_m	membrane potential
V_{cmd}	command potential
VNC	ventral nerve cord
v/v	measure for concentration: volume of a fluid per total volume of solution

WT	wildtype
w/v	a measure of concentration: weight of a solid per total volume of solution (%), 1% w/v corresponds to one gram solid in 100ml solution

9 Table of figures and tables

10 Acknowledgements

First of all, I have to thank Tobias Langenhan and Robert J Kittel, who brought me to neuroscience world and allowed me to work independently. They encouraged me to design my own experiments and gave me a hand with scientific points of view when I got bunkered in the research road. Apart from the scientific issues they always had an ear for personal concerns.

I have to thank Georg Nagel and Manfred Heckmann, who shared with me their expertise on the optogenetic and electrophysiological issues and read my doctoral thesis.

I have to thank Matthias Pawlak, who introduced me to thermosensory analysis and was always fun to talk to.

I have to thank Vetrivel Lakshmanan, who helped me solve lots of technical problems during the development of recording setup and shared with me his international research experiences.

I have to thank Nicole Scholz, Matthias Nieberler, and Jennifer Gehring, with whom I worked on the dCIRL projects and who provided me genetic modified flies for functional screening.

I want to thank Nadine Ehmann and Dmitrij Ljaschenko, who taught me larval preparation and TEVC recording technique.

I have to thank Christian Geiger, Armin Liebenstein, and Franz-Josef Sauer, whom I could always ask for technical assistances.

I would give my most special thanks to my wife Debin, with whom I got home feeling and went through thick and thin.

At last my parents Jianhua and Hongxue, who always supported and comforted me during my living and studying in Germany.

11 Appendix

11.1 List of publications

Scholz N*, Gehring J*, **Guan C***, Ljaschenko D, Fischer R, Lakshmanan V, Kittel RJ[#], LangenhanT[#] (2015) The Adhesion GPCR Latrophilin/CIRL Shapes Mechanosensation. Cell Rep 11(6): 866-874.

Terpitz U*, Letschert S*, Bonda U, Spahn C, **Guan C**, Sauer M, Zimmermann U, Bamberg E, Zimmermann D, Sukhorukov VL (2012) Dielectric analysis and multi-cell electrofusion of the yeast Pichia pastoris for electrophysiological studies. J Membr Biol 245(12): 815-826

Eschbach C, Cano C, Haberkern H, Schraut K, **Guan C**, Triphan T, Gerber B (2011) Associative learning between odorants and mechanosensory punishment in larval Drosophila. Journal of Experimental Biology 214(23): 3897-3905.

*Equal contribution / [#] shared correspondence

11.2 Curriculum Vitae